FACULTY OF SCIENCE
UNIVERSITY OF COPENHAGEN

Master's Thesis in Physics

Raffael Gawatz

Matrix Product State Based Algorithms

for Ground States and Dynamics

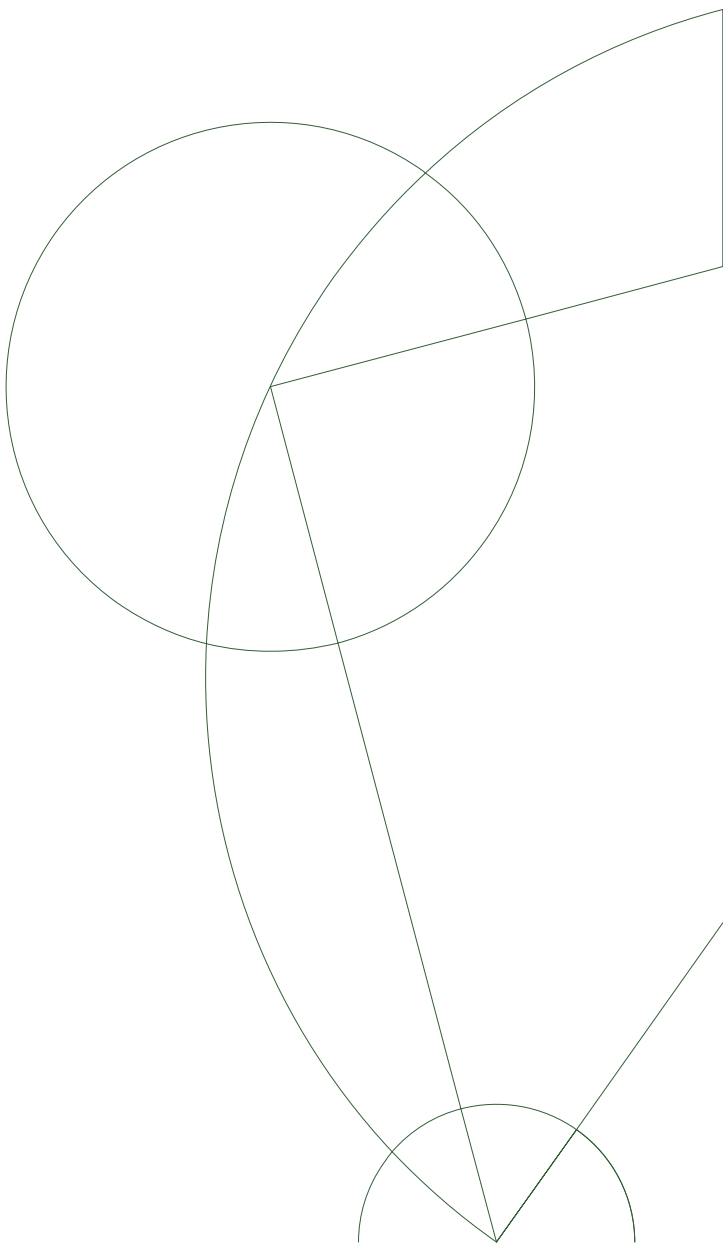

Supervisors: Prof. Mark Rudner & Dr. Ajit C. Balram

September 4, 2017

Matrix Product State Based Algorithms

Raffael Gawatz

Abstract

Strongly correlated systems are arguably one of the most studied systems in condensed matter physics. Yet, the (strong) interaction of many particles with each other is most of the times a strong limitation on practicable analytical methods, such that usually collective phenomenas are studied. To overcome this limitation, numerical techniques become more and more indespensable in the study of many-body systems. A fast growing field of numerical techniques which relies on the notion of entanglement in strongly correlated systems thoroughly analyzed in this thesis is usually referred to as Matrix Product States routines (in one dimension).
In the following we will present such different numerical Matrix Product State routines and apply them to several interesting pehnomena in the field of condensed matter physics. Hereby, the motivation is to verify the accuracy of the implemented routines by matching them with well established results of interesting physical models. The algorithms will cover the exact computation of ground states as well as the dynamics of strongly correlated systems. Further, effort has been put in pointing out for which systems the routines work best and where possible limitations might occure. In this manner the with our routines studied physical models, will complete the picture by giving some hands-on examples for systems worth studying with Matrix Product State algorithms.

Contents

1. Introduction

1.1. A Pinch of Quantum Information

Already during the times of the formulation and interpretation of quantum mechanics in the early 20th century, entanglement was one of the most disputed consequences of the Copenhagen interpretation. This led many renowned physicists to believe in an incompleteness of the proposed quantum theory. One of the most prominent examples is the EPR paradox named after its authors Einstein, Podolsky and Rosen in 1935, who argued that the inclusion of the possibility of entangled states in the formulation of quantum mechanics leads to the possibility to violate classical locality. Consider for instance the decay of a neutral pi meson π^0 into an electron and positron with opposite momentum. Since the pion is initialized in a singlet configuration

$$|\Psi\rangle = \frac{1}{\sqrt{2}} \left(|\uparrow\rangle_+ |\downarrow\rangle_- + |\downarrow\rangle_- |\uparrow\rangle_+ \right), \tag{1}$$

the apart moving electron and positron are in an „entangled" state. Einstein proclaimed that the measurement of the spin configuration of the electron would lead to a collapse of the wave function and instantly determine the outcome of a measurement on the positron. Since both particles move with opposite momentum, this would also hold over very large length scales which strikingly violates the limit imposed by the speed of light. Therefore, Einstein referred to entanglement as „spooky action at a distance" and claimed that quantum mechanics is in fact incomplete. Nevertheless, the introduction of new variables known as „hidden variables" as proposed by Einstein, to solve the EPR pradox were proven to be wrong by Bell in 1965. Moreover, the limit of speed of light is preserved by standard quantum theory, since even though person A would have measured the spin of the electron as long as person B does not know about the result, the measurement on the positron would still be indeterministic: person B would still have a fifty-fifty chance to measure the positron in spin up or down unless person A would send him a note about the result of the measurement on the electron. Thus, one may say that entanglement is shared information between a pair of particles which interacted or were generated in the past, such that none of them can be independently described.

1.2. Separability and Schmidt Decomposition

Much clearer, though more abstract, is the mathematical definition of entanglement. Suppose we have two particles, A and B, with their corresponding Hilbert spaces, $\mathcal{H}_A$ and $\mathcal{H}_B$. The composite Hilbert space describing both particles A and B is given by the tensor product between their individual Hilbert spaces,

$$\mathcal{H} = \mathcal{H}_A \otimes \mathcal{H}_B. \tag{2}$$

In this new composite Hilbert space we now distinguish two types of states. One kind of states that can be decomposed into a tensor product of pure states

$$|\Psi\rangle = |\Psi_A\rangle \otimes |\Psi_B\rangle, \tag{3}$$

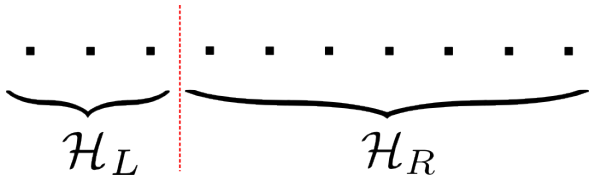

Figure 1: Bipartition: of a composite Hilbert space of 10 sites between site 3 and 4, red doted line. A local Hilbert space is denoted by a black square, such that $\mathcal{H}_L = \mathcal{H}_1 \otimes ... \otimes \mathcal{H}_3$ and $\mathcal{H}_R = \mathcal{H}_4 \otimes ... \otimes \mathcal{H}_{10}$

where $|\Psi_A\rangle \in \mathcal{H}_A$ and $|\Psi_B\rangle \in \mathcal{H}_B$, and the other that cannot. The first type of states are the so called product[1] or separable states, while the latter are the entangled states. Entangled states are precisely those that cannot be separated.
The simplest example of a composit Hilbert space are two spin 1/2 for which each local Hilbert space is spanned by $span\left(\mathcal{H}_{A,B}\right) = \{|\uparrow\rangle, |\downarrow\rangle\}$ and thus the composite system, $span\left(\mathcal{H}_A \otimes \mathcal{H}_B\right) = \{|\uparrow\uparrow\rangle, |\uparrow\downarrow\rangle, |\downarrow\uparrow\rangle, |\downarrow\downarrow\rangle\}$. As one can easily verify, the state

$$|\Psi\rangle = \frac{1}{\sqrt{2}}\left(|\uparrow\rangle \otimes |\downarrow\rangle - |\downarrow\rangle \otimes |\uparrow\rangle\right) \tag{4}$$

cannot be decomposed into a product in the above described fashion. The state, therefore, is an example of an entangled state. However entangled states still might be decomposed as a sum of tensor products. For instance can equation (4) be written as

$$|\Psi\rangle = \frac{1}{\sqrt{2}}|\uparrow\rangle \otimes |\downarrow\rangle - \frac{1}{\sqrt{2}}|\uparrow\rangle \otimes |\downarrow\rangle, \tag{5}$$

which is an example of a Schmidt Decomposition. In general, the Schmidt decomposition of a pure normalized state in composite Hilbert spaces, $\mathcal{H}_{1\otimes...\otimes N} = \mathcal{H}_1 \otimes ... \otimes \mathcal{H}_N$, can be constructed as

$$|\Psi\rangle = \sum_{\alpha=1}^{\chi} \lambda_\alpha |\Phi\left[L\right]_\alpha\rangle \otimes |\Phi\left[R\right]_\alpha\rangle, \tag{6}$$

where $|\Phi\left[L\right]_\alpha\rangle$ and $|\Phi\left[R\right]_\alpha\rangle$ are vectors from an orthonormal set of $\mathcal{H}_L$ and $\mathcal{H}_R$ respectively (referred to as left respectively right Schmidt vectors). Hereby, $\mathcal{H}_L$ and $\mathcal{H}_R$ are the composition of all Hilbert spaces to the left respectively right of an arbitrary chosen bipartition of $\mathcal{H}_{1\otimes...\otimes N}$ (see figure 1). Due to normalization of the state $|\Psi\rangle$, the Schmidt coefficients λ_α are constrained to fulfil $\sum_\alpha \lambda_\alpha^2 = 1$. The number of non-vanishing Schmidt coefficients is called the Schmidt rank χ and can at most take the value $\chi = min\left(dim\left(\mathcal{H}_L\right), dim\left(\mathcal{H}_R\right)\right)$.
If a state is separable, the Schmidt rank χ is exactly one. An entangled state, on the other hand, will have a Schmidt rank strictly greater than one, as the above example suggests.

1.3. Quantitative Measure of Entanglement

Beyond the qualitative information above, the Schmidt rank allows us to give a quantitative measure of entanglement. Since entanglement is the occurrence of a certain phenomenon in

[1] Disclaimer: equivalence of product and separable state just applies for pure states

an experimental set-up rather than an actual measurable property (e.g the spin of a particle), it is a involved task defining a meaningful quantitative measure. This is an important detail which is left out in this work but can be found in [1, 2].
One possible realization of measuring entanglement of pure states is by the entanglement entropy, the von Neumann entropy of the reduced density operator of a pure state

$$S_{vN}\left(\hat{\rho}_A\right) = -Tr\left[\hat{\rho}_A \ \log\left(\hat{\rho}_A\right)\right], \quad \hat{\rho}_A = Tr_B\left[\hat{\rho}\right]. \tag{7}$$

Hereby, $\hat{\rho} = |\Psi\rangle\langle\Psi|$ is the density operator of the state. Having the Schmidt Decomposition in mind (6), the connection to the Schmidt coefficients,

$$S_{vN}\left(\hat{\rho}_A\right) = -\sum_{\alpha} \lambda_\alpha^2 \ \log\left(\lambda_\alpha^2\right), \tag{8}$$

gets immediately obvious by tracing out the right Schmidt vectors. Separable states thus have a vanishing entanglement entropy since the Schmidt rank, and the corresponding Schmidt coefficient, is one. On the other hand, all non-separable (entangled) states are strictly bigger than zero. The maximum of S_{vN} is reached if the state is maximally entangled, a state where $\lambda_\alpha^2 = \frac{1}{\chi}$ while χ is the full rank.
After tracing out one subsystem, an entangled bipartite pure state becomes a mixed state in the remaining other half of the system. For instance, $|\Psi\rangle = 1/\sqrt{2} \cdot (|\uparrow_A\downarrow_B\rangle - |\downarrow_A\uparrow_B\rangle)$ would lead to $\rho_A = 1/2 \cdot (|\uparrow_A\rangle\langle\uparrow_A| - |\downarrow_A\rangle\langle\downarrow_A|)$. It is important to understand that by tracing out one part of the system, all information contained in it and its correlations with the remaining subsystem are lost. Therefore, the fact that tracing out part of the system leads to a mixed state, reveals the incompleteness of the information compared to the original state. This non-locality of entangled state is the defining property of entanglement. Since the von Neumann entropy measures the uncertainty of a system, we have a good quantitative measure of entanglement at hand.[2] Furthermore, note that tracing out the left Schmidt vectors would lead to exactly the same entanglement entropy and therefore, $S_{vN}(\hat{\rho}_A) = S_{vN}(\hat{\rho}_B)$.
An upper bound of the amount of entanglement can be defined by the logarithm of the Schmidt rank, $E_\chi = \log(\chi)$. As desired, it vanishes for $\chi = 1$ and since the Schmidt coefficients have to fulfil $\sum_\alpha \lambda_\alpha^2 = 1$, S_{vN} cannot exceed E_χ and $\chi \geq e^{S_{vN}}$.
It is important to note that the entanglement entropy, as well as the Schmidt rank, can differ for different bipartition as not all parts of the composite system have to be equally codependent (in the above sense).

[2] Further: Since a mixed state would have uncertainty from beginning the von Neumann entropy would dilute the measurement of the entanglement.

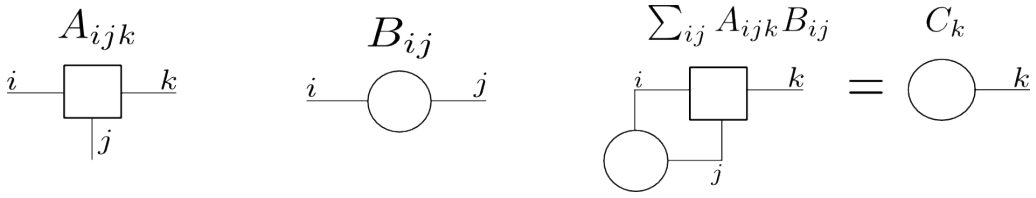

Figure 2: Tensor: graphical representation of a rank 3 A_{ijk} and rank 2 tensor B_{ij} contracted by connecting legs of the same corresponding indices. In the following we will always depict tensors with rank ≤ 2 as circles while tensors with rank ≥ 3 as squares.

2. Theoretical Backbone

2.1. Preliminaries

The concept of tensors is fundamental throughout this thesis. A tensor is a multilinear scalar valued function

$$T : V_1 \times V_2 \times ... \times V_N \longrightarrow \mathbb{C}. \tag{9}$$

The rank of a tensor is the number of vector spaces which the tensor T takes as argument. Usually the tensor is represented such that T becomes an array. For instance one can denote a rank 3 tensor as T_{ijk}, where the indices ijk label the basis states of each vector space V_n; $n \in \{1, 2, 3\}$. The rank can be seen as the dimensionality of such an array to represent the tensor. A vector is therefore represented by a tensor of rank one while a matrix is of rank two.

The meaning of a contraction of tensors is the summation over one or more pair of indices. For instance, a contraction between a rank three tensor A_{ijk} and a rank two tensor B_{ij} over the indices ij is a rank one tensor:

$$C_k = \sum_{ij} A_{ijk}B_{ij}. \tag{10}$$

Since carrying around indices in long terms of equations is a cumbersome task, it is convenient to represent tensors as graphical objects as in figure 2. Hereby a contraction is depicted by connecting legs of the graphical representation of two tensors, where each leg is associcated to an index of a tensor. Further note that if not stated otherwise sums may be left out in which case Einstein summation holds. The sum above is then just written as

$$C_k = A_{ijk}B_{ij}. \tag{11}$$

2.2. Matrix Product States (MPS)

Suppose we have a composition of N identical local Hilbert spaces $\mathcal{H}^{\otimes N} = \mathcal{H}_1 \otimes ... \otimes \mathcal{H}_N$, where each Hilbert space itself is of dimension $dim\,(\mathcal{H}_i) = d$. Each pure state living in the composite Hilbert space can be written as a linear combination

$$|\Psi\rangle = \sum_{s_1 s_2 ... s_N}^{d} \mathrm{c}_{s_1 s_2 ... s_N} |s_1\rangle \otimes |s_2\rangle \otimes ... \otimes |s_N\rangle = \sum_{\bar{s}}^{d} c_{\bar{s}} |\bar{s}\rangle \tag{12}$$

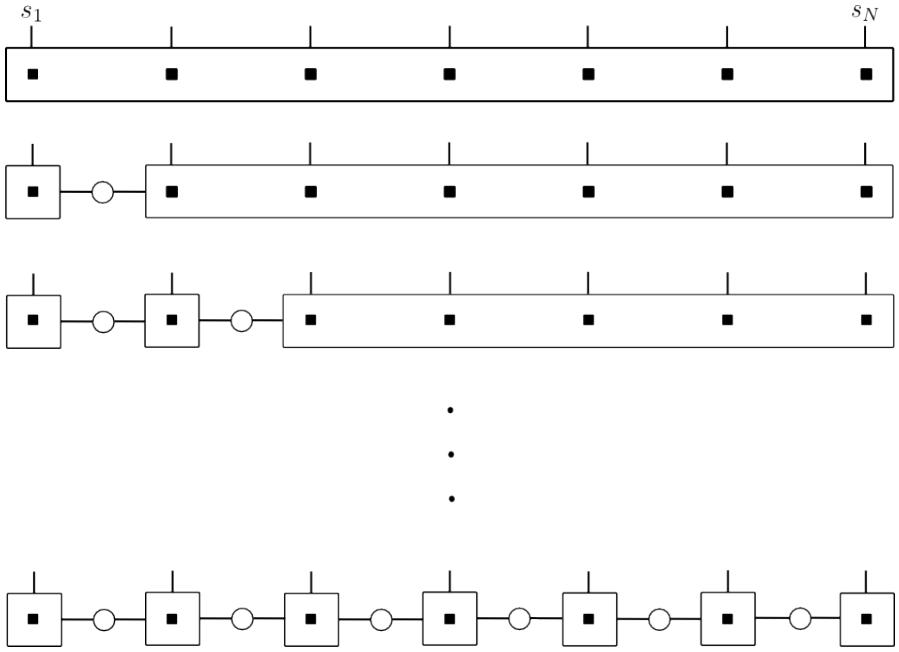

Figure 3: Decomposition: Top line depicts the coefficients of a state $|\Psi\rangle$, a rank N tensor. At the bottom line, this tensor is fully decomposed into a chain of tensors with smaller rank. The second line corresponds to equation (15) in the main text as the third line to equation (18)

of the composite basis states. In this way, a general pure state is described by d^N complex numbers $c_{s_1 s_2 ... s_N}$. These coefficients of the state can be seen as a tensor of rank N, mapping the N basis states onto the according complex number (the coefficient). A Matrix Product State (MPS) is nothing else than a decomposition of the $c_{s_1 s_2 ... s_N}$ tensor of rank N into N tensors of smaller rank in one dimensional systems

$$|\Psi\rangle = \sum_{\bar{s}}^{d} \sum_{\alpha_1 ... \alpha_{N-1}} M[1]_{\alpha_1} M[2]_{\alpha_1 \alpha_2} ... M[N-1]_{\alpha_{N-2} \alpha_{N-1}} M[N]_{\alpha_{N-1}} |\bar{s}\rangle \,. \tag{13}$$

To illustrate the concept, let us look at a specific decomposition of the coefficients step by step (see figure 3) as described in [3]. Consider the local Hilbert spaces laid out on a line (a one dimensional system), as it would be the case for a spin chain for instance. First we form a bipartition of the state $|\Psi\rangle$ by splitting the system between the first site and the rest. We then write the Schmidt decomposition (see equation (6)):

$$|\Psi\rangle = \sum_{\alpha_1=1}^{d} \lambda[1]_{\alpha_1} |\Phi[1]_{\alpha_1}\rangle \otimes |\Phi[2, ..., N]_{\alpha_1}\rangle \,, \tag{14}$$

where $\lambda[1]_{\alpha_1}$ are the corresponding Schmidt coefficients. The attentive reader may claim that the sum does not necessarily have to run up to d (the dimension of $\mathcal{H}_L$); the number of non vanishing Schmidt coefficients depends on the amount of entanglement of site 1 with the rest of the system. For the moment this is neglected (consider a completely entangled state), even though these vanishing Schmidt coefficients in fact lead to the most notable advantage of

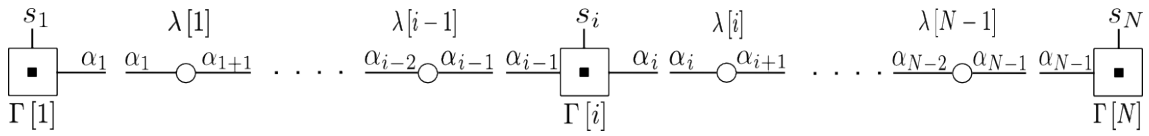

Figure 4: obc MPS: MPS decomposition with open boundary conditions

MPS, as introduced in the later section 2.3. Continuing the decomposition, the basis of site 1 is changed $|\Phi[1]_{\alpha_1}\rangle = \sum_{s_1} \Gamma[1]^{s_1}_{\alpha_1} |s_1\rangle$ into the local basis $\{|s_1\rangle\}$

$$|\Psi\rangle = \sum_{s_1}^{d} \sum_{\alpha_1}^{d} \Gamma[1]^{s_1}_{\alpha_1} \lambda[1]_{\alpha_1} |s_1\rangle \otimes |\Phi[2...N]_{\alpha_1}\rangle \,, \tag{15}$$

introducing a linear map $\Gamma[1]^{s_1}_{\alpha_1}$ from the local basis to the Schmidt basis. The remaining Schmidt basis vector $|\Phi[2...N]_{\alpha_1}\rangle$ is further expanded in the local basis of site 2

$$|\Phi[2,...,N]_{\alpha_1}\rangle = \sum_{s_2} |s_2\rangle \, |\omega[3,...,N]_{\alpha_1 s_2}\rangle \,. \tag{16}$$

Next we express the state $|\omega[3...N]_{\alpha_1 i_2}\rangle$ by the $\chi = d^2$ right Schmidt vectors of a cut of the system between site 2 and 3

$$|\omega[3,...,N]_{\alpha_1 s_2}\rangle = \sum_{\alpha_2}^{\chi} \Gamma[2]^{s_2}_{\alpha_1 \alpha_2} \lambda[2]_{\alpha_2} \, |\Phi[3,...,N]_{\alpha_2}\rangle \,. \tag{17}$$

Inserting the expression above into equation (16) and further into equation (15) gives us an expression for $|\Psi\rangle$ decomposed with sites 1 and 2 in their local computational bases:

$$|\Psi\rangle = \sum_{s_1 s_2} \sum_{\alpha_1 \alpha_2} \Gamma[1]^{s_1}_{\alpha_1} \lambda[1]_{\alpha_1} \Gamma[2]^{s_2}_{\alpha_1 \alpha_2} \lambda[2]_{\alpha_2} \, |s_1\rangle \, |s_2\rangle \, |\Phi[3...N]_{\alpha_2}\rangle \,. \tag{18}$$

The system can now be completely decomposed by iteratively applying equation (16) and (17). Note that hereby the upper bound of the sum in eq. 17 will change according to $\chi = min\left(dim\left(\mathcal{H}^{s_1} \otimes ... \otimes \mathcal{H}^{s_{cut}}\right), dim\left(\mathcal{H}^{s_{cut+1}} \otimes ... \otimes \mathcal{H}^{s_N}\right)\right)$, since as outlined beforehand, the reduction of the Schmidt rank due to vanishing Schmidt ceof. is neglected. Putting the whole expression together, one arrives at

$$|\Psi\rangle = \sum_{s_1 s_2 ... s_N}^{d} \sum_{\alpha_1 ... \alpha_{n-1}} \Gamma\left[1\right]^{s_1}_{\alpha_1} \lambda\left[1\right]_{\alpha_1} \Gamma\left[2\right]^{s_2}_{\alpha_1 \alpha_2} \lambda\left[2\right]_{\alpha_2} \Gamma\left[3\right]^{s_3}_{\alpha_2 \alpha_3} ... \Gamma\left[N\right]^{s_n}_{\alpha_{n-1}} |s_1 ... s_N\rangle \tag{19}$$

where the rank N tensor $c_{s_1 s_2 ... s_N}$ (the coefficients) is decomposed into N tensors $\{\Gamma[1], ..., \Gamma[N]\}$ and $N-1$ vectors $\{\lambda[1], ..., \lambda[N]\}$. Consequently the decomposition reveals that it is possible to describe any pure state of a composite Hilbert space in the depicted manner, in other words the MPS representation is complete.

Before investigating the new obtained tensors Γ and vectors λ further, let us look at their graphical representation (see figure 4). The Γ tensor at each site i, except of the boundaries, is a rank 3 tensor, depicted by the 3 legs in the figure above. One leg marked s_i, is the index of the physical local Hilbert space and hence, has the dimension $d = dim\left(\mathcal{H}_i\right)$. The legs to

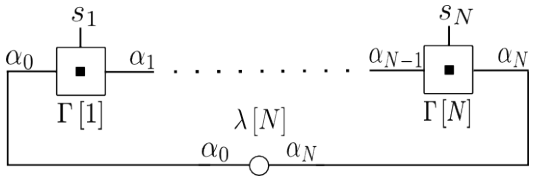

Figure 5: pbc MPS: MPS decomposition with periodic boundary conditions

the left α_{i-1} and to the right α_i are called bond indices (or auxiliary or virtual indices), which are connecting the tensor at site i with the previous tensor to the left and the next tensor to the right. Their dimensionality, denoted as D_{α_i} for bond indices α_i, varies in general since at each cut we summed over $\chi = min\left(dim\left(\mathcal{H}^{s_1} \otimes ... \otimes \mathcal{H}^{s_{cut}}\right), dim\left(\mathcal{H}^{s_{cut+1}} \otimes ... \otimes \mathcal{H}^{s_N}\right)\right)$. Throughout this thesis, bond indices are labelled with subscript Greek letters while physical are given by upper Latin ones. The vector λ_α of equation (19), obtained from the Schmidt coefficients, is depicted in figure 4 as a rank 2 tensor. At the boundaries (site 1 and N) the Γ tensor is of rank 2 as there is no tensor to connect to at the left respectively right.
Revealing the origin of the name, the coefficients of a state $|\Psi\rangle$ to a certain basis state $|\bar{s}\rangle = |s_1...s_n\rangle$ are obtained by

$$\langle \bar{s'}|\Psi\rangle = \sum_{\alpha_1...\alpha_{n-1}} \Gamma\left[1\right]^{s'_1}_{1\alpha_1} \lambda\left[1\right]_{\alpha_1\alpha_1} \Gamma\left[2\right]^{s'_2}_{\alpha_1\alpha_2} \lambda\left[2\right]_{\alpha_2\alpha_2} \Gamma\left[3\right]^{s'_3}_{\alpha_2\alpha_3} ...\Gamma\left[N\right]^{s'_n}_{\alpha_{n-1}1}, \tag{20}$$

where the Schmidt coefficient vector λ_{α_i} is rewritten into a diagonal matrix $\lambda_{\alpha_i\alpha_i}$. This is nothing else than a product of matrices: by considering the physical index of each tensor Γ as fixed, we have a contraction of rank 2 tensors, which can be expressed as matrices (where the first and last site can be seen as row and column vectors).
In the case where the state is subjected to specific boundary conditions, enforced at the left and right end of the one dimensional composite system. The system might be compared with adding a new local Hilbert space with local dimension $d = 1$ (otherwise the boundary is not fixed) at both ends of the chain. A cut between the left boundary condition and the state in this scenario would correspond to a Schmidt decomposition between site 1 and 2. Obviously the first site of the actual state (site 2) now becomes a rank 3 tensor like the rest in the bulk, since entanglement between the boundary and the actual system have to be incorporated. One step further, periodic systems can be thought of as a connection between the last site and the first (see fig. 5). This is natural, since tensors at site k and $k + N$ $\forall k \in \{1, ..., N\}$ should be equal and further should display possible entanglement at a cut between the first and the last site. Hence, a periodic system with a unit cell of N sites may be described by N rank 3 tensors, $\{\Gamma\}$, and N vectors, $\{\lambda\}$.
The above decomposition as introduced by Vidal [3], makes the connection to the Schmidt decomposition and separation of systems in bipartite blocks, and hereby entanglement, immediately accessible. For clarification of this matter, let us start with equation (15), which when transforming site 1 back into its Schmidt basis $|\Phi[1]_{\alpha_1}\rangle = \sum_{s_1} \Gamma[1]^{s_1}_{\alpha_1} |s_1\rangle$, can be reformulated into

$$|\Psi\rangle = \sum_{s_2\alpha_1\alpha_2} \lambda[1]_{\alpha_1}\Gamma[2]^{s_2}_{\alpha_1\alpha_2}\lambda[2]_{\alpha_2} |\Phi[1]_{\alpha_1}\rangle \otimes |s_2\rangle \otimes |\Phi[3...N]_{\alpha_2}\rangle . \tag{21}$$

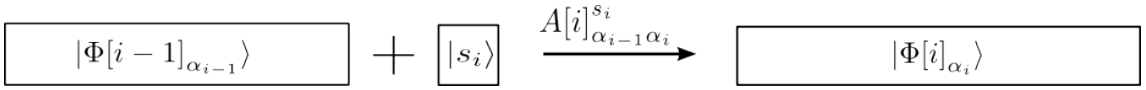

Figure 6: Mapping of increased block: the block in Schmidt basis, build up of all sites to the left of site i is increased by adding the local basis of site i and projected (by $A[i]$ to a new effective Schmidt basis of the by one site increased block.

After contraction and regrouping of $\lambda[1]$ and $\Gamma[2]$ into a new tensor which we define as $A[2]^{s_2}_{\alpha_1\alpha_2} \coloneqq \lambda[1]_{\alpha_1}\Gamma[2]^{s_2}_{\alpha_1\alpha_2}$, the latter equation gives us a new expression

$$|\Psi\rangle = \sum_2 \lambda[2]_{\alpha_2}\left(\sum_{s_1\alpha_1} A[2]^{s_2}_{\alpha_1\alpha_2}|\Phi[1]_{\alpha_1}\rangle \otimes |s_2\rangle\right) \otimes |\Phi[3...N]_{\alpha_2}\rangle\,. \tag{22}$$

Comparison with the Schmidt decomposition of the system between site 2 and 3, then directly leads to the deduction that $A[2]$ transforms $|\Phi[1]_{\alpha_1}\rangle \otimes |s_2\rangle$ into the Schmidt vectors of an enlarged block $|\Phi[1,2]_{\alpha_2}\rangle = \sum_{s_1 s_2 \alpha_1} \Gamma[1]^{s_1}_{\alpha_1}\lambda[1]_{\alpha_1}\Gamma[2]^{s_2}_{\alpha_1\alpha_2}|s_1\rangle \otimes |s_2\rangle$. The reduced density containing site 1 and 2 tracing out the right part of the system (site 3 to N), i.e. tracing over $|\Phi[3...N]_{\alpha_2}\rangle$, then reads as

$$\begin{aligned}\hat{\rho}_{1,2} &= \sum_{\substack{s_1 s_2\\ s_1' s_2'}}\sum_{\substack{\alpha_1\alpha_1'\\ \alpha_2\alpha_2'}} \Gamma[1]^{s_1}_{\alpha_1}\lambda[1]_{\alpha_1}\Gamma[2]^{s_2}_{\alpha_1\alpha_2}\lambda[2]_{\alpha_2}\lambda[2]^*_{\alpha_2'}\Gamma[2]^{s_2'*}_{\alpha_2'\alpha'_1}\lambda[1]^*_{\alpha_1'}\Gamma[1]^{s_1'*}_{\alpha_1'}|s_1 s_2\rangle\langle s_1' s_2'| \\ &= \sum_{\alpha_2\alpha_2'}\lambda[2]_{\alpha_2}\lambda[2]^*_{\alpha_2'}|\Phi[1,2]_{\alpha_2}\rangle\langle\Phi[1,2]_{\alpha_2'}|\,,\end{aligned} \tag{23}$$

from which the direct access by the entries of the λ tensor to the entanglement entropy, as introduced previously, is

$$S_{vN}(\hat{\rho}_{1,2}) = -\sum_{\alpha_2}|\lambda[2]_{\alpha_2}|^2 \cdot \log\left(|\lambda[2]_{\alpha_2}|^2\right). \tag{24}$$

It is this direct access to the entanglement of a state in MPS form opposing the „encryption" in coefficients which leads people to speak of the „entanglement picture" [4]
Note that this holds for any decomposition since $|\Phi[3...N]_{\alpha_2}\rangle$ in equation (22) could be decomposed with equation (16) and (17) such that an expression of the form (21) is retrieved. Consequently, identifying $\Gamma[1]^{s_1}_{\alpha_1}$ with $A[1]^{s_1}_{\alpha_1}$, the whole MPS may be reformulated in terms of the new tensors $A[i]^{s_i}_{\alpha_{i-1}\alpha_i} \coloneqq \lambda[i-1]_{\alpha_{i-1}}\Gamma[i]^{s_i}_{\alpha_{i-1}\alpha_i}$ as

$$|\Psi\rangle = \sum_{s_1 s_2 ... s_N}^{d} Tr\left[A\,[1]^{s_1}_{\alpha_1}\,A\,[2]^{s_2}_{\alpha_1\alpha_2}\,A\,[3]^{s_3}_{\alpha_2\alpha_3}\,...A\,[N]^{s_n}_{\alpha_{n-1}}\right]|s_1...s_N\rangle\,. \tag{25}$$

Besides the fact that this new form looks similar to the general expression (13), it is also a widely used notation in references as well as in this thesis. To motivate this rewriting, consider building up the composite Hilbert space by adding one local Hilbert space after the other to the previous set-up, going from the first to last site (see fig. 2.2). After adding a site, the new Hilbert space is spanned by $|\Phi[i-1]_{\alpha_{i-1}}\rangle \otimes |s_i\rangle$, where $\{|s_i\rangle\}$ is the basis of the

local Hilbert space just added to the system. A general basis transformation

$$|\Phi[i]_{\alpha_i}\rangle = \sum_{s_i}\sum_{\alpha_{i-1}} A[i]_{\alpha_i(\alpha_{i-1},s_i)}\,|\Phi[i-1]_{\alpha_{i-1}}\rangle \otimes |s_i\rangle \tag{26}$$

is defined by the matrix $A[i]_{\alpha_i(\alpha_{i-1},s_i)}$. In the case that $\{|\Phi[i]_{\alpha_i}\rangle\}$ and $\{|\Phi[i-1]_{\alpha_{i-1}}\rangle\}$ are sets of orthonormal basis vectors, the matrix A has to fulfill $A^\dagger A = AA^\dagger = 1$ ($dim(1) = dim(\alpha_i) \times dim(\alpha_i)$). Rewriting and transposing A into a tensor of rank 3

$$|\Phi[i]_{\alpha_i}\rangle = \sum_{s_i}\sum_{\alpha_{i-1}} A[i]^{s_i}_{\alpha_{i-1}\alpha_i}\,|\Phi[i-1]_{\alpha_{i-1}}\rangle \otimes |s_i\rangle\,, \tag{27}$$

equation (25) becomes just an iterative application of adding sites. The rank 3 tensor A inherits hereby from the orthonormality the so called *left* canonical form

$$\sum_{s_i}(A[i]^{s_i}_{\alpha_{i-1}\alpha_i})^\dagger A[i]^{s_i}_{\alpha_{i-1}\alpha_i} = 1_{(D_{\alpha_i}\times D_{\alpha_i})}, \tag{28}$$

which straightforward leads for the decomposition defined by Γ and λ

$$\sum_{s_i} \Gamma[i]^{s_i}_{\alpha_i\alpha_{i-1}}{}^*\lambda[i-1]^*_{\alpha_{i-1}}\lambda[i-1]_{\alpha_{i-1}}\Gamma[i]^{s_i}_{\alpha_{i-1}\alpha_i} = 1_{(D_{\alpha_i}\times D_{\alpha_i})}. \tag{29}$$

Similarly, the process of adding sites could be run from the right to the left

$$|\Phi[i-1]_{\alpha_{i-1}}\rangle = \sum_{s_i}\sum_{\alpha_i} B[i]_{\alpha_{i-1}(\alpha_i s_i)}\,|\Phi[i]_{\alpha_i}\rangle\,|s_i\rangle\,, \tag{30}$$

which in equation (21) would translate into a regrouping

$$|\Psi\rangle = \sum_{\alpha_{i-1}} \lambda[i-1]_{\alpha_{i-1}}\,|\Phi[1..i-1]_{\alpha_{i-1}}\rangle \otimes \left(B^{s_i}_{\alpha_{i-1}\alpha_i}\,|s_i\rangle \otimes |\Phi[i+1..N]_{\alpha_i}\rangle\right), \tag{31}$$

with $B[i] \coloneqq \Gamma[i]_{\alpha_{i-1}\alpha_i}\lambda[i]_{\alpha_i}$ and $B[N] \coloneqq \Gamma[N]_{\alpha_{N-1}\alpha_i}$. Following the same reasoning as for the tensor $A[i]$, the tensor $B[i]$ also fulfils the orthonormality condition

$$\sum_{s_i} B[i]^{s_i}_{\alpha_{i-1}\alpha_i}(B[i]^{s_i}_{\alpha_{i-1}\alpha_i})^\dagger = 1_{(D_{\alpha_{i-1}}\times D_{\alpha_{i-1}})}, \tag{32}$$

referred to as *right* canonical form. For the associated Vidal decomposition this translates into

$$\sum_{s_i} \Gamma[i]^{s_i}_{\alpha_{i-1}\alpha_i}\lambda[i]_{\alpha_i}\lambda[i]^*_{\alpha_i}\Gamma[i]^{s_i*}_{\alpha_{i-1}\alpha_i} = 1_{(D_{\alpha_{i-1}}\times D_{\alpha_{i-1}})}. \tag{33}$$

For decomposing actual coefficients of a state in implementation, one usually iteratively uses Singular Value Decomposition (SVD)[3] (see Appendix A) by which one obtains the above tensors A or B directly. A step by step protocol, which besides an in general very strong review on MPS (especially different algorithms and implementation details), is described in [5].
For completeness note that Matrix Product States are the one dimensional example of Tensor Network states.[4] There are no restrictions of decomposing higher dimensional states. Nonetheless the question is rather if these decompositions are desirable, which is briefly answered in the upcoming section.

[3] the Schmidt Decomposition is strongly connected to SVD see Appendix A
[4] highly recommanded is Orus review [4] for conceptual insights

2.3. Area Law

One major reason why many numerical techniques fail in many body Hilbert spaces is its exponential growth. Consider, for example, a spin 1/2 system for which the Hilbert space grows as 2^N where N is the number of spins. This means that if all coefficients are stored with double precision (real+complex part: 16 Byte), a state with $N = 53$ sites would fill the storage of the currently largest memory of 120 petabyte[5]. Numerical techniques, such as exact diagonalization of the Heisenberg model, are thus almost certain to break down at around $N \approx 40$ sites even with exploiting as many symmetries as possible.
As mentioned, Matrix Product states are complete. Any pure state can be represented by replacing the coefficients, a *rank* N tensor, by N *rank* 3 tensors and 2 *rank* 2 tensors[6] at the boundaries of our system. But how may this help to overcome the restrictions of the vast many body Hilbert spaces?
Other than the coefficients of a state, Matrix Product States reveal the amount of entanglement immediately by their bond dimension. In equation (14) and (18) one sums over the whole range of Schmidt vectors. For a not fully entangled state this is redundant since some of the Schmidt coefficients will eventually vanish and the Schmidt rank χ (an upper bound for the entanglement entropy, see section 1.3) will in general not have full rank. To illustrate this let us have a look at a popular example from quantum information theory, the GHZ state:

$$|GHZ\rangle = \frac{1}{\sqrt{2}} \left(|1, 1, ..., 1\rangle + |0, 0, ..., 0\rangle \right), \tag{34}$$

a superposition of a state with all spins up and one with all spins down. Even though the system size N might grow arbitrarily large, the GHZ state can be represented in the Hilbert space by $4 \cdot D_\chi + 2 \cdot (D_\chi \times D_\chi)$ with $(D_\chi = 2)$ parameters of the MPS representation (see eq. 13)

$$\begin{aligned}
M^{\uparrow}[1] &= \frac{1}{\sqrt{2}} \cdot \begin{pmatrix} 0 & 1 \end{pmatrix} & M^{\downarrow}[1] &= \frac{1}{\sqrt{2}} \cdot \begin{pmatrix} 1 & 0 \end{pmatrix} \\
M^{\uparrow}[i] &= \begin{pmatrix} 0 & 0 \\ 0 & 1 \end{pmatrix} & M^{\downarrow}[i] &= \begin{pmatrix} 1 & 0 \\ 0 & 0 \end{pmatrix}; \quad i \in \{1, ..., N-1\} \\
M^{\uparrow}[N] &= \begin{pmatrix} 0 \\ 1 \end{pmatrix} & M^{\downarrow}[N] &= \begin{pmatrix} 1 \\ 0 \end{pmatrix}.
\end{aligned} \tag{35}$$

To verify that the bond dimension $D_\chi = 2$ is indeed sufficient, we look at the reduced density matrix of an arbitrary cut in the system. Written in the Schmidt basis, the reduced density operator will always have just two non zero contributions
$\hat{\rho}_{reduced} = \frac{1}{2} \left(|1, ..., 1\rangle \langle 1, ..., 1| + |0, ..., 0\rangle \langle 0, ..., 0| \right)$. While this is a very special example, a more general state might also exhibit vanishing Schmidt coefficients which would allow a reduction of the parameters to describe it in MPS form. Apart from that, the example also highlights strongly that the entanglement entropy, as the Schmidt rank χ as its upper bound,

[5] see [6]
[6] for open boundary conditions

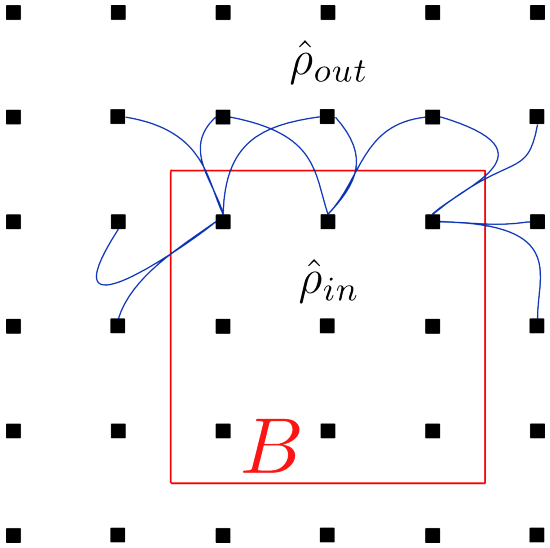

Figure 7: Area law: Cut (red) of an $D = 2$ system in an inner and outer system. The reduced density operator $\hat{\rho}_{in} = \hat{\rho}_{out}$ agree with each other, leading to on an boundary B dependent scaling behaviour. Blue lines illustrate a next nearest neighbour interaction across the boundary leaving the center site untouched.

is all about the quantitative measure of entanglement rather than the qualitative one, since the GHZ state is correlated over the whole system.

It remains to clarify for which states the MPS form is desirable. Or better, to clarify what properties a state should have in order to be efficiently representable in MPS form. A thorough analysis of a periodic composite system of N identical local d dimensional Hilbert spaces (see fig. 5), shows that for a "standard" description with coefficients, d^N parameters are requiered, while for Matrix Product States there are $(d \cdot \chi^2 + \chi) \cdot N$ parameters. Consequently, describing states in MPS form has a linear explicit system size dependency rather than an exponential one. Unfortunately, the bond dimension χ, respectively the entanglement entropy, S_{vN}, is not system size independent, such that in a generic case the number of parameters must grow exponentially with the system size.

However, there are many systems in manybody theories, where interactions are local (for instance next and next nearest neighbour interactions), such that correlations tend to establish in finite ranges (correlation should drop off exponentially [7, 8]). Considering a cut in a system, it seems hence reasonable to assume that the entanglement entropy of low-energy eigenstates will just depend on the amount of quantum correlations between finite layers across the boundary of the cut, leading to a scaling of the entropy with the boundary (area) of the cut (see fig. 7). Even though this seems to contradict the extensive property of entropy it seems to agree with the observation that the entanglement entropy is the same regardless of which part of the bipartite Hilbert space is traced out to receive the reduced density operator: $S_{vN} = -Tr\left[\hat{\rho}_{in} \log\left(\hat{\rho}_{in}\right)\right] = -Tr\left[\hat{\rho}_{out} \log\left(\hat{\rho}_{out}\right)\right]$. Consequently, it is reasonable to assume that S_{vN} will depend on a common property as the boundary [9]. Howsoever, this boundary (area) scaling behaviour may break down for gapless systems where corrections have to be incorporated [10]. An example would be a critical system where the correlation

length diverges and the assumption of an interplay in a finite region across the boundary of a cut breaks. On the contrary, for gapped local Hamiltonians the scaling behaviour of the entanglement entropy for the ground state

$$S_{vN} \sim L^{D-1}, \tag{36}$$

can be proven to hold [7], where D is the real space dimension of the system and L its lenght scale.

In light of equation (36), the entanglement of the ground state of a one dimensional $D = 1$ gapped system with local interactions therefore is constant and does not scale with the system size at all. Ergo the Schmidt rank (respectively the bond dimension $\chi \geq e^{S_{vN}}$) will not depend on L^{D-1} either and the MPS representation can be described by linearly with system size increasing number of parameters.

Less desirable is the scaling in higher dimensional Tensor Networks which will not be topic of this thesis. Though lowering ones sights by applying approximative methods, there have been many successful applications in 2 dimensional tensor networks also referred to as Projected Entangled Pair States (PEPS) [4, 11].

Accompanying the discussion up to this point we can approach from a slightly different point of view. Consider a state $|\Psi\rangle$ in a composite Hilbert space $\mathcal{H}^{\otimes N}$ which should be approximated as closely as possible by another state $|\widetilde{\Psi}\rangle$. Both states are in this scenario Schmidt decomposed at an arbitrary cut in the system

$$|\Psi\rangle = \sum_{i}^{M} \lambda_i \, |\Phi[L]_i\rangle \, |\Phi[R]_i\rangle \quad \text{with} \quad |\widetilde{\Psi}\rangle = \sum_{\alpha}^{N} \lambda_\alpha \, |\Phi[L]_\alpha\rangle \, |\Phi[R]_\alpha\rangle \,, \tag{37}$$

where $N \leq M$ such that the approximated state is described by a smaller basis than the original. Inserting the Schmidt decomposition of both states at this arbitrary cut and minimizing the distance of the states in the two norm $|| \, |\Psi\rangle - |\widetilde{\Psi}\rangle \, ||_2^2$ (see [12]), then boils down to keeping the highest Schmidt coefficients while disregarding the $M - N$ lowest. The error of such an approximation is directly given by

$$|| \, |\Psi\rangle - |\widetilde{\Psi}\rangle \, ||_2^2 = \epsilon \qquad \epsilon = 1 - \sum_{\alpha}^{N} \lambda_\alpha^2, \tag{38}$$

the sum of all disregarded Schmidt coefficients squared. In other words, regarding the reduced density matrix of the state $|\Psi\rangle$ at an arbitrary cut, the approximation is a neglection of its $M - N$ smallest eigenvalues. Think of neglecting all those Schmidt states which contribute to the state $|\Psi\rangle$ the least. How well a state can be approximated, obviously depends on the distribution of the Schmidt coefficients. Most desirable the Schmidt coefficients λ drop off fast, perfectly exponentially, such that a state even in large systems might be faithfully described by a much smaller basis. Accordingly for MPS it is possible to reduce the size of tensor Γ and λ (where λ is assumed to be sorted in decreasing order) at an arbitrary cut

$$\sum_{\alpha_{i-1}}^{M} \lambda_{\alpha_{i-1}} \Gamma^{s_i}_{\alpha_{i-1}\alpha_i} \to \sum_{\alpha_{i-1}}^{N} \lambda_{\alpha_{i-1}} \Gamma^{s_i}_{\alpha_{i-1}\alpha_i}, \tag{39}$$

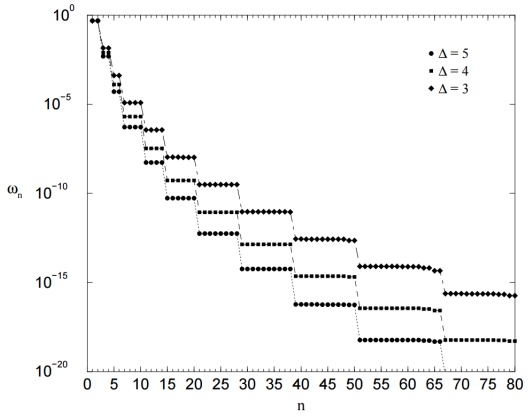

Figure 8: Schmidt coefficents XXZ-modell: Schmidt coefficents of the ground state of a $N = 98$ site long XXZ-chain. [13]

such that after truncation at every cut (every λ) the state can be represented by a MPS with smaller bond dimension.
As one might expect, the systems for which this works best are the ones satisfying the area law. Let us look for instance at the Schmidt coefficients of the exact ground state at half length in a XXZ-model spin chain, which is known to be gapped for $\Delta \geq |1|$, see fig. 8.

2.4. The Valence Bond Picture

Other than motivating Matrix Product States as a technical decomposition of the coefficients of a quantum state into tensors, the Valence Bond Picture (VBP) gives a more physically intuitive motivation which eases the generalization to higher dimensions. Consider a one dimensional system with N particles described by local Hilbert space with dimension d.[7] In the valence bond picture each particle is replaced by two virtual particles with dimension χ. Each of the virtual particles is in a maximally entangled state with the respective neighbouring site (see fig. 9)

$$|\mathcal{I}\rangle_i = \frac{1}{\sqrt{\chi}} \sum_{\alpha_i=1}^{\chi} |\alpha_i\rangle_i \, |\alpha_i\rangle_{i+1} \tag{40}$$

In order to describe a state of the physical particles, we need to map from states on the composite (local) Hilbert space of the virtual particles to the physical local Hilbert space

$$|\Psi\rangle = P_1 \otimes .. \otimes P_N \prod_i^{N-1} \otimes |\mathcal{I}\rangle_i \, . \tag{41}$$

Each map $P : \mathbb{C}^\chi \otimes \mathbb{C}^\chi \to \mathbb{C}^d$ can here be depicted as

$$P_i = \frac{1}{\sqrt{\chi}} \sum_{s_i=1}^{d} \sum_{\alpha_{i-1}\alpha_i}^{\chi} M^{s_i}_{\alpha_{i-1}\alpha_i} \, |s_i\rangle \, \langle \alpha_{i-1}\alpha_i| \, . \tag{42}$$

[7] The generalization to particles with different local Hilbert space dimension is possible

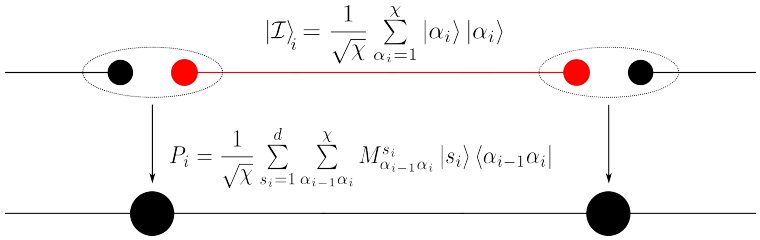

Figure 9: VBP: Valence Bond Picture of a Matrix Product State. P_i maps the maximally entangled states $|\mathcal{I}\rangle_i$ from the valence (auxiliary) into the pyhsical space.

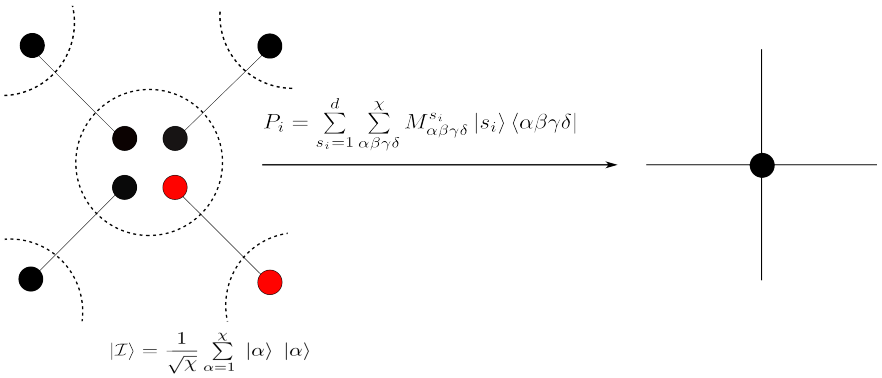

Figure 10: PEPS: Projected Entangled Pair States the two dimensional analogon to MPS

Note that the rank 3 tensors $M^{s_i}_{\alpha_{i-1}\alpha_i}$ now correspond to the previous representation of the MPS (13). By this construction, it also seems more natural to impose periodic boundary conditions which eventually boils down to assigning a virtual, maximally entangled pair between the last site and the first site, and thus automatically leads to the shared bond index in the matrices. The abstraction to higher dimension corresponds to additional shared maximally entangled virtual particle by one physical particles with neighbouring sites. A two dimensional system with physical particles in a square lattice can hence be represented as depicted in figure 10, and is called PEPS (Projected Entangled Pair States). For an example of the construction of a MPS state in this valence bond picture see Appendix B.

2.5. Gauge Freedom and Canonical Forms

The Matrix Product State representation is not unique.This can be easily verified by inserting an identity $X[i]\,X[i]^{-1} = 1$ between each site of equation (13). The state is unchanged, but the matrices M change according to a set of non singular matrices $\{X[i]\}$ of size $D_{\alpha_i} \times D_{\alpha_i}$

$$M[i]^{s_i} \rightarrow X[i-1]^{-1}\, M[i]^{s_i}\, X[i] \tag{43}$$

Despite this arbitrariness the gauge freedom is actually highly of help and is one of the most utilized property of MPS to overcome computational bottlenecks (see section 3.1). Part of the gauge freedom can be eliminated by enforcing left or right orthonormality constraints on

the matrices

$$\text{(left)} \qquad \sum_{s_i} M\left[i\right]^{s_i\dagger} M\left[i\right]^{s_i} = 1 \tag{44}$$

$$\text{(right)} \qquad \sum_{s_i} M\left[i\right]^{s_i} M\left[i\right]^{s_i\dagger} = 1. \tag{45}$$

In the case of left orthonormality, we speak of a left canonical MPS and write their matrices as already discussed in the end of section 2.2, from this point on strictly with an A. On the other hand right canonical MPS are written with matrices B. Unspecified matrices, which do not obey any of the above canonical forms are written with a M.

3. Matrix Product Operators

This introduction in Matrix Product Operators (MPO) is quite brief since the generalization from Matrix Product States is rather clear, for a discussion in depth consider [5]. The same procedure decomposing the coefficients of a state can be used to decompose the entries of an operator of a compost system

$$\hat{O} = \sum_{s_1,..,s_N,s'_1,...,s'_N} c_{(s_1...s_N)(s'_1,...s'_N)} \left|\bar{s}\right\rangle \left\langle\bar{s}'\right| \tag{46}$$

by a set of $N-2$ rank 4 tensors and 2 rank 3 tensors at the boundaries (see figure 11)

$$\hat{O}_{MPO} = \sum_{s_1,...,s_N,s'_1,...,s'_N} W^{s_1,s'_1} W^{s_2,s'_2} ... W^{s_N,s'_N} \left|\bar{s}\right\rangle \left\langle\bar{s}'\right|. \tag{47}$$

Application of a MPO on a MPS is straight forward and leads to

$$\begin{aligned}
\hat{O}_{MPO} \left|\Psi\right\rangle_{MPS} &= \sum_{s_1,...,s_N,s'_1,...,s'_N} \left(W^{s_1,s'_1} W^{s_2,s'_2} ... W^{s_N,s'_N}\right) \left(M^{s'_1} M^{s'_2} ... M^{s'_N}\right) \left|\bar{s}\right\rangle \\
&= \sum_{s_1,...,s_N,s'_1,...,s'_N} \sum_{\alpha_1...\alpha_{N-1},\beta_1...\beta_{N-1}} \left(W^{s_1,s'_1}_{\beta_1} M^{s'_1}_{\alpha_1}\right) \left(W^{s_2,s'_2}_{\beta_1,\beta_2} M^{s'_2}_{\alpha_1,\alpha_2}\right) .... \left(W^{s_N,s'_N}_{\beta_{N-1}} M^{s'_N}_{\alpha_{N-1}}\right) \left|\bar{s}\right\rangle \\
&= \sum_{s_1,...,s_N} \sum_{\alpha_1...\alpha_{N-1},\beta_1...\beta_{N-1}} N^{s_1}_{(\alpha_1,\beta_1)} N^{s_2}_{(\alpha_1,\beta_1),(\alpha_2,\beta_2)} ... N^{s_N}_{(\alpha_{N-1}\beta_{N-1})}, \left|\bar{s}\right\rangle
\end{aligned} \tag{48}$$

a new MPS with higher bond dimension which, in a generic case increases the computational complexity for further calculations. Note that this has far-reaching consequences for time evolution (see section 4.2). In principal it is not necessary to decompose operators. However, applying operators directly has an undesirable consequence. Consider an operator acting on two sites of the system $\hat{O}_[ii+1 = \sum_{s_i,s_{i+1},s'_i,s'_{i+1}} c^{s_i s_{i+1} s'_i s'_{i+1}} \left|s_i, s_{i+1}\right\rangle \left\langle s'_i, s'_{i+1}\right|$ while leaving all other sites untouched. Unlike the application of a MPO on a MPS, applying this operator at site 2 and 3 for instance

$$\begin{aligned}
\hat{O}_{23} \left|\Psi\right\rangle &= \sum_{s_1,...,s_N,s'_1,...,s'_N} \sum_{\alpha_1...\alpha_{N-1}} M^{s'_1}_{\alpha_1} \delta^{s'_1 s_1} M^{s'_2}_{\alpha_1\alpha_2} c^{s_2 s_3 s'_2 s'_3} M^{s'_3}_{\alpha_2,\alpha_3} ... M^{s'_N}_{\alpha_{N-1}} \delta^{s'_N s_N} \left|\bar{s}\right\rangle \\
&= \sum_{s_1,...,s_N} \sum_{\alpha_1...\alpha_{N-1}} M^{s_1}_{\alpha_1} N^{s_2 s_3}_{\alpha_1\alpha_3} M^{s_4}_{\alpha_3\alpha_4} ... M^{s_N}_{\alpha_{N-1}} \left|\bar{s}\right\rangle,
\end{aligned} \tag{49}$$

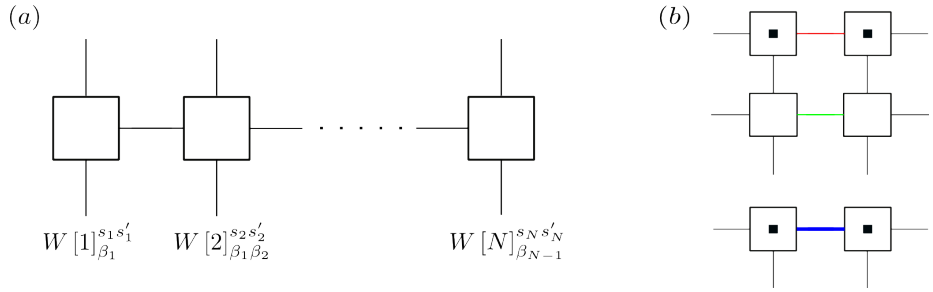

Figure 11: MPO: a) Matrix Product Operator representation b) Increase of bond dimension due to application of an MPO on a state $D_{blue} = D_{red} + D_{green}$.

changes the decomposition of the state. Instead of 2 rank 3 tensors for site 2 and 3, one is now left with a new tensor N of rank 4, encoding both sites at once. Even though it is clear how to decompose such a tensor back into MPS form, it is more convenient to directly work in an environment leaving the form of the MPS unchanged.
The construction of MPO by decompositioning its entries is in principal possible (see [5]). However, it is much easier to construct them by sequential graphs (Markov chain) [14, 15].

3.1. MPS Algebra

After the introduction of the fundamentals, we shall proceed with simple calculus, for instance the overlap of two states or the expectation value of an operator. To begin with, the overlap between two states with open boundary conditions is given by the multiplication of their coefficients

$$\langle \Phi | \Psi \rangle = \sum_{\bar{s}} \widetilde{M}^{s_1 *} ... \widetilde{M}^{s_N *} M^{s_1} ... M^{s_N}, \tag{50}$$

where the set $\{\widetilde{M}\}$ represents the tensors describing the coefficients of $\langle \Phi |$, while $\{M\}$ are the ones of $|\Psi\rangle$. Transposing the coefficients given by the matrix product of $\langle \Phi |$, which is an identity operation, leads to a cleaner expression

$$\langle \Phi | \Psi \rangle = \sum_{\bar{s}} \widetilde{M}^{s_N \dagger} ... \widetilde{M}^{s_1 \dagger} M^{s_1} ... M^{s_N}, \tag{51}$$

as this might be represented graphically by figure 12. This first example already indicates an important detail of MPS calculus, the order of contraction matters. Rewriting the expression above as an iterative process from first to last site

$$\langle \Phi | \Psi \rangle = \sum_{s_N} \widetilde{M}^{s_N \dagger} \left(.. \left(\sum_{s_1} \widetilde{M}^{s_1 \dagger} M^{s_1} \right) .. \right) M^{s_N}, \tag{52}$$

yields a huge computational speed up. The approximately required computation time scales for the hardest computation of the first case with the order of $\mathcal{O}(d^N \cdot D_\alpha)$, while the whole computation of the latter is of the order $\mathcal{O}(N \cdot d \cdot D_\alpha^3)$ (see figure 12).
Before looking at the calculation of expectation values with MPO let us investigate the action of operators in their usual representation, in particular, an operator acting on one site

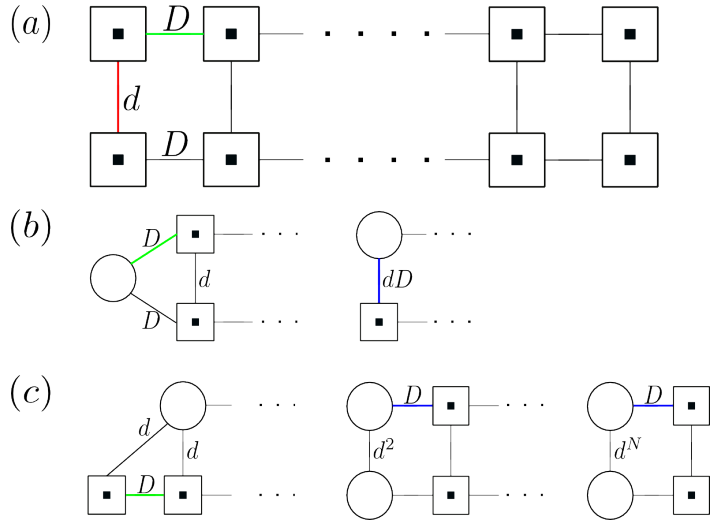

Figure 12: Contraction matters: a) calculation of the norm (overlap) $\langle\Psi|\Psi\rangle$. Contracting the red indices first leads to contraction procedure b) while the green contraction leads to c). The different contraction scheme (contracted indices are coloured) b) & c) correspond to equation (52) respectively (51) leading to different computational complexity as outlined in the text.

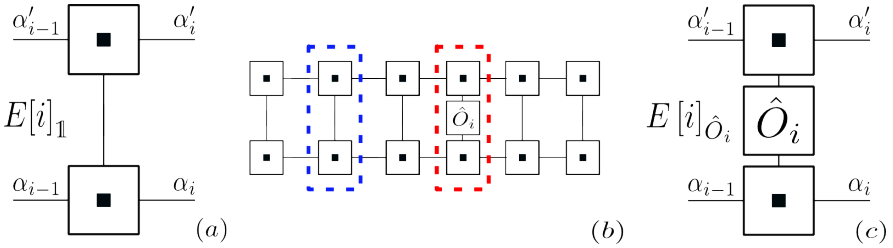

Figure 13: Transfer matrix: b) Graphical representation of a single site exp. value $\langle\Psi|\hat{O}_i|\Psi\rangle_{MPS}$, in blue identity transfer matrix a) and in red the generalized transfer matrix incorporating operator $\hat{O}_i$ c).

$\hat{O}_i = \sum_{s_i s_i'} O^{s_i s_i'} |s_i\rangle \langle s_i'|$. This one site operator can be seen as a tensor with two physical indices (legs), such that calculating $\langle\Psi|\hat{O}_i|\Psi\rangle$ boils down to connecting these legs at the corresponding site with the ones from $\langle\Psi|$ and $|\Psi\rangle$ whereas all others are contracted as in the overlap calculation (see fig. 14). Similar to the example in the above calculation of the expectation value of a single site operator, exploiting the gauge freedom of he MPS representation leads to huge computational speed up. This speed up, as in general MPS calculus, is more comprehensible when working with the concept of transfer operators. Consider the overlap of a state with itself, its norm $\langle\Psi|\Psi\rangle$ is given by (52) where $\widetilde{M}^{s_i} = M^{s_i} \quad \forall i \in \{1, ..., N\}$. It looks quite natural to rewrite equation (52) as a recursive operation $C_i = \mathcal{E}_1^*[i](C_{i-1})$ with

$$\mathcal{E}_1^*[i](\cdot) \coloneqq \sum_{s_i} M^{s_i\dagger} \cdot M^{s_i}, \tag{53}$$

where $\mathcal{E}_1^*[i]$ defines a superoperator transfering an operator from the virtual space $\alpha_i \times \alpha_i$ to $\alpha_{i+1} \times \alpha_{i+1}$. For further simplification, the calculation of the norm can be written into a

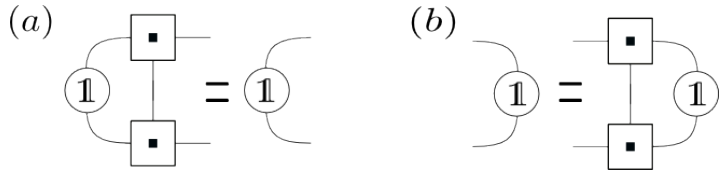

Figure 14: Transfer matrix eigenvector: a) identity transfer matrix in left canonical form respectively right b).

chain product of matrices (see fig. 12) known as transfer matrices

$$\langle\Psi|\Psi\rangle = Tr\left[E_1[1]E_1[2]...E_1[N]\right]. \tag{54}$$

The transfer matrices $E_i[i]$ are hereby a matrix representation of the recursive operator $\mathcal{E}_1^*[i]$

$$E_1[i] = \sum_{s_i} M^{s_i*}_{\alpha'_{i-1}\alpha'_i} \otimes M^{s_i}_{\alpha_{i-1}\alpha_i}, \tag{55}$$

also referred to as Choi Matrix in quantum information. The previous elements $(C_{i-1})_{\alpha'_{i-1}\alpha_{i-1}}$ are then denoted by vectors acting on the left of the transfer matrix. In the case of calculating the expectation value of a single site operator the concept of the transfer matrix can be generalized to incorporate these operators (see fig. 14)

$$E_{\hat{O}_i}[i] = \sum_{s_i s'_i} \langle s_i|\hat{O}_i|s'_i\rangle\, M^{s_i*}_{\alpha'_{i-1}\alpha'_i} \otimes M^{s'_i}_{\alpha_{i-1}\alpha_i} \tag{56}$$

such that the expectation value $\langle\Psi|\hat{O}_i|\Psi\rangle$ can be written as the norm replacing $E_i[i]$ accordingly to the site by $E_{\hat{O}_i}[i]$

$$\langle\Psi|\hat{O}_i|\Psi\rangle = Tr\left[E_1[1]E_1[2]...E_1[i-1]E_{\hat{O}_i}[i]E_1[i+1]...E_1[N]\right]. \tag{57}$$

How do the gauge condition now speed up these type of calculations? Consider first the MPS to be fully expressed by left canonical matrices (44), equation (52) in the case where $\widetilde{M}^{s_i} = M^{s_i} \quad \forall i \in \{1...N\}$, the norm of a state, is trivially equal to one. Consequently this property is shared by the superoperator (53) defining our recursive formulation of the norm respectively the transfer matrix. In other words, in the case of the transfer matrix constructed with left canonical matrices, the identity is a left eigenvector with eigenvalue one. Accordingly, in the right canonical form (45), the identity is a right trivial eigenvector of the transfer matrix (see. fig. 14). Consequently, the calculation of a single site operator, as denoted above as the trace over a product of transfer matrices, can be in fact reduced to the calculation of

$$\langle\Psi|\hat{O}_i|\Psi\rangle = Tr\left[E_{\hat{O}_i}[i]\right] \tag{58}$$

if all matrices of $|\Psi\rangle$ to the left of site i are in left canonical respectively to the right in right canonical form.

In the case the system is under certain fixed or periodic boundary conditions, the situation is less convenient. As pointed out in section 2.2, fixed boundary conditions can be incorporated

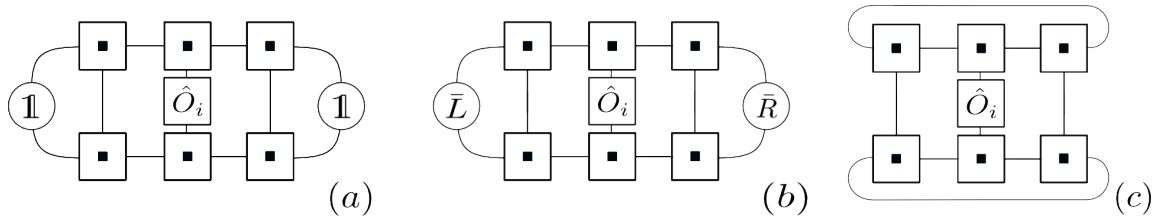

Figure 15: Overview single site expectation value: single site operator expectation values for : a) open chain b) open chain with fixed boundary conditions c) periodic chain

into additional tensors of *rank* 1 at both ends of the system. To account for these boundaries in the transfer matrix notation, vectors $\left(\bar{L}\right)_{1,(\alpha'_0\alpha_0)}$ and $\left(\bar{R}\right)_{(\alpha'_N\alpha_N),1}$ are formed out of the corresponding left respectively right boundary tensors and applied to the left and right end of the tensor product of transfer matrices

$$\langle\Psi|\hat{O}_i|\Psi\rangle = Tr\left[\bar{L}E_1[1]E_1[2]...E_1[i-1]E_{\hat{O}_i}[i]E_1[i+1]...E_1[N]\bar{R}\right]. \tag{59}$$

Therefore, either the boundary vectors are the identity vector, in which case the system would be open and we would regain the expression derived above, or we are left with this unsatisfying expression since even exploiting canonical forms would not facilitate it. The same issue applies for periodic boundary conditions, except that here the problem is intrinsic in the structure of the MPS. Think of the MPS tensors being thread on a ring, such that the first tensor and the last tensor do have a connection. The transfer matrices for those sites hence, change to

$$\begin{aligned}(E_1[1])_{1,\alpha'_1\alpha_1} &\to (E_1[1])_{\alpha'_N\alpha_N,\alpha'_1\alpha_1}\\ (E_1[N])_{\alpha'_{N-1}\alpha_{N-1},1} &\to (E_1[N])_{\alpha'_{N-1}\alpha_{N-1},\alpha'_N\alpha_N},\end{aligned}$$

such that the identity cannot be applied on either site. See figure 15 for comparison of the different situations.

So far, all expectation values are of single site operators. But what is the procedure for terms of operators acting on multiple sites? Section 3 motivated how such terms might be decomposed into MPOs, now it remains to point out how to efficiently use them. Let us look at the calculation of expectation values with a MPO (see figure 16). As done previously, considering the role of contraction in the MPS formalism, the most favoured computation is an iterative computation

$$C[i]_{\alpha_i\beta_i\alpha'_i} = \sum_{s_i\alpha_{i-1}} (M[i]^{s_i*})_{\alpha_i\alpha_{i-1}} \left(\sum_{s'_i\beta_{i-1}} W[i]^{s_i s'_i}_{\beta_{i-1}\beta_i} \left(\sum_{\alpha'_{i-1}} C[i-1]_{\alpha_{i-1}\beta_{i-1}\alpha'_{i-1}} M[i]^{s'_i}_{\alpha'_{i-1}\alpha'_i}\right)\right), \tag{60}$$

coming with an operation count of $\mathcal{O}(D^3_\alpha D_\beta d)$. Other than before it is not possible to rewrite this recursive expression into a trace over "MPO" transfer matrices. However, it is often usefull and eases the understanding for beginners to consider the MPO expectation value as such a trace. Thus, even though with an higher computational effort we can write the MPO

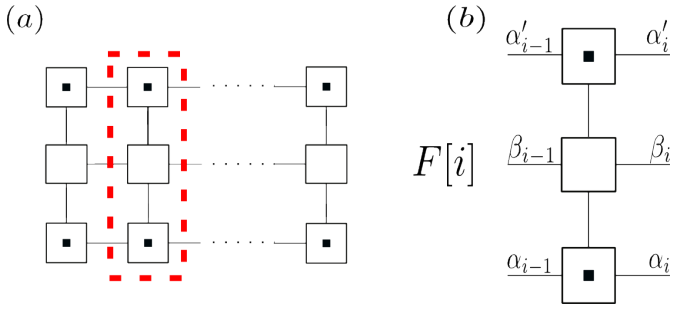

Figure 16: Expectation value of a MPO: a) threads of basic constituents b) in the calculation of a MPO expectation values.

expectation value as a trace of "MPO" transfer matrices $F[i]$ (see fig. 16)

$$\langle \hat{O}_{MPO} \rangle = Tr\left[F[1]...F[N]\right] \tag{61}$$

3.2. Infinite Systems and Strictly Finite Correlation

Up until this point all MPS have finite system size either with open boundary conditions or periodic ones. Beyond Matrix Product State formalism also incorporates infinite MPS (iMPS). An infinite MPS can be seen as some unit cell of N rank 3 tensors such that the infinite system would be translation invariant by a shift of N sites. Since both the first and last tensor in this unit cell of N sites have un-contracted bond indices to the previous respectively next site, we can think of the unit cell being repetitively added to the last site of the previous unit cell. This seems highly similar to the case of a finite MPS with periodic boundary conditions, where the bond indices of the last and first site of one unit cell are contracted. The difference of both methods is stressed in the calculation of a single site expectation value. As an example, consider the simple case of a unit cell of size $N = 1$. The expectation value for a site operator $\hat{O}$

$$\langle \Psi_{inf} | \hat{O} | \Psi_{inf} \rangle = Tr \left[... E_1 E_{\hat{O}} E_1 ... \right] = Tr \left[... E_1 E_{\hat{O}} \right] \tag{62}$$

is given by the trace over an infinite product of the transfer matrix acting on $E_{\hat{O}}$. How to proceed with the infinite product of transfer matrices? In general, the transfer matrix can be represented in the basis of its left and right eigenvectors

$$E_1 = \sum_{i=1}^{D^2} \lambda_i \left| R_i \right\rangle \left\langle L_i \right| , \tag{63}$$

where the eigenvalues are strictly smaller or equal to one. In mathematical terms, the transfer matrix is said to have a spectral radius of one.[8] In the following we will assume the eigenvalues to be orderd by decreasing absolut value $|\lambda_1| \geq |\lambda_2| \geq ... \geq |\lambda_{D^2}|$. Expressing the above equation slightly differently and looking at a product of translation invariant identity transfer matrices

$$E_1^x = (\lambda_1)^x \left(\left| R_1 \right\rangle \left\langle L_1 \right| + \sum_{i=2}^{D^2} \left(\frac{\lambda_i}{\lambda_1} \right)^x \left| R_i \right\rangle \left\langle L_i \right| \right) , \tag{64}$$

it becomes clear that, if the highest eigenvalue one is non degenerate, an infinite product of transfer matrices is suppressing all contributions from eigenvectors other than the one corresponding to the largest eigenvalue $\lambda_1 = 1$

$$\lim_{x \to \text{inf}} (E_1)^x = \lambda_1 \left| R_1 \right\rangle \left\langle L_1 \right| . \tag{65}$$

The expectation value of a single site operator (62) therefore, results in

$$\langle \Psi_{inf} | \hat{O} | \Psi_{inf} \rangle = \langle L_1 | \hat{O} | R_1 \rangle , \tag{66}$$

which is a fairly easy expression even though the system is assumed to be infinite.

As mentioned any state of a many body Hilbert space might be represented as long as one pays the price in form of an increase of bond dimension D_{α_i}. However, things are certainly different for infinite system as the bond dimension cannot grow without boundaries. The

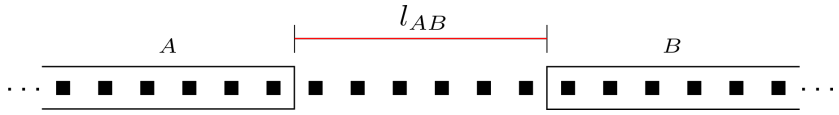

Figure 17: $|\Psi_{inf}\rangle$**:** the infinite MPS is decomposed into 3 blocks A, B, C, while C is finite and of size l_{AB}, A and B are infinite.

question is, which infinite states are at all representable as an iMPS?
To clear this question, consider a decomposition of an infinite state into 3 blocks (see fig. 17)

$$|\Psi_{inf}\rangle \simeq \sum_{i\alpha_A\alpha_B} M^i_{\alpha_A\alpha_B} |\Phi_{\alpha_A}\rangle \otimes |C_i\rangle \otimes |\Phi_{\alpha_B}\rangle , \tag{67}$$

where in general the sum over α_A and α_B would have to be infinite. Yet, in the case that block A is completely separated from block B, which for now means that correlations vanishe for distances smaller than the size l_{AB} of block C, we can expresse $M^i_{\alpha_A\alpha_B}$ finitely. Just consider the decomposition into the three blocks A,B and C shifted by l_{AB} to the right or left. Assuming that the correlation between block A and B still vanishes over the distance l_{AB}, we just showed that M^i only depends on a finite number of sites in block $A(B)$ for a shift to the right(left) [11].
Therefore the correlation lenght of an infinite system seems to be a good criterion to determine is representability as a MPS. Starting with a finite translation invariant MPS (unit cell size one) with N sites the correlation $\langle \hat{O}_i \hat{O}_{i+r} \rangle$ between two site operators $\hat{O}_i$ and $\hat{O}_j$

$$\langle \hat{O}_i \hat{O}_{i+r} \rangle = \frac{Tr\left[E_1 ... E_1 E_{\hat{O}_i} E_1 ... E_1 E_{\hat{O}_{i+r}} E_1 ... E_1\right]}{Tr\left[E_1 ... E_1\right]}, \tag{68}$$

is obtained by a trace over a product of N transfer matrices. Exploiting the equality of the trace under cyclic permutations $Tr\left[ABC\right] = Tr\left[CAB\right] = Tr\left[BCA\right]$, the latter expression can be compressed as

$$= \frac{Tr\left[E_{\hat{O}_i} E_1^{r-1} E_{\hat{O}_{i+r}} E_1^{N-r-1}\right]}{Tr\left[E_1^N\right]}, \tag{69}$$

by merging the identity transfer matrices E_1 at the ends of the system. As previously done for the calculation of a site operator expectation value, the identity transfer matrix can be decomposed in its corresponding eigenvectors. Simplifying the study to an infinite system, the identity transfer matrices, to the power N, can be exchanged

$$\lim_{N\to\infty} \langle \hat{O}_i \hat{O}_{i+r} \rangle = \frac{Tr\left[E_{\hat{O}_i} E_1^{r-1} E_{\hat{O}_{i+r}} \lambda_1^{N-r-1} |R_1\rangle \langle L_1|\right]}{\lambda_1^N}. \tag{70}$$

Moreover, focusing on long range order $r \gg 1$, the product of the identity transfer matrices between the two site operators can be approximated by expansion up to the μ degenerate second eigenvalues of E_1

$$E_1^x \sim \lambda_1^x \left(|R_1\rangle \langle L_1| + \sum_{i=2}^{\mu} \left(\frac{\lambda_2}{\lambda_1}\right)^x |R_i\rangle \langle L_i| \right), \tag{71}$$

[8] Proof of this claim: [5, 16]

such that the correlation between the two site operators can be simply expressed by

$$\lim_{\substack{N\to\infty \\ r\gg 1}} \langle \hat{O}_i \hat{O}_{i+r} \rangle = \langle \hat{O}_i \rangle \langle O_{i+r} \rangle + \left(\frac{\lambda_2}{\lambda_1}\right)^r \frac{\langle R_1 | E_{\hat{O}_i} | L_2 \rangle \langle R_2 | E_{\hat{O}_{i+r}} | L_1 \rangle}{\langle R_1 | L_1 \rangle}. \tag{72}$$

Considering the connected correlation $C(r) = \langle \hat{O}_i \hat{O}_{i+r} \rangle - \langle \hat{O}_i \rangle \langle O_{i+r} \rangle$, one finds a correlation length ϵ

$$C(r) \sim e^{-r/\epsilon} \quad \text{with} \quad \epsilon \coloneqq -1/log(|\lambda_2/\lambda_1|), \tag{73}$$

which stays finite as long as there is one non-degenerate highest eigenvalue λ_1. As stated formerly, it can be proven that in all gapped systems the correlation is decaying exponentially (also known as correlation clustering). Somehow not surprisingly, iMPS can merely represent systems which are most feasible for finite systems as well.
However, bear in mind that there are indeed states such as the previous example of the GHZ state (see sec. 2.3), which are long range correlated but still can be expressed as an iMPS. On the other hand, there are also systems with vanishing correlation that cannot be represented as a tensor product. A more suitable indication whether a state can be decomposed as an iMPS/MPS is the exponential decay of mutual information [17].

4. Matrix Product State Routines

4.1. Variational Ground State Search (vMPS/DMRG)

The Rayleigh-Ritz-variational principal states that the lowest expectation value to every self-adjoint operator, as quantum operators, serves as a lower bound for the expectation value of a trial state $|\Psi\rangle$. For the ground state energy E_0 of a generic system, this translates into

$$\frac{\langle\Psi|\hat{H}|\Psi\rangle}{\langle\Psi|\Psi\rangle} \geq E_0, \tag{74}$$

which consequently means that the ground state energy can be found by optimizing a set of parameters describing a trial state, such that the expectation value becomes minimal. If the trial state is expressed as a MPS, this ground state search is referred to as the variational Matrix Product State algorithm (short vMPS).
Imposing normalization on the trial state $|\Psi\rangle$ by a Lagrange multiplier, the ground state search

$$\underset{|\Psi\rangle_{MPS}}{min} \Big(\langle\Psi|\hat{H}|\Psi\rangle - \lambda\left(\langle\Psi|\Psi\rangle - 1\right)\Big), \tag{75}$$

is given by a global variation over all MPS parameters (entries of each tensor at all sites). The MPS can thus be seen as a variational ansatz. However, instead of solving this multi-linear optimization problem at once, it is highly advantageous, regarding computational efficiency, to split up the process. In order to do so, we optimize the parameters of a tensor of one site at a time, while keep all the other tensors fixed. This leads to a simple quadratic optimization problem

$$\underset{M_i}{min}\left(\bar{M}_i H[i]_{eff} M_i - \lambda\left(\bar{M}_i N[i] M_i - 1\right)\right), \tag{76}$$

which can be solved by searching for the extremum with respect to variations in $\bar{M}_i$

$$\frac{\partial}{\partial\bar{M}_i}\left(\bar{M}_i H[i]_{eff} M_i - \lambda\left(\bar{M}_i N[i] M_i - 1\right)\right) = 0, \tag{77}$$

where M_i are the elements of the tensor at site i. The hereby new defined effective hermitian matrices $(H[i]_{eff})_{(s_i' a_{i-1}' a_i')(s_i a_{i-1} a_i)}$ and $(N[i]_{eff})_{(s_i' a_{i-1}' a_i')(s_i a_{i-1} a_i)} = \left(\widetilde{N}[i]_{eff}\right)_{(a_{i-1}' a_i'),(a_{i-1} a_i)} \otimes \delta_{s_i' s_i}$ (see fig. 18), are obtained by reshaping the contraction of all indices in $\langle\Psi|\hat{H}|\Psi\rangle$ respectively $\langle\Psi|\Psi\rangle$ after removing the tensor ($\bar{M}[i]$ and $M[i]$) of site i. Since the optimization is conducted locally on one site after the other it is in general uncertain if the global minimum is reached. Regarding the case of a many body system, the proposed optimization routine does find the global minimum nontheless [11]. From expression (77), we obtain a simple general eigenvalue problem of the form

$$H[i]_{eff} M_i = \lambda N[i]_{eff} M_i, \tag{78}$$

where the elements of the tensor $(M_i)_{s_i \alpha_{i-1} \alpha_i}$ of site i can be seen as a $d \cdot D_\chi^2$ large vector acting on the matrices $H[i]_{eff}$ and $N[i]_{eff}$, respectively. The Lagrange multiplier λ corresponds hereby, to the eigenenergy. Even though the space over which we wish to find eigenvectors

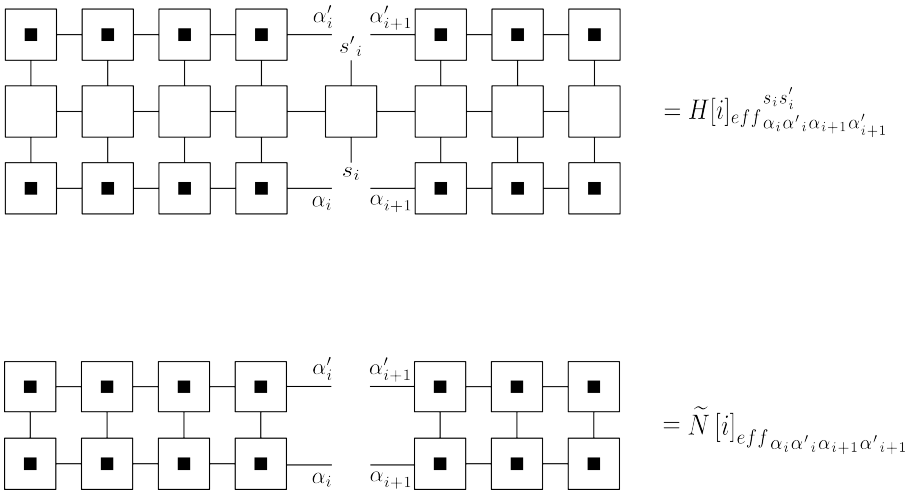

Figure 18: $H[i]_{eff}$ **and** $\widetilde{N}[i]_{eff}$**:** Construction of the effective matrices in the optimization protocol (77) at site i

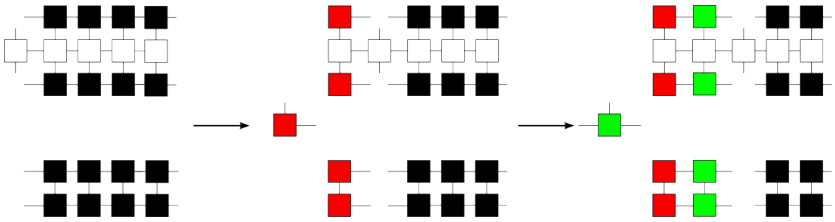

Figure 19: **update blocks:** After optimizing site 1 the red tensor $M'[1]^{s_1}_{\alpha_1}$ is retrieved. For the following optimization of site 2 $H[2]_{eff}$ and $N[2]_{eff}$ is formed with the already optimized $M'[1]^{s_1}_{\alpha_1}$ of site 1. In the same manner, for site 3 $H[3]_{eff}$ and $N[3]_{eff}$ are constructed with $M'[2]^{s_2}_{\alpha_1 \alpha_2}$ (green) and so forth.

is $d \cdot D^2_\chi$ large, we are fortunate to only be interested in the eigenvector corresponding to the lowest lying eigenenergy λ. Henceforth, aiming for solely the lowest eigenvalue we can accelerate numerics by the use of iterative eigensolver such as Lanczos or Jacobi-Davidson. The locally at site i optimized parameters $M'[i]_i$ of the variational MPS ansatz are then given by the eigenvector of the lowest eigenvalue of the generalized eigenvalue problem (78).
Considering the calculation of the effective matrices, it seems reasonable to start optimizing from one end of the system and sweep through it back and forth, sequentially updating $H[i]_{eff}$ and $\widetilde{N}[i]_{eff}$, respectively.
Rather than optimizing randomly one site after the other, we can simply attach the updated transfer operator elements to the pre existing $H[i]_{eff}$ and $N[i]_{eff}$ instead of calculating it each time from scratch (see fig. 19) and thereby, save computation time.[9]
Moreover, for open boundary conditions (obc) the generalized eigenvalue problem (78), can be brought into a simple one. In order to do so, at each optimization step at site i all MPS tensors to the left have to be in the left canonical form while all tensors to right are in the right canonical form. As a consequence, the computation of $\widetilde{N}[i]_{eff}$ is trivially equal to the identity. Since, tensors are optimized sequentially from first to last site and vice versa, bring-

[9] see Appendix D for pseudocode

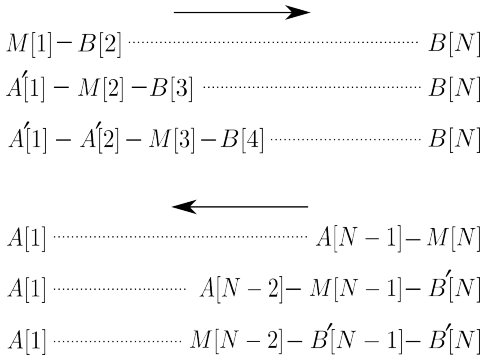

Figure 20: Canonical form during sweep: while going forth and back all tensor to the left and right of the to be optimized tensor $M[i]$ are in left respectively right canonical form. After the optimization the updated tensor $M'[i]$ is directly gauged into $A'[i]$ ($B'[i]$) for a sweep from $1 \rightarrow N$ site ($1 \leftarrow N$ site).

ing the MPS in the desired canonical form can be conducted with little numerical effort (see fig. 20).

In the case of periodic boundaries however, it is unfortunately impossible to transform the general eigenvalue problem into a simple one. Because $\widetilde{N}[i]_{eff}$ cannot become the identity, no matter the gauge of the trial MPS (see sec. 3.1). The viability of a generalized eigenvalue problem strongly depends on the conditioning of $\widetilde{N}[i]_{eff}$, yet with additional care most of such issues can be overcome [18]. Apart from the stiffness of the routine it is also computationally more demanding. The construction of $H[i]_{eff}$ comes due to the pbc with a computational complexity of $\mathcal{O}(D_\alpha^5 D_\beta^2 d^2)$ and additionally, since $\widetilde{N}[i]_{eff}$ is no longer trivial it has to be computed at each optimization (with $\mathcal{O}(d^2 D_\alpha^5)$ step, slowing down the vMPS for pbc significantly. Workarounds for a complexity similar to vMPS with obc $\mathcal{O}(d^2 D_\alpha^3)$ exist [**?**], and mainly work with introducing effective boundary vectors.

Nonetheless, the scaling for constructing the effective matrices $H[i]_{eff}$ and $N[i]_{eff}$, in the presented routine most operations are carried out during the sparse eigensolver (e.g. Lanczos), which are mainly matrix multiplication of $H[i]_{eff}$ with the vector M_i. One of these multiplication comes with a numerical cost of $\mathcal{O}(D^4 d^2)$ such that the whole optimization procedure is governed by an overall computation time of $\mathcal{O}(D^4 d^2) \cdot N_{sites} \cdot N_{sweeps} \cdot N_{matrixmul.}$.

Error Analysis:

As denoted, the vMPS ground state search is an optimization of the entries of a trial MPS and subsequently, it is in principal a variational search in a Hilbert space subspace, which states represented as MPS have the same bond dimension as the trial state.

How close the actual ground state is reached thus depends strongly on the bond dimension of the actual ground state and whether it lies in the scope of the subspace or not. Consequently, it is desirable to choose the subspace as large as possible in such manner that it covers most of the entire Hilbert space. On the other hand the ground state search is restricted by the numerical costs and therefore, becomes infeasible for large bond dimensions. This tradeoff can partly be overcome by dynamically increasing the bond dimension. Consider starting with a

trial MPS of low bond dimension, such that the algorithm is fast but the trial MPS is lacking parameters to fully represent the ground state. After several sweeps and/or observation of convergence of the eigenenergy, additional free parameters in form of an increase in the bond dimension (by adding rows and columns of zeros to each matrix $M[i]^{s_i}$) are introduced, hopefully allowing the trial state to reach the actual ground state closer.
However, in the case our system is characterized as gapped and therefore, the ground state is represented by small bond dimension. This trade off between computation time and accuracy is fixed and high precisions can be achieved. Note that this does not mean that it is in principal impossible to find ground states or make estimates about the ground state behaviour in gapless systems (see sec.5.1.1).
To exclude large errors and to have an estimate of the quality of the ground state, it is advisable to counter check all ground state results with another run conducted with larger bond dimensions. Eventually, in hope to observe a stable result rather than a drift off in the eigenenergy. A good measure of the convergence of the latter described scheme, is either directly given by the eigenenergy or by the variance

$$var(\hat{H}) = \langle\Psi|\hat{H}^2|\Psi\rangle - \langle\Psi|\hat{H}|\Psi\rangle^2, \tag{79}$$

with which the quality of the eigenvector as well as possible degeneracy, can be quantified.

Connection to NRG and DMRG:
Apart from, the variational picture presented so far, there is an accompanying physical interpretation of the scheme, which unlike MPS does not originates in quantum information but rather in renormalization. To be precise, the vMPS routine is equivalent to the Density Matrix Renormalization Group (DMRG) [12], an improvement of Wilson's Numerical Renormalization Group (NRG) [19].
Starting in chronological order, NRG was first introduced in 1975 by Wilson to compute the low energy spectrum of spin chains. Motivated by the assumption that low-energy states contribute the most to the low-energy behaviour of a enlarged system. The basic idea is relatively simple, we start with a small system of initially n sites $\hat{\mathcal{H}}_n$ spanned by $\{|\Phi[n]_\alpha\rangle\}_{\alpha=1,..,m}$, which is completely exact diagonalizable. Second, the system is enlarged by adding an additional local Hilbert space $\hat{h}_{n+1}$ spanned by $\{|s_i\rangle\}_{i=1,..,d}$ to the pre-existing one. Proceeding in this manner and adding site after site, the system $\hat{\mathcal{H}}_n$ quickly becomes too large for exact numerics, luckily though the only interest lies in the low energy physics therefore, not all eigenstates are equally important. Consequently, after every enlargement of the system, the m lowest energy eigenstates are calculated in order to project $\hat{\mathcal{H}}_n \otimes \hat{h}_{n+1}$ into the according low energy subspace

$$\hat{\mathcal{H}}_{n+1} = \hat{O}\hat{\mathcal{H}}_n\hat{O}^\dagger, \tag{80}$$

where the rows of $\hat{O}$ are exactly the low energy eigenstates. In this manner more and more sites can be added while keeping the effective Hilbert space, describing low energies, limited. NRG has been proven to be very powerfull in the sudies of impurity systems, where the coupling to a bath is discretized into a semi infinite spin chain with exponentially decreasing tight

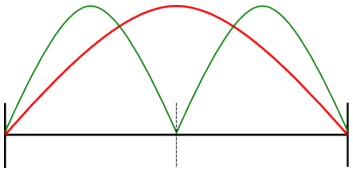

Figure 21: Ground state: Gloabl system of a particle in a box described by the first exitation of a string (red). Trying to build up solution by attaching solution of subplocks leads to an highly exited state of the global system (green).

binding couplings [20]. However NRG becomes very inaccurate for the usual tight binding model without an exponential decrease of couplings. The reason for the poor performance in strongly correlated systems is that NRG is deficient on the global picture. Consider a particle in a box (see figure 21). Its ground state is given by a string excitation spanned in the box. Now let us assume that we want to calculate the ground state of the box by splitting it in half (dashed line) and proceed with one single NRG step. The ground state of the initial block (with open boundary conditions to the right) is the same as the global solution with double periodicity. However constructing the enlarged block out of the low energy spectrum of the initial block, is an insufficient choice since it would almost take all the excited harmonics of the inital block to faithfully represent the global optimum [21]. White solved this issue in 1992 by introducing the Density Matrix Renormalitzation Group (DMRG) [12], which latest interpretation is known as the vMPS. Instead of just building up the system from the left leaving out any feedback from unreached sites to the current system, he incorporated the global view. Let us briefly compare the two, to sort out the difference more clearly. Note that in fact the NRG scheme might as well be expressed as an MPS

$$|\Phi[n]_{\alpha_{n+1}}\rangle = \sum_{s_i}\sum_{\alpha_n} P[n]^{s_i}_{\alpha_{n+1}\alpha_n}\,|\Phi[n-1]_{\alpha_n}\rangle \otimes |s_i\rangle\,, \tag{81}$$

where $P[n]^{s_i}_{\alpha_{n+1}\alpha_n}$ incorporates the basis transformation and truncation to the lower m eigenstates of the system.[10] It is important to point out that in this MPS description, other than the previously introduced one (as used in vMPS), reduction of the representation originates from neglection of higher energy scales rather than optimizing the preservation of entanglement. The effective Hamiltonian in the renormalized basis in a NRG scheme given after n steps thus, can be written as

$$\hat{\mathcal{H}}^n_{\alpha\alpha'} = \langle\Phi[n]_{\alpha_{n+1}}|\hat{\mathcal{H}}^n|\Phi[n]_{\alpha'_{n+1}}\rangle\,, \tag{82}$$

which is diagonalized in the following step to obtain the new reduced basis for $P[n+1]^{s_i}_{\alpha_{n+2}\alpha_{n+1}}$. Accordingly, the effective Hamiltonian in a vMPS sweep at site i

$$(H[i]_{eff})_{(s'_i a'_{i-1} a'_i),(s_i a_{i-1} a_i)}\,, \tag{83}$$

together with the fig. 18 reveals the missing link of NRG. It fails to incorporate all sites to its right, which is acceptable for impurity problems where the energy scale drops off but

[10] In fact there exist reformulation of NRG as vNRG incorporating feedback from lower to higher energy scale improving results for impurity systems even further [22].

eventually, it renders unsuitable for constant couplings, which stands in complete contrast to vMPS.

So why the name Density Matrix Renormalization Group? To be short and on the point, the variational search space of the trial MPS is in principal a renormalization of the density operator. As pointed out, the Schmidt coefficients of a state and the dimensionality of a Matrix in the MPS-representation are related (see sec. 2.3). Moreover, the Schmidt coefficients are in a one to one correspondence to the weight of a density matrix at the according cut $\rho_{ii'} = \delta_{ii'}\lambda_i^*\lambda_{i'}$. Neglecting entanglement between a bipartition is therefore, equivalent to neglecting states contributing the least to the density matrix of the global state the system is in. However we are not interested in any state but the ground state[11], assuming orthogonality of the trial state, the variational optimization procedure can be seen as solving for the local minimum

$$\frac{\partial Tr\left[\hat{\rho}\hat{\mathcal{H}}\right]}{\partial M^*[i]} = 0 \tag{84}$$

of the density operator, which eventually, after several sweeps, ends up in the ground state.

4.2. Time Evolution (TEBD, iTEBD)

Besides the calculation of ground state energies, MPS allows highly efficient numerics for short range time evolution. In other words, we would like to apply unitary time evolution to an arbitrary MPS

$$U(t,t_0)\left|\Psi(t_0)\right\rangle = e^{-i\hat{H}(t-t_0)}\left|\Psi(t_0)\right\rangle. \tag{85}$$

Even though this might seem as a simple task for small enough systems such that calculating the exponent of $\hat{H}$ sets no restriction, it becomes instantly impractical for bigger systems. A possible workaround is decomposing the time evolution operator such that it can be expressed as a chain application of a feasible small operator $U(t-t_0) = \left(\widetilde{U}(\Delta t)\right)^n$ with $\Delta t = \frac{t-t_0}{n}$. For simplification, in the following the Hamiltonian is assumed to have at most nearest neighbour terms

$$\hat{H} = \sum_i^N \hat{h}_{i,i+1}. \tag{86}$$

Unfortunately, in most cases, even and odd nearest neighbour terms do not commute

$$e^{-i\sum_i^N \hat{h}_{i,i+1}t} \neq e^{-i\sum_{i\ odd}^N \hat{h}_{i,i+1}t}e^{-i\sum_{i\ even}^N \hat{h}_{i,i+1}t} \quad \text{if} \quad \left[\hat{h}_{even},\hat{h}_{odd}\right] \neq 0, \tag{87}$$

such that for further decompositions, approximations are inevitable.

Consider two operators $\hat{A}$ and $\hat{B}$ which do not commute. From Baker-Campbell-Hausdorff formula it follows that

$$e^{\hat{A}t}e^{\hat{B}t} = e^{(\hat{A}+\hat{B})t+\left[\hat{A},\hat{B}\right]\frac{t^2}{2}+\mathcal{O}(t^3)}, \tag{88}$$

In effect, regarding our time evolution, the nearest neighbour time evolution operator can, in principal, be split up with an error of $\mathcal{O}(t^2)$. To suppress this error further , we take the n-th

[11] other than in NRG, where the interest lies in the low energy spectrum

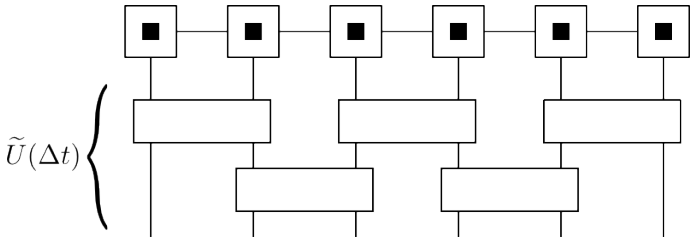

Figure 22: Applying $\widetilde{U}(\Delta t)$: evolution by one time step Δt

root of $e^{At}e^{Bt}$ by replacing t with $\Delta t = \frac{t}{n}$. The full expression

$$e^{\hat{A}t}e^{\hat{B}t} = \left(e^{\hat{A}\frac{t}{n}}e^{\hat{B}\frac{t}{n}}\right)^n = \left(e^{(\hat{A}+\hat{B})\frac{t}{n}} + \mathcal{O}\left(\frac{t^2}{n^2}\right)\right)^n \Rightarrow e^{(\hat{A}+\hat{B})t} = \left(e^{\hat{A}\Delta t}e^{\hat{B}\Delta t}\right)^n + \mathcal{O}\left(\Delta t^2\right), \tag{89}$$

then comes with an error of $\mathcal{O}(\Delta t)^2$. This type of decomposition is widely known as the Lie-Trotter-Suzuki Decomposition [23]. Consequently, the time evolution operator of our interest can be obtained by applying

$$\widetilde{U}(\Delta t) = \prod_{i\in even} e^{-i\hat{h}_{i,i+1}\Delta t} \prod_{i\in odd} e^{-i\hat{h}_{i,i+1}\Delta t} = e^{-i\sum_{i\in odd}\hat{h}_{i,i+1}\Delta t}e^{-i\sum_{i\in even}\hat{h}_{i,i+1}\Delta t}, \tag{90}$$

n times in a row. Instead of exponentiating one huge matrix $\hat{H}$, the task is reduced to smaller matrices $\hat{h}$. The resulting operator for site i, $\widetilde{U}(\Delta t)_i = e^{-i\hat{h}_{i,i+1}\Delta t}$ is an operator acting only on two sites and is referred to as bond operator. A full time step Δt can be achieved by first sequentially (going from site 1 to N) applying all odd bond operations and then in the same manner (going from first to last site) evolve the even bonds (see fig. 23). As mentioned in section 3, applying a two site operator as a bond operation, will eventually destroy the decomposition of the MPS. Thus, after each applied bond operator, the MPS has to be brought back into its original shape. Let us go through the evolution of one bond step by step (see fig. 23). We assume the MPS to be in Vidal's mixed canonical notation (see sec. 2.2). Before applying the bond operator, contract all tensors

$$M^{s_i s_{i+1}}_{\alpha_{i-1}\alpha_{i+1}} = \lambda[i-1]_{\alpha_{i-1}\alpha_{i-1}}\Gamma[i]^{s_i}_{\alpha_{i-1}\alpha_i}\lambda[i]_{\alpha_i\alpha_i}\Gamma[i+1]^{s_{i+1}}_{\alpha_i\alpha_{i+1}}\lambda[i+1]_{\alpha_{i+1}\alpha_{i+1}}, \tag{91}$$

belonging to the to be evolved bond. Next apply the bond operator (i) which leads to

$$M'^{s_i' s_{i+1}'}_{\alpha_{i-1}\alpha_{i+1}} = \sum_{s_i s_{i+1}} U^{s_i' s_{i+1}' s_i s_{i+1}} M^{s_i s_{i+1}}_{\alpha_{i-1}\alpha_{i+1}}, \tag{92}$$

a rank 4 tensor with two physical indices (legs). To retrieve an expression of the same form, we started with (91), the rank 4 tensor is shaped into a matrix $M_{(s_i\alpha_{i-1}),(s_{i+1}\alpha_{i+1})}$ which in the next step, (ii) is singular value decomposed (SVD) to

$$M'^{s_i' s_{i+1}'}_{\alpha_{i-1}\alpha_{i+1}} = U_{(s_i\alpha_{i-1}),\alpha_i}\lambda_{\alpha_i}(V^\dagger)_{\alpha_i,(s_{i+1}\alpha_{i+1})}. \tag{93}$$

As the entanglement between two sites sharing a bond usually grows by application of an interaction, such as the bond operator, the amount of non-singular singular values (Schmidt

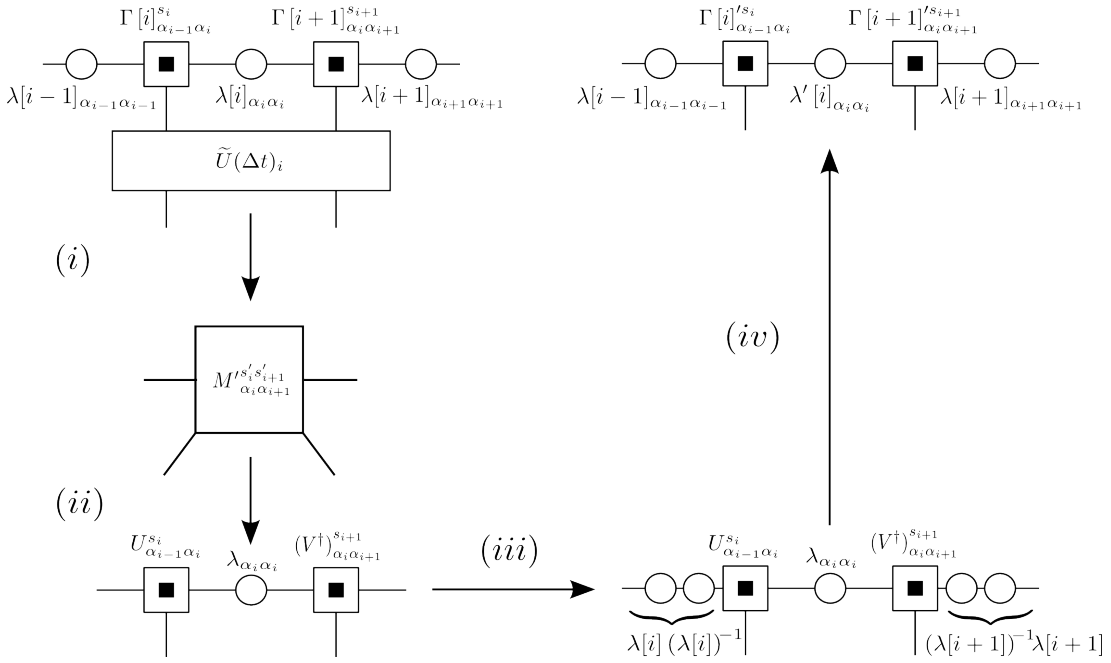

Figure 23: TEBD: scheme of a single bond evolution in the TEBD algorithm.

coefficients)[12] $D_{\alpha_i} = dim(\lambda_{\alpha_i})$ will grow to unmanageable size. However, not all of the newly established correlations are equally important. Therefore, as indicated in section 2.3 it is possible to truncate the dimension D_{α_i} by disregarding smaller singular values. The truncated state $|\widetilde{\Psi}\rangle$ hereby, as mentioned earlier in equation (38), minimizes the distance to the true state $|\Psi\rangle$ (in the two norm). The corresponding error ϵ_{α_i}, by disregarding the $D_{\alpha_i} - D_{trunc.}$ smallest singular values, is given by

$$1 - \sum_{\alpha_i}^{D_{trunc.}} (\lambda_{\alpha_i})^2 = \epsilon_{\alpha_i} \tag{94}$$

which is the trace difference of the reduced density (the disregarded probability) keeping the $D_{trunc.}$ highest eigenvalues. The still missing singular values are inserted by identities $1 = \lambda[i-1]\,(\lambda[i-1])^{-1}$ and $1 = (\lambda[i+1])^{-1}\,\lambda[i+1]$ (step (iii)) respectively, such that the time evolved tensors $\Gamma'[i]$, $\Gamma'[i+1]$ and $\lambda'[i]$ can be read off

$$M'^{s'_i s'_{i+1}}_{\alpha_{i-1}\alpha_{i+1}} = \lambda[i-1]_{\alpha_{i-1}\alpha_{i-1}} \underbrace{\left(\lambda[i-1]_{\alpha_{i-1}\alpha_{i-1}}\right)^{-1} U^{s_i}_{\alpha_{i-1},\alpha_i}}_{=\Gamma'^{s_i}_{\alpha_{i-1},\alpha_i}} \lambda'_{\alpha_i\alpha_i} \underbrace{(V^\dagger)^{s_{i+1}}_{\alpha_i,\alpha_{i+1}} \left(\lambda[i+1]_{\alpha_{i+1}\alpha_{i+1}}\right)^{-1}}_{=\Gamma'^{s_{i+1}}_{\alpha_{i+1}\alpha_{i+1}}} \lambda[i+1]_{\alpha_{i+1}\alpha_{i+1}}. \tag{95}$$

Proceeding in this fashion, the from of the decomposition of the MPS is unchanged and the next odd or even bond can be evolved by contracting the required tensors (as in equation (91)) to shape $M'^{s'_{i+2}s'_{i+3}}_{\alpha_{i+1}\alpha_{i+3}}$.

Imaginary Time Evolution:

Besides real time evolution, TEBD can also be used to find ground states of gapped systems.

[12] see Appendix A

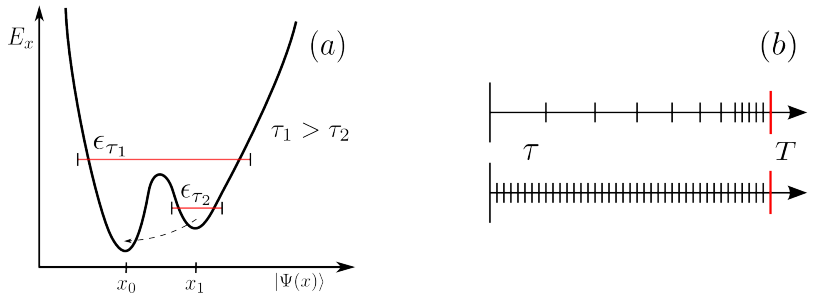

Figure 24: **Time steps:** a) eigenenergy E_x depending on position x. and ϵ_{τ_2} represent trotter errors. Assume that after a first time step with trotter error ϵ_{τ_1}, the imaginary TEBD process ends up in a state located in the valley around the local minimal x_1. Reducing τ_1 to τ_2 the new trotter error ϵ_{τ_2} might not overreach the potential barrier to the global minima x_0 such that the process is trapped. Note that this does not mean the state will not eventually (after an infeasible time) end up in x_0, since all excitations are still damped. b) time steps to reach a final time T at which all contributions from excitations are sufficiently small. The lower sizing as depicted needs far more steps and therefore, computational time than the upper process.

The way to do so is by imaginary time evolution

$$t \to -i\tau, \tag{96}$$

which transforms the unitary time evolution operator into the non-unitary imaginary time evolution operator $U(\tau) = e^{-\tau \hat{H}}$. Assuming a random state $|\Phi\rangle$ which has some non-vanishing overlap with the ground state

$$\langle \Psi_0 | \Phi \rangle \neq 0 \quad \text{with} \quad \hat{H} = \sum_i E_i \, |\Psi_i\rangle \langle \Psi_i| \, ; \quad E_0 < E_1 \leq E_2 ... \leq E_{dim(\hat{H})}, \tag{97}$$

the action of $e^{-\tau \hat{H}}$ is projecting out all contributions from excitations

$$e^{-\tau \hat{H}} \, |\Phi\rangle = \underbrace{e^{-\tau(E_0 - E_0)}}_{=1} \cdot \sum_i c_i e^{-\tau E_i} \, |\Psi_i\rangle = c_0 e^{-\tau E_0} \, |\Psi_0\rangle + e^{-\tau E_0} \sum_i c_i e^{-\tau(E_i - E_0)} \, |\Psi_i\rangle \, . \tag{98}$$

Note that this method highly depends on distinct ground states, such that on large gap-less systems it is almost certain to fail. Moreover, due to the necessary discretization of the imaginary time evolution, the algorithm has the tendency to get stuck in local minima. In principal we would like to choose τ as big as possible to damp all excitation, the trade off though is the trotter error $\mathcal{O}(\Delta t^2)$. Thus, an iterative application of $e^{-\tau \hat{H}}$ with a reasonable large enough τ would leave the result with a rather large error. By choosing a small τ, we manage a vanishing error for the later time steps. On the other hand, excitations are rarely projected out such that the process after a feasible computation time might still have contributions besides the desired ground state one. Concluding, the process might get trapped, never reaching the ground state (see fig. 24). A simple workaround is lowering τ, depending on the convergence of the trial states energy, such that if the energy is not decreasing any longer it is assumed to be due to the trotter error.

Error Analysis:
For the real time evolution there are two sources of errors, both already mentioned in the general description above. The first error is due to the Trotter decomposition of the time evolution operator, which is mentioned in above with the order of $\mathcal{O}(\Delta t^2)$. This error can be decreased by taking higher orders of the Trotter decomposition into account, for a p-th Trotter decomposition, after $n = \frac{t}{\Delta t}$ time steps, follows an overall error of $\mathcal{O}(\Delta t^p \cdot t)$. The second error comes from the necessary truncation and is specific to the system at hand. The reason for the entanglement growth of a generic system is explained best by looking at a simple exampl, for instance a global quench of a transverse Ising chain (see Appendix C). Let us assume the system of size L is at $t = 0$ in a product state of all spins down $|\Psi(t=0)\rangle = \prod_i^L \otimes |\downarrow\rangle_i$ and evolves for all time $t > 0$ under the Hamiltonian

$$\hat{\mathcal{H}} = -J \sum_i \hat{\sigma}_i^x \hat{\sigma}_{i+1}^x - B \sum_i \hat{\sigma}_i^z. \tag{99}$$

Following the arguments in [24], we can say that the initial state under the evolution of the quenched Hamiltonian acts as a source for pairs of entangled quasiparticles with opposit momentum at each site. Thinking of the system being bipartite in the middle (see figure 25), we can explain the growth of entanglement between the two halfs of the system by the opposing movement of the constituents of the entangled pairs. Since as soon as a quasiparticle crosses from one half to the other while its entangled partner remains, the entanglement between both halfs increased. The velocity of the quasiparticles is hereby essential since it is in a one to one correspondense to the growth rate. To illustrate this a bit have a look at figure 25 b) where TEBD results for the half length entanglement entropy S_{vN} for different chain length of the above model are plotted. The growth of entanglement is almost linear until it peaks where it starts to decreas. As already mentioned the linear increase should be in correspondence to the velocity of the quasiparticles. Let us consider only the fastest quasiparticles $max(v_k)$ obtained by $\frac{\partial v_k}{\partial k} \stackrel{!}{=} 0$ with $v_k = \frac{\mathrm{d}\epsilon_k}{\mathrm{d}k}$,[13] which for $B \geq J$ yields $max(v_k) = 2J$. Hence, the time a fastest quasiparticle would need to cross the middle of the system starting from one edge is given by $T = \frac{N}{2 \cdot v_{max}}$. Tracking the end of the linear slope (grey vertical lines in fig. 25) and compare it with the analytic result, we find that for $N = 10, 15$ and a bond dimension of $D_\alpha = 60$ the time T matches the numerical results (except for $N = 20$). Thus it seems that the growth of entanglement is mainly gorverned by the fastest moving quasiparticles and more importantly, it is bounded. This bound is referred to as the Lieb-Robinson bound [25] and is far more general than our simple example. In general it states that apart of relativistic thoughts a quantum system still possess an upper non-universal limit in the speed of information (entanglement). This limit can be an indication of systems worth studying with TEBD. In a later example (see section 5.3) we will actually see a model where this bond is even stronger and information grows logarithmically.

Note that for a bond dimension of $D_\alpha = 60$ we actually hope that the evolution for $N = 10$

[13] for the dispersion relation ϵ_k see Appendix C

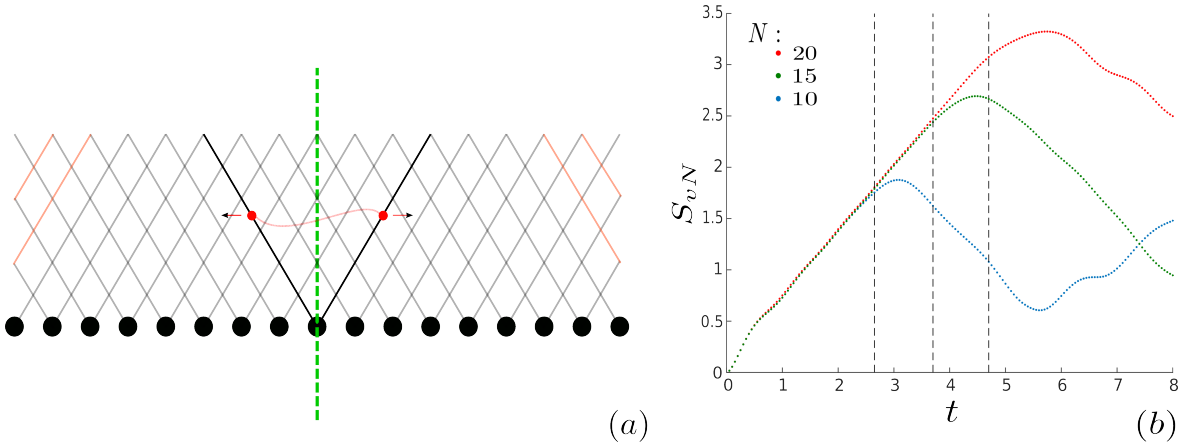

Figure 25: Lieb Robinson: a) cartoon picture of entangled quasiparticles moving in opposit direction and thus leading to entanglement growth between the green cut of the system. b) Entanglement growth in a global quenched transverse Ising model ($B = 1.0$, $J = 1.0$) obtained by TEBD for different chain lengths N with $max(D_\alpha) = 60$. Black dashed line corresponds to the time needed for the fastest quasiparticle to travel half the chain, see main text. (for ED results see [26]).

(Hilbert spaces needs $D_\alpha = 2^5$ for full representation) is up to the Trotter error exact, since the evolution goes without any truncation. For $N = 15$ the truncation from $D_\alpha = 2^7$ to 60 seems to have little effects. However for $N = 20$ sites which correspondse to $D_\alpha = 2^{10}$ for the full representation our choosen maximal bond dimension of 60 is far off, and as we can see the linear growth stops before the analytic estimated one ($T_{20} = 5$). This illustrates the unpreventable error due to truncation of entanglement.

infinite TEBD (iTEBD):

In the upcoming section 5.2 we will make use of the infinite TEBD which is a adapted version of TEBD suited for "infinite" systems with translation invariance [27]. The changes to the previous discussed TEBD routine are very subtle, such that the causes for possible inaccuracies, discussed in the previous paragraph, persist.

The starting point of the routine is an infinite MPS for translation invariant systems, which as discussed in section 3.2 can be thought of as stringing together the unit cell of the system (ensuring translation invariance) infinitely many times. Time evolution of the iMPS thus boils down to evolve only one of its single constituents, one unit cell. Since the evolved unit cell represents the whole time evolved "infinite" system. Let us for simplification consider a two site translation invariant system. The unit cell of the infinite system can thus be described by two tensors $\Gamma[1]$, $\Gamma[2]$ and their Schmidt coefficients $\lambda[1]$, $\lambda[2]$ (see blue frame in fig. 26 a)). Proceeding with the iTEBD routine by evolving our two site unit cell:

- we first evolve the bond between $\Gamma[1]$ and $\Gamma[2]$ (inside the unit cell, see fig. 26 a))
- second evolve the bond between unit cells (between $\Gamma[2]$ and $\Gamma[1]$) by reordering the tensors (see fig. 26 b))

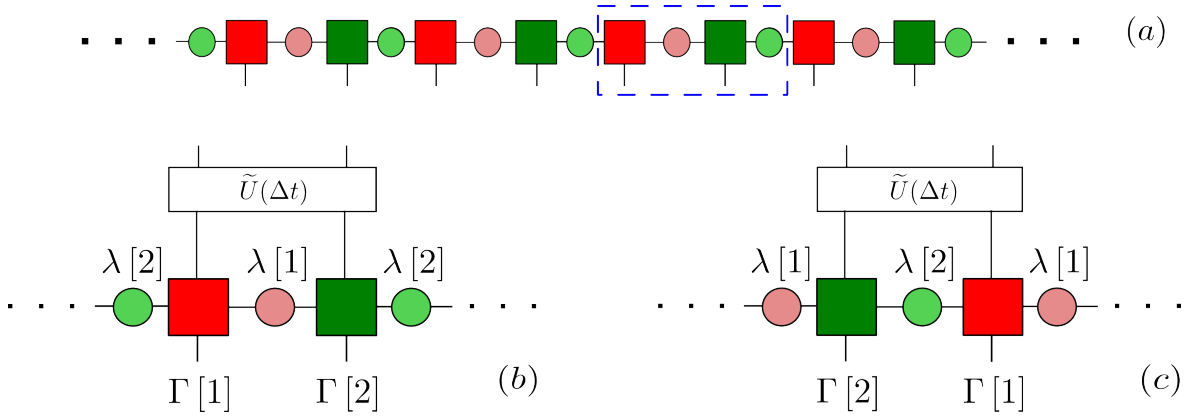

Figure 26: iTEBD: a) illustration of the two site translation invariant iMPS represented by stringing the blue framed tensors ifinite many times together b) evolution of the intra bond in the two site unit cell c) evolution of the inter bond between the unit cells

The evolution operator $\widetilde{U}(\Delta t)$ is hereby still a Trotter decomposition of the translation invariance Hamiltonian (90). Compared to the TEBD routine the only difference between the two is the second step, where the bond between the end and beginning of the unit cell is evolved. The generalization to bigger unit cells is therefore straight forward. First evolve the the unit cell as discussed for TEBD and afterwards the bond between the last and first site. Of course the evolution between unit cells (last and first site) can be directly incorporated in the unit cell evolution, saving a computational step.

4.3. Tangent Plane Methods (TDVP)

One of the conclusions of the previous section 4.2, is that for a generic system under unitary time evolution, the entanglement grows with time. The latter leads to the eventual necessity of truncating the bond dimension, since the state under evolution leaves the MPS representation feasible corner of the Hilbert space. Unfortunately, in general the truncation does not respect conservation laws (in particular, energy conservation) under time evolution. How can we avoid truncation in order to preserve symmetries? The goal is to time evolve a MPS while keeping its bond dimensions fixed and symmetries conserved. An abstraction of this problem is to restrict the time evolution of the full Hilbert space $\mathcal{H}$ governed by the time dependent Schrödinger equation

$$\left(i\frac{\mathrm{d}}{\mathrm{d}t} - \hat{\mathcal{H}}\right)|\Psi\rangle = 0, \tag{100}$$

to a manifold $\mathcal{M} \subset \mathcal{H}$ described by a set of parameters, $\{\mathbf{z}\}$

$$\mathcal{M} = \{|\Psi(\mathbf{z})\rangle\,, \mathbf{z} \in \mathbb{C}^n\}. \tag{101}$$

This type of problem is known as the Dirac-Frenkel time-dependent variatonal principle or in short TDVP [28, 29]. Note that the Schrödinger equation (TDSE) can be deduced from the

principal of least action $\delta\mathcal{S} = 0$ by variation of the action

$$\mathcal{S}\left[\Psi(t), \bar{\Psi}(t)\right] = \int_{t_1}^{t_2} \mathcal{L}\left[\Psi(t), \bar{\Psi}(t)\right] \mathrm{d}t, \tag{102}$$

where the Lagrangian $\mathcal{L}$, as it is easy to prove, is given by $\mathcal{L}\left[\Psi(t), \bar{\Psi}(t)\right] = \langle\Psi(t)|i\frac{\partial}{\partial t} - \hat{\mathcal{H}}|\Psi(t)\rangle$. In the same fashion, we can form a Lagrangian for states restricted to the manifold $\mathcal{M}$, written in terms of the parameter $\mathbf{z}$:

$$\mathcal{L}\left[\Psi(\bar{\mathbf{z}}), \bar{\Psi}(\mathbf{z})\right] = \frac{i}{2}\left(\langle\Psi(\bar{\mathbf{z}})|\dot{\Psi}(\mathbf{z})\rangle - \langle\dot{\Psi}(\bar{\mathbf{z}})|\Psi(\mathbf{z})\rangle\right) - \langle\Psi(\bar{\mathbf{z}})|\hat{\mathcal{H}}|\Psi(\mathbf{z})\rangle\,. \tag{103}$$

The Euler Lagrange equations $\dfrac{\mathcal{L}}{\partial\bar{z}^{\bar{i}}} - \dfrac{\partial}{\partial t}\dfrac{\partial\mathcal{L}}{\dot{\bar{z}}^{\bar{i}}} = 0$, lead to equations of motion describing the path of the parameters $\mathbf{z}(t)$ on the manifold $\mathcal{M}$ (see fig. 27)

$$i\underbrace{\langle\partial_{\bar{i}}\Psi(\bar{\mathbf{z}})|\partial_j\Psi(\mathbf{z})\rangle}_{=:\,G_{\bar{i}j}}\cdot\dot{z}^j - \langle\partial_{\bar{i}}\Psi|\hat{\mathcal{H}}|\Psi\rangle = 0. \tag{104}$$

The parameters $\mathbf{z}$ and $\bar{\mathbf{z}}$ are hereby treated as completely separated variables consequently, varying $\mathbf{z} \to \mathbf{z}+\delta\mathbf{z}$ corresponds to the equation of motion for $\dot{\bar{z}}^{\bar{j}}$. To find solutions to the latter equations, the inverse of $\langle\partial_{\bar{i}}\Psi(\bar{\mathbf{z}})|\partial_j\Psi(\mathbf{z})\rangle$[14]has to exist, in other words the vectors $\{|\partial_i\Psi(\mathbf{z})\rangle\}$ have to be linear independent. Let us proceed by assuming for now $G_{\bar{i}j}$ to be non-singular, such that we can derive the parameter e.q.o.m

$$\dot{z}^j = -iG^{j\bar{i}}\langle\partial_{\bar{i}}\Psi|\hat{\mathcal{H}}|\Psi\rangle \qquad \dot{\bar{z}}^{\bar{j}} = \; iG^{\bar{j}i}\langle\Psi|\hat{\mathcal{H}}|\partial_i\Psi\rangle\,, \tag{105}$$

with $G^{j\bar{i}}$ being the inverse of $G_{\bar{i}j}$. This equation has a strong resemblance to the pair of equations for the canonical coordinates in classical mechanics ($\dot{\mathbf{p}} = -\dfrac{\partial\mathcal{H}}{\partial\mathbf{q}}$, $\dot{\mathbf{q}} = \dfrac{\partial\mathcal{H}}{\partial\mathbf{p}}$). And in fact, as in the classical case, we can define a Poisson bracket for functions on the phase space $f(\mathbf{z}, \bar{\mathbf{z}})$, $g(\mathbf{z}, \bar{\mathbf{z}})$

$$\{f, g\} \coloneqq \left(\partial_i f\partial_{\bar{j}}g - \partial_i g\partial_{\bar{j}}f\right)G^{j\bar{i}}, \tag{106}$$

such that the e.q.o.m translate into

$$\dot{z}^j = i\{H, z^j\} \qquad \dot{\bar{z}}^{\bar{j}} = \; i\{H, \bar{z}^{\bar{j}}\}, \tag{107}$$

where $H(\mathbf{z}, \bar{\mathbf{z}}) = \langle\Psi(\bar{\mathbf{z}})|\hat{\mathcal{H}}|\Psi(\mathbf{z})\rangle$ is the Hamilton function. By a restriction of the action to a subset of the whole Hilbert space $\mathcal{H}$, we end up with the classical equations of motion for our parameters. Moreover, as the change in time of the parameters is governed by the Poisson bracket, so will the functions on the phase space. For simplicity, let us neglect the complex conjugate parameters $\bar{\mathbf{z}}$ for a moment and assume $\mathbf{z}$ is real. A function O to an operator $\hat{O}$ defined as its expectation value $O = \langle\Psi(\mathbf{z})|\hat{O}|\Psi(\mathbf{z})\rangle$ evolves in time as

$$\dot{\hat{O}} = i\{\hat{\mathcal{H}}, \hat{O}\}, \tag{108}$$

since $\{\hat{\mathcal{H}}, \hat{O}(z_i)\} = \{\hat{\mathcal{H}}, z_i\}\dfrac{\partial\hat{O}}{\partial z_i} = -i\dot{z}_i\dfrac{\hat{O}}{\partial z_i} = -i\dfrac{\hat{O}}{\partial t}$.

[14]following the supplementaries of [30] we introduce $\partial_i = \dfrac{\partial}{\partial z^i}$ and $\partial_{\bar{j}} = \dfrac{\partial}{\partial\bar{z}^{\bar{j}}}$ to ease the notation

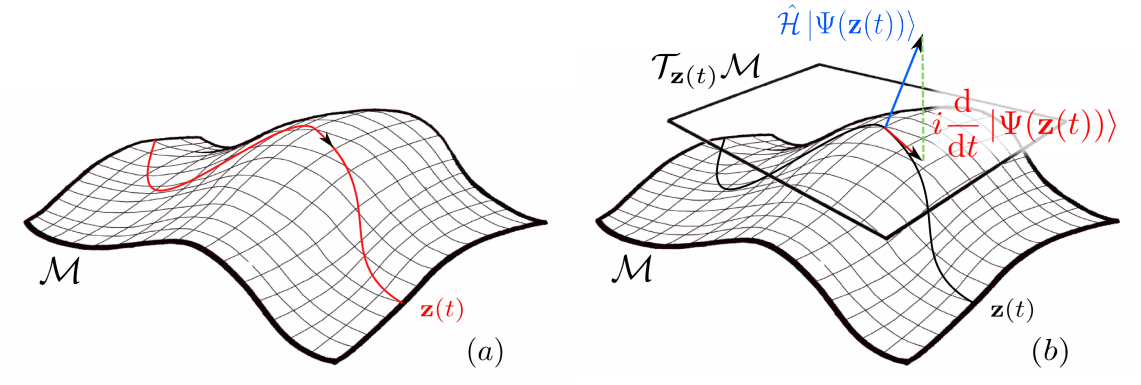

Figure 27: TDVP in $\mathcal{M}$: a) path $\mathbf{z}(t)$ of the TDVP, follows the tangent vectors constructed by orthogonal projecting the evolution of $\hat{\mathcal{H}}$ at each point onto the tangent plane b).

- **conservation of energy:** Note that the Poisson bracket is antisymmetric $\{f, g\} = -\{g, f\}$, as a direct consequence, we obtain energy conservation $\Rightarrow \{H, H\} = 0$
- **conservation of symmetries:** Generator of Lie-groups which are conserved in the Hilbert space evolution $\left[\hat{J}, \hat{\mathcal{H}}\right] = 0$ are as well conserved under the TDVP e.q.o.m as long as a state $|\Psi(\mathbf{z})\rangle$ under the to the generator $\hat{J}$ associated symmetry operation $\hat{U}(\epsilon) = exp(i\hat{J}\epsilon)$ does not leave the manifold $\hat{U}(\epsilon)\,|\Psi(\mathbf{z})\rangle \in \mathcal{M}$. For a discussion in depth, see supplementaries of [30].

Besides the derivation by variation of the action, the same equation can be obtained from a geometric approach. Consider figure 27 b) where at a point $\mathbf{z}(t)$, of the manifold the tangent plane is spanned by the directional derivatives of the parameters $span\left(\mathcal{T}_{\mathbf{z}(t)}\mathcal{M}\right) = \{|\partial_i \Psi(\mathbf{z}(t))\rangle\,, i \in \{1..n\}\}$. Evolution with $\hat{\mathcal{H}}\,|\Psi(\mathbf{z}(t))\rangle$, as depicted, would in general leave the manifold. The closest this evolution can be approximated in the manifold at point $\mathbf{z}(t)$ in z^j direction, is obtained by minimization of

$$\dot{z}^j_{ext.}(t) = \underset{\dot{z}^j(t)}{argmin}\left(|| \underbrace{i\dot{z}^j(t)\,|\partial_j \Psi\left(\mathbf{z}(t)\right)\rangle}_{=\frac{\mathrm{d}}{\mathrm{d}t}|\Psi(\mathbf{z}(t))\rangle} - \hat{\mathcal{H}}\,|\Psi(\mathbf{z}(t))\rangle\,||^2\right), \tag{109}$$

or, in other words, an orthogonal projection (measurement) of $\hat{\mathcal{H}}\,|\Psi(\mathbf{z}(t))\rangle$ on the tangent plane

$$\mathrm{P}_{\mathcal{T}_{\mathbf{z}}\mathcal{M}}\left(\bar{\mathbf{z}}, \mathbf{z}\right) = |\partial_j \Psi(\mathbf{z})\rangle\, G^{j\bar{i}}\, \langle \partial_{\bar{i}} \Psi(\bar{\mathbf{z}})|\,. \tag{110}$$

It is exactly this projection causing the indeterministic behaviour of the state $|\Psi(\mathbf{z})\rangle$ to collapse into a set of classical equation of motions. Let us return to opening of our discussion. We started with the Schrödinger equations and derived e.q.o.m for a set of canonical coordinates $\mathbf{z}$, $\bar{\mathbf{z}}$. However, the Schrödinger equation alone is not sufficient to describe quantum mechanics, an important detail which is completely ignored so far. To give the solutions of the TDSE a physical meaning, it has to obey Born's rule, being normalized at all time, such that it can be interpreted as the propagation of probabilities. For evolution under the

TDSE, the probability is conserved meaning that, if the initial state is normalized, it will preserve normalization at all time during the time evolution. Unfortunately, this is not the case for the projected evolution. The choice of trial states hence, has to be restricted to the ones preserving norm in the manifold evolution by default. To free the trial state from this restriction, the Lagrangien can be transformed

$$\mathcal{L}\left[\Psi(t), \bar{\Psi}(t)\right] \rightarrow \frac{\mathcal{L}\left[\Psi(t), \bar{\Psi}(t)\right]}{\langle\Psi(t)|\Psi(t)\rangle}, \tag{111}$$

such that, by variation of the action, norm preserving equations of motion are obtained (see supp. [30]). The derivation is rather direct, and leads to a modification of equation (104)

$$i\widetilde{G}_{\bar{i}j}\dot{z}_j = \frac{\langle\partial_{\bar{i}}\Psi(\bar{\mathbf{z}})|\hat{\mathcal{P}}_0\hat{\mathcal{H}}|\Psi(\mathbf{z})\rangle}{\langle\Psi(\bar{\mathbf{z}})|\Psi(\mathbf{z})\rangle} \quad \text{with} \quad \widetilde{G}_{\bar{i}j} = \frac{\langle\partial_{\bar{i}}\Psi(\bar{\mathbf{z}})|\hat{\mathcal{P}}_0|\partial_j\Psi(\mathbf{z})\rangle}{\langle\Psi(\bar{\mathbf{z}})|\Psi(\mathbf{z})\rangle}, \tag{112}$$

where the projector $\hat{\mathcal{P}}_0 = 1 - \frac{|\Psi(\mathbf{z})\rangle\langle\Psi(\bar{\mathbf{z}})|}{\langle\Psi(\bar{\mathbf{z}})|\Psi(\mathbf{z})\rangle}$, projects out all contributions along $|\Psi(\mathbf{z})\rangle$. This leads to the conclusion that phase and norm are preserved as long as the tangent plane is perpendicular to $|\Psi(\mathbf{z})\rangle$. The same constraint (though sufficient) on the trial state can be deduced from arguing that the total time derivative of the phase space distribution function $\rho(\bar{\mathbf{z}}, \mathbf{z}) = \langle\Psi(\bar{\mathbf{z}})|\hat{\rho}|\Psi(\mathbf{z})\rangle$ should vanish in order to ensure norm preservation of the evolution in the phase space

$$\frac{\mathrm{d}}{\mathrm{d}t}\rho(\bar{\mathbf{z}}, \mathbf{z}) = 2\left(\dot{\bar{z}}^i\langle\partial_i\Psi(\bar{\mathbf{z}})|\Psi(\mathbf{z})\rangle + \langle\Psi(\bar{\mathbf{z}})|\partial_i\Psi(\mathbf{z})\rangle\dot{z}^i\right) \stackrel{!}{=} 0. \tag{113}$$

Fortunately, in the case of using TDVP with MPS, the gauge freedom of the MPS representation allows to enforce norm preservation by ensuring orthogonality of $|\Psi(\mathbf{z})\rangle$ to the tangent plane $|\Psi(\mathbf{z})\rangle \perp \mathcal{T}_{\mathbf{z}}\mathcal{M}$.

Before adapting the discussed method in the MPS framework and explaining the role of the gauge, let us recapture. By orthogonal projecting the evolution of the full Hilbert space in the tangent plane, we derived equation of motions never leaving the initial manifold $\mathcal{M}$, and thus being represented by the same amount of parameters at all time. For clarification, this does not mean the evolution is faithful, represented by those parameters. The quality of a variational ansatz, as $|\Psi(\mathbf{z})\rangle$, strongly depends on the choice of its parameters. A good choice in general, is if they capture physical properties of the system they aim to describe.

In the case of a MPS, the representation of a state

$$|\Psi(\{A[i]\})\rangle = \sum_{\bar{s}} M[1]^{s_1}M[2]^{s_2}...M[n]^{s_n}\,|\bar{s}\rangle\,, \tag{114}$$

is a parametrization by the elements of each site tensor $A[i]$[15]. It is known from section 2.3 that this representation is faithful as long as the entanglement is bonded to a feasible amount. That being said, it is clear that TDVP will fail to reproduce exact results as soon as the bond dimension and with that the amount of parameters fails to incorporate the

[15] it can be shown that $\mathcal{M}_{MPS} = \{|\Psi(\{A[i]\})\rangle\}$ for fixed bond dimensions fulfils the manifold and the corresponding tangent plane axioms [31]

states entanglement, and to that extend TDVP performs as badly as TEBD. However, other than TEBD where the truncation maps the evolved state back to the feasible bond dimensions (amount of parameters), the TDVP projector preserves energy and symmetries of the system.

TDVP with MPS:
This section is intended to give conceptual insights into the gauge freedom of the tangent plane and the derivation of TDVP e.q.o.m for the MPS entries. For all, who are less concerned about technicalities this section might be skipped, even though the tangent plane of MPS is used in several other routines [32, 33] and seems to be an enriching concept. Before jumping to the generic case of a finite size MPS [34], where each site is parametrized by a different tensor $M[i]$, consider for simplicity a uniform infinite MPS (uMPS) [30]

$$|\Psi(M)\rangle = \sum_{\bar{s}} \bar{L} \left[\prod_{i\in\mathbb{Z}} M^{s_i} \right] \bar{R} \, |\bar{s}\rangle \,, \tag{115}$$

uniform in the sense that each site i is represented by the same matrices M^{s_i} such that the system is completely translation invariant. Without loss of generality, the boundary conditions, $\bar{L}$ and $\bar{R}$, are set to identity describing an open system. The evolution according to the TDVP thus, follows a path in the manifold parametrized by all elements of the tensor, $\mathcal{M} = \{|\Psi(M)\rangle_{MPS}, M \in \mathbb{C}^{d\times D_\alpha \times D_\alpha}\}$. Further, let us define a generic vector in the tangent plane $|\Phi(T;M)\rangle \in \mathcal{T}_M\mathcal{M}$ of $\mathcal{M}$ at point M as

$$|\Phi(T;M)\rangle \coloneqq \sum_i T^i \frac{\partial}{\partial M^i} |\Psi(M)\rangle \quad \text{with } i = \{n, s_n, \alpha_{prev.}, \alpha_{next}\}, \tag{116}$$

which in the composite basis reads as

$$\sum_i T^i \frac{\partial}{\partial M^i} |\Psi(M)\rangle = \sum_{n\in\mathbb{Z}} \sum_{\bar{s}} ...M^{s_{n-1}} T^{s_n} M^{s_{n+1}} ... \, |\bar{s}\rangle \,, \quad \text{with} \quad |\bar{s}\rangle = |...s_{n-1}s_n s_{n+1}...\rangle \,. \tag{117}$$

Two problems of the tangent plane $\mathcal{T}_M\mathcal{M}$ can be identified, the first more obvious one is that $A^i \, |\partial_i \Psi(M)\rangle \in \mathcal{T}_M\mathcal{M}$ is a valid tangent vector. This, as mentioned, allows the state to change its norm and phase. The second problem is the gauge freedom in the MPS representation $M^s \to XM^sX^{-1}$ with $X \in \mathbb{C}^{D_\alpha \times D_\alpha}$ (see sec. 2.5), which is inherited to the tangent plane. To understand why this is an issue, considering a one parameter gauge transformation $G(\epsilon) = exp(\epsilon X)$ the state should stay invariant due to small changes in ϵ

$$\frac{\mathrm{d}\,|\Psi(M(\epsilon))\rangle}{\mathrm{d}\epsilon} = \underbrace{\frac{\mathrm{d}M(\epsilon)^i}{\mathrm{d}\epsilon}}_{\coloneqq T_X^i} |\partial_i \Psi(M(\epsilon))\rangle = 0, \tag{118}$$

$$|\Phi\left(T_X;M\right)\rangle \coloneqq \frac{\mathrm{d}M(\epsilon)^i}{\mathrm{d}\epsilon} |\partial_i \Psi(M(\epsilon))\rangle$$

with T_X fulfilling $T_X^s = XM^s - M^sX + \mathcal{O}(\epsilon^2)$. This gauge freedom in the tangent plane causes trouble solving equation (104), where $G_{\bar{i}j}$ has to be inverted, since T_x^i is a null vector of the Gram matrix $G_{\bar{i}j}T_X^j = 0$. In other words, the tangent plane is over-complete and not

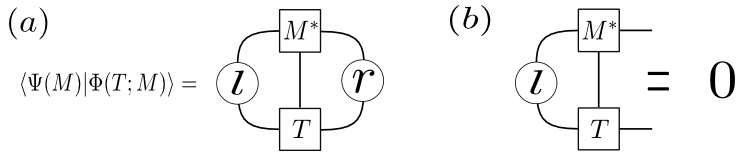

Figure 28: Overlap and Gauge: a) overlap of tangent vector with state from the manifold $\mathcal{M}$ b) left gauge fixing condition.

all vectors T^i are linearly independent ($T' = T + T_X$).
In order to determine the redundant degrees of freedom note that the invariance of the state $|\Psi(M(\epsilon))\rangle = |\Psi(M(\epsilon))\rangle + \epsilon\,|\Phi(T_X; M)\rangle$ leads to a constraint on the overlap (and eventually on T_X) $\langle\Psi(M)\rangle\,|\Phi(T_X; M) = 0$. To facilitate the calculation let us assume that the identity transfer matrix $E = \sum_i M^{s_i *} \otimes M^{s_i}$ (see section 3.1) of the uMPS has a non degenerate eigenvalue 1 with normalized ($Tr\,[lr] = 1$) right and left eigenvectors of full rank[16], denoted as l respectively r. Such that the calculation of the states expectation values and norm follows the outlines of an infinite MPS (see sec. 3.2). Proceeding with the evaluation of the condition above reveals that there are $D_\alpha^2 - 1$ independent ways for T_X to obey the constraint, since

$$\langle\Psi(M)\rangle\,|\Phi(T_X; M) = Tr\left[lE^M_{T_X} r\right] = 0 \qquad \text{with} \quad E^M_{T_X} \coloneqq \sum_s M^{s*} \otimes T^s_X \tag{119}$$

leads to

$$lE^M_{T_X} = \sum_{s=1}^{d} (M^s)^\dagger\, lT^s_X = \sum_{s=1}^{d} (M^s)^\dagger\, lXM^s - \underbrace{(M^s)^\dagger\, lM^s}_{=l} X = 0, \tag{120}$$

which only has one solution for $X = 1$. To eliminate these additional degrees of freedom of the tangent vectors the gauge has to be fixed. Imposing the gauge fixing condition

$$\sum_{s=1}^{d} (M^s)^\dagger\, lT^s = 0, \tag{121}$$

both drawbacks of the tangent plane are solved at once. First note that the overlap of (fig. 28)

$$\langle\Psi(M)|\Phi(T; M)\rangle = Tr\left[lE^M_T r\right] = 0 \qquad \text{with} \quad E^M_T \coloneqq \sum_s M^{s*} \otimes T^s \tag{122}$$

vanishes and hence, the tangent plane is orthogonal to $|\Psi(M)\rangle$. Second, it eliminates the $D_\alpha^2 - 1$ additional degree of freedom in T, such that the remaining tangent plane is of dimensionality $(d-1)D_\alpha^2$ and the inverse of $G_{i\bar{j}}$ is well behaved. For the constructions of a parametrization of T which fulfils the just formulated gauge fixing constraint, let us define the map $(L)_{\alpha'(d\alpha)} = (M^s)^\dagger l^{1/2}$, $L : dD_\alpha \to D$. The kernel of L is of dimension $D_\alpha(d-1)$ and spanned by the $D_\alpha(d-1)$ last columns of V, obtained from the non-reduced singular value decomposition of $L = USV^\dagger$. Note that besides, spanning the kernel of L, the columns of V (from now denoted as V_L), by construction, form an orthonormal basis $V_L^\dagger V_L = 1$. Transforming V_L from a matrix

[16] proof of these properties in [16]

of dimension $dD \times D(d-1)$ into a tensor V_L^s, a tangent vector fulfilling constraint (121) can be parametrized by

$$T^s(Z) = l^{-1/2} V_L^s Z r^{-1/2}, \tag{123}$$

where the only free parameters are the elements of the matrix Z with dimension $D(d-1) \times D$. Note that due to the orthonormality of V_L, the overlap of two tangent vectors reduces to

$$\langle \Phi(T(Z'); M) | \Phi(T(Z); M) \rangle = Tr \left[Z'^{\dagger} Z \right]. \tag{124}$$

Knowing the parametrization of the gauge fixed tangent plane we are now in the position to orthogonality project the evolution of the full Hilbert space $\hat{\mathcal{H}} |\Psi(M)\rangle$ onto the tangent plane by minimization of

$$\min_Z \left(|| \hat{\mathcal{H}} |\Psi(M)\rangle - |\Phi(Z; M)\rangle ||^2 \right). \tag{125}$$

Variations in $\bar{Z}$ lead to an extremum for the parameters Z given as

$$Z_{ext.} = \partial_{\bar{Z}} T(\bar{Z}) \partial_{\bar{T}} \langle \Phi(T(\bar{Z}); M) | \hat{\mathcal{H}} | \Psi(M) \rangle = \partial_{\bar{Z}} T(\bar{Z}) \partial_T \langle \Phi(T(\bar{Z}); M) | \hat{\mathcal{H}} | \Psi(M) \rangle, \tag{126}$$

such that the projected vector in the tangent plane can be written as $T^i(Z_{ext.}) |\partial_i \Psi(M)\rangle$. From the time evolution of the state $|\Psi(M)\rangle$

$$i \frac{\mathrm{d}}{\mathrm{d}t} |\Psi(M(t))\rangle = i \dot{M}^i |\partial_i \Psi(M(t))\rangle, \tag{127}$$

a comparison of the coefficient with $T^i(Z_{ext.}) |\partial_i \Psi(M)\rangle$ concludes to a solution of the TDSE in the tangent plane

$$\dot{M} = -iT(Z_{ext.}). \tag{128}$$

For real time evolution, these non-linear coupled differential equations can be solved with e.g. the Runge-Kutta integration scheme, while others as a simple Euler-step routine, do not respect the symplectic structure and are only appropriate for imaginary time evolution [30].

After being familiar with the general concepts and difficulties, let us now come to finite systems for which the formulation becomes less convenient. From the general from of a finite MPS (13), we deduce that a generic vector in the tangent plane $\mathcal{T}_{\{M\}}\mathcal{M}$ can be expressed as

$$T^i |\partial_i \Psi(\{M\})\rangle = \sum_{n=1}^{N} \sum_{s_n=1}^{d} M^{s_1}[1] ... T^{s_n}[n] ... M^{s_n}[N] |\bar{s}\rangle \quad \text{with } i = \{s_n, n, \alpha_{n-1}, \alpha_{n-}\}. \tag{129}$$

The issues of the tangent plane, namely overcompleteness and vialation of norm preservation, persist in the case of a generic finite size MPS. Even worse, unlike the former case, matrices $M^{s_n}[n]$ are site dependent, such that we have to impose site dependent gauge-fixing conditions

$$(M^{s_n})^{\dagger} l(n-1) T^{s_n}[n] = 0 \qquad \forall n \in \{1....N-1\}, \tag{130}$$

where $l(n-1) = l(n-2) E_1[n-1]$, to overcome the gauge freedom $M^{s_n}[n] \to X^{-1}[n-1] M^{s_n}[n] X[n]$. In principal, it is possible to reformulate the above approach for finite systems. However, the TDVP scheme presented so far acquires numerical frauds as it incorporates the

square root inverse of l and r. A recent reformulation for finite systems [34] allows an inverse free implementation of TDVP with strong resemblance to the vMPS routine, allowing a rather direct implementation (as part of this thesis). The general idea is, that it is in principal known how to avoid the necessity of $l(n)$ and $r(n)$ by bringing the state in mixed canonical form. Meaning, that all tensors of the MPS to the left of site n are in left canonical form and to the right, in right canonical form

$$|\Psi(\{M\}\rangle = \sum_{\bar{s}} A[1]^{s_1}...A[n-1]^{s_{n-1}}M[n]^{s_n}B[n+1]^{s_{n+1}}...B[N]^{s_N}\,|\bar{s}\rangle\,, \tag{131}$$

such that the expectation value of a site operator is trivially $\langle\hat{O}_i\rangle = Tr\left[E[i]_{\hat{O}_i}\right]$ (see section 3.1). The gauge freedom in the mixed canonical form, for the tangent plane, further translates into

$$T^{s_n}_{\{X\}}[n] = X[n-1]B^{s_n}[n] - A^{s_n}[n]X[n], \tag{132}$$

which can be fixed, as in the uMPS case, by imposing the gauge-fixing condition

$$(A^{s_n}[n])^\dagger \widetilde{T}^{s_n}[n] = 0 \qquad \forall n \in \{1....N-1\}. \tag{133}$$

Note, that $\widetilde{T}^{s_n}[n]_{\alpha_{n-1}\alpha_n}$ however, is not the same as T^i any longer, since tangent vectors are now represented in a different basis than the previous $\{|\partial_i\Psi(\{M\})\rangle\}$,

$$|\Theta(\{\widetilde{T}\};\{A\},\{B\})\rangle = \sum_{n=1}^{N}\sum_{\alpha_{n-1},\alpha_n,s_n}\widetilde{T}^{s_n}[n]_{\alpha_{n-1}\alpha_n}\,|\Phi_{\alpha_{n-1}}[1..n-1]\rangle\,|s_n\rangle\,|\Phi[n+1..N]_{\alpha_{n+1}}\rangle\,. \tag{134}$$

In analogy to the uMPS routine, we construct a tensor V_L such that $(M^{s_n}[n])^\dagger V_L^{s_n} = 0$ and $V_L^{s_n\dagger}V_L^{s_n} = 1$, allowing us to parametrize a tangent vector naturally fulfilling the gauge fixing condition by $\widetilde{T}^{s_n}(Z) = V_L^{s_n}Z$. It remains to clear how the tangent plane projector $\mathrm{P}_{|\Psi\{M\}\rangle}$ of the inverse free parametrization looks like and what the parameters Z stand for, if not for the components of $|\partial_i\Psi\rangle$. For the latter purpose, let us look at the orthogonal projection of a generic state $|\Xi\rangle$ onto the tangent plane by minimizing

$$\min_{\bar{Z}}\left(||\,|\Xi\rangle - |\Theta(\{\widetilde{T}\};\{A\},\{B\})\rangle\,||^2\right), \tag{135}$$

which results in[17]

$$Z_{ext.}(n) = \partial_{\bar{Z}(n)}\langle\Theta(\{\widetilde{T}(\bar{Z})\};\{A\},\{B\})|\Xi\rangle \;=$$

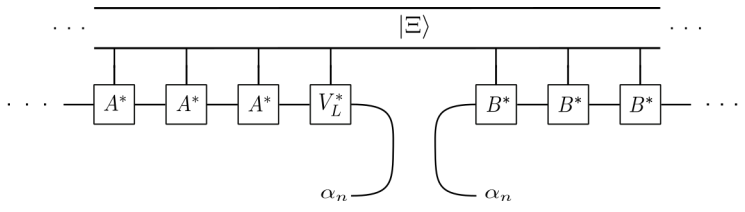

Consequently, the tangent plane projector $P_{|\Psi(\{M\})\rangle}$, as defined in the new tangent plane basis
$\{|\Phi_{\alpha_{n-1}}[1..n-1]\rangle\,|s_n\rangle\,|\Phi[n+1..N]_{\alpha_{n+1}}\rangle\}$, reads as

[17] graphical depiction adopted from [32]

$$P_{\mathcal{T}_{|\Psi(\{M\})\rangle}\mathcal{M}} = \sum_{n}$$

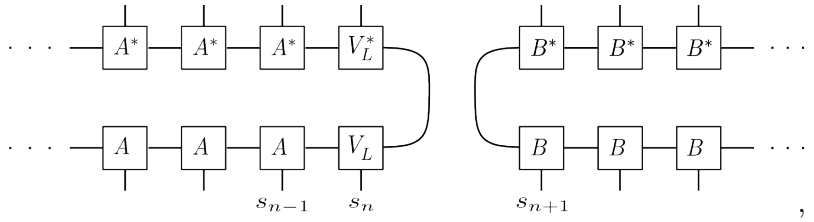

,

which can be further simplified by realising that $V_L^{s_n}(V_L^{s_n'})^\dagger$ is a projection in the orthogonal complement of $A^{s_n}A^{s_n'\dagger}$. Allowing us to interchange

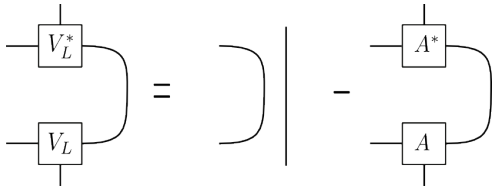

,

such that the tangent plane projector yields

$$P_{\mathcal{T}_{|\Psi(\{M\})\rangle}\mathcal{M}} = \sum_{n}^{N}$$

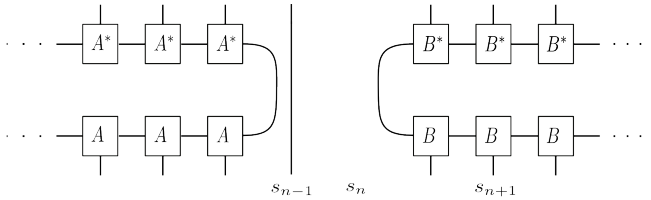

$$- \sum_{n}^{N-1}$$

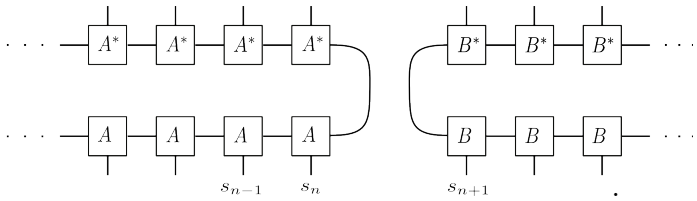

.

Given the form of projector, we could in principal, try to solve the TDSE in the tangent plane

$$\frac{\mathrm{d}}{\mathrm{d}t}\left|\Psi(\{M\})\right\rangle = -i\hat{\mathcal{P}}_{\mathcal{T}_{|\Psi(\{M\})\rangle}\mathcal{M}}\hat{\mathcal{H}}\left|\Psi(\{M\})\right\rangle, \tag{136}$$

by integrating the components at each site at once. However, not suprisingly for large systems this is impracticable. Fortunately, Lubich et al. [35,36] showed that it is possible to integrate above equations by a Lie-Trotter splitting of $\hat{\mathcal{P}}_{\mathcal{T}_{|\Psi(\{M\})\rangle}\mathcal{M}}\hat{\mathcal{H}}\left|\Psi(\{M\})\right\rangle$, resulting in a scheme evolving each site seperatly.

The finite MPS-TDVP routine:

As depicted in the latter section, ensuring norm preservation and non-singularity of $G_{\bar{j}i}$, the projector into the tangent plane

$$\hat{\mathcal{P}}_{\mathcal{T}_{|\Psi(\{M\})\rangle}\mathcal{M}} = \sum_{n}^{N}\underbrace{\hat{P}[1..n-1]_L \otimes \hat{1}_n \otimes \hat{P}[n+1..N]_R}_{:=\hat{\mathrm{P}}_1(n)} - \sum_{n}^{N-1}\underbrace{\hat{P}[1..n]_L \otimes \hat{P}[n+1..N]_R}_{:=\hat{\mathrm{P}}_2(n)}, \tag{137}$$

can be expressed in terms of the Schmidt basis

$$\hat{P}[1..n]_L = \sum_{\alpha} |\Phi[1..n]_\alpha\rangle \langle\Phi[1..n]_\alpha| \qquad \hat{P}[n..N]_R = \sum_{\alpha} |\Phi[n..N]_\alpha\rangle \langle\Phi[n..N]_\alpha| \,. \tag{138}$$

Ensuring an easy comparison of coefficients in equation (136), the MPS can be expressed in the same basis reading at site n as

$$|\Psi\rangle = \sum_{s_n\alpha\beta} M^{s_n}_{\alpha\beta} |\Phi[1..n-1]_\alpha\rangle |s_n\rangle |\Phi[n+1..N]_\beta\rangle \,. \tag{139}$$

This form is equivalent (as denoted in sec. 2.2) as bringing all tensors to the left/right of site n into left/right canonical form. As shown in, [34,35] the projector (137) enables us to apply an integration scheme evolving the entries of an MPS sequentially, one site after the other. Thereby, the evolution consists of two steps corresponding to the two projectors $\hat{\mathrm{P}}_1(n)$ and $\hat{\mathrm{P}}_2(n)$:

- evolve center site forward in time $M^{s_n}(t+\Delta t) = exp\left[-i\mathrm{H}_n\Delta t\right] M^{s_n}(t)$, with H_n being the components of $\hat{\mathrm{P}}_1(n)\hat{\mathcal{H}} |\Psi(\{M\})\rangle$ along $|\Phi[1..n-1]_\alpha\rangle |s_n\rangle |\Phi[n+1..N]_\beta\rangle$ (see fig. 29)
- evolve bond back in time $\lambda_n(t) = exp\left[i\mathrm{K}_n\Delta t\right] \lambda_n(t+\Delta t)$, with K_n being the components of $\hat{\mathrm{P}}_2(n)\hat{\mathcal{H}} |\Psi(\{M\})\rangle$ along $|\Phi[1..n]_\alpha\rangle |\Phi[n+1..N]_\beta\rangle$ (see fig. 29).

For the second step, reading of the components of $\hat{\mathrm{P}}_2(n)\hat{\mathcal{H}} |\Psi(\{M\})\rangle$, the MPS after the evolution of M^{s_n} is transformed into a Schmidt decomposition between site n and $n+1$

$$|\Psi\rangle = \sum_{\alpha\beta} \lambda_{\alpha\beta} |\Phi[1..n]_\alpha\rangle |\Phi[n+1..N]_\beta\rangle \,, \tag{140}$$

by bringing site n into left canonical form $M^{s_n} \to A^{s_n}$. After the back evolution of the bond $\lambda_n(t)$, it is absorbed into the next site $n+1$ leading to a MPS in the form we started with

$$|\Psi\rangle = \sum_{s_{n+1}\alpha\beta} M^{s_{n+1}}_{\alpha\beta} |\Phi[1..n]_\alpha\rangle |s_{n+1}\rangle |\Phi[n+2..N]_\beta\rangle \,. \tag{141}$$

Continuing in this manner the finite MPS can be evolved in time $|\Psi(t)\rangle \to |\Psi(t+\Delta t)\rangle$, sweeping through the chain from left to right. Note that K_n and H_n are always constructed respecting the previous evolved matrices (see fig. 29). This simple sweep algorithm comes with an error of $\mathcal{O}(\Delta t^2)$. By imposing a symmetric scheme, sweeping back and forth, this error can be further shrunk to $\mathcal{O}(\Delta t^3)$. Since there are no new insights involved in the implementation of the symmetric routine, this section is concluded by referring to the pseudo code for the symmetric routine presented in Appendix D.

5. Results

In the following section, results of the implemented routines are presented. Other than showing dry benchmark results, the schemes are applied to study quantum phases of three

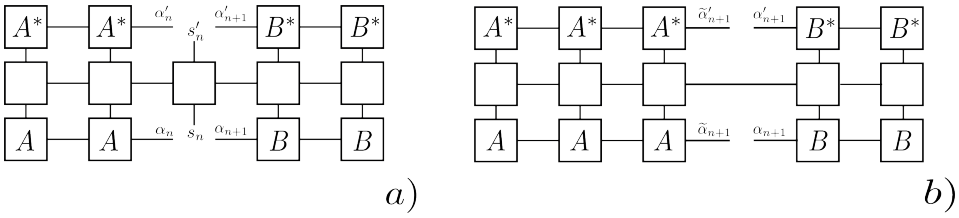

Figure 29: effective H_n and K_n: a) effective matrix H_n for the evolution of the tensor at site n b) effective matrix K_n for the evolution of the bond between site n and $n+1$.

different intriguing physical models, displaying the strength and possible drawbacks of the routines. In this regard, this section completes the picture of the theoretical part. Moreover, it will highlight recent findings in the study of symmetry protected topological order (SPT) and many-body localization (MBL). The covered examples of MPS routines include:

- quantum phase transition of the transverse Ising model
- Symmetry Protected Topological Phase in the Spin 1 Heisenberg Chain
- logarithmic growth of entanglement in the MBL-phase

In an effort to present a coherent story, in each section, the model and its underlying physical fundamentals are covered without going into too much detail. For readers interested in the latter we refer to the given references on the way.

5.1. Quantum Phase Transition of the Transverse Ising Model

When implementing new routines, it is advisable to compare the numerical results with well known theoretical models, for instance the transverse Ising model

$$\hat{\mathcal{H}} = -J \sum_i \hat{\sigma}_i^z \hat{\sigma}_{i+1}^z - h \sum_i \hat{\sigma}_i^x. \tag{142}$$

Besides being exactly solvable (see Appendix C), it is probably the most common model of phase transition in statistical and quantum physics. Moreover, it enables us to introduce some terminology, sharpening the distinction from the Symmetry Protected Topological phase (subject of the upcoming section).
The model for $J > 0$ can be interpreted as a ferromagnet along the z-axis which feels an external perpendicular in x-axis applied magnetic field of strength h. Furthermore, we will restrict this study to ground states at $T = 0$, such that the influence of thermal phase transitions can be neglected and all observed effects are indeed, completely quantum physical. In the case the magnetic field is switched off $h = 0$, the ground state of the Hamiltonian for a system of size N is double degenerate, since

$$|\bar{\uparrow}\rangle = |\uparrow\rangle^{\otimes N} \quad \text{or} \quad |\bar{\downarrow}\rangle = |\downarrow\rangle^{\otimes N}, \tag{143}$$

possess the same eigenenergy. This double degeneracy is the manifestation of the Hamiltonian's $\hat{\mathcal{H}}$ symmetry, namely being invariant under inversion (π rotation) of the z-axis referred

to as the second cyclic group $\mathbb{Z}_2$. Even though we would expect the ground state to be in some sort of superposition of the latter to degenerate ones, e.g.

$$|\Psi_{sym}\rangle = \frac{1}{\sqrt{2}}\left(|\bar{\uparrow}\rangle + |\bar{\downarrow}\rangle\right), \tag{144}$$

this is not the case in the thermodynamic limit $N \to \infty$, where the ground state can just be either of them. This phenomenon is referred to as spontaneous symmetry breaking, since the ground state exhibits less symmetries than its underlying Hamiltonian. In the other limit of the parameters $J = 0, h > 0$, the spins align with the externally applied field resulting in a ground state

$$|\bar{+}\rangle = \frac{1}{\sqrt{2}}\left(|\downarrow\rangle + |\uparrow\rangle\right)^{\otimes N}, \tag{145}$$

where each spin points in the x direction as the magnetic field. Other than before, this state has still the same symmetry properties as $\hat{\mathcal{H}}$ and is thus said to be in a different phase than for $h = 0, J > 0$.

It is important to point out that the breaking of symmetries is the characteristic of two "truly" distinct phases which cannot be adiabatically connected. For instance, the phase transition between liquid and solid water break the translation invariance of the system while the phases liquid and vapor do not. Therefore, even though one may witness a phase transition at a certain parameter regime, there exists an adiabatically connection between the vapor and liquid phases of water beyond the critical point. In this manner, vapor and liquid are of the same phase.

In Landau theory, phase transitions are detected by the continuous or discontinuous (second or first oder) change of (local) order parameters which only take non zero values in the "ordered" phase. For the discussed transverse Ising Model, the (local) order parameter is given by the expectation value (magnetization) $\langle \hat{s}_z \rangle$, which is essentially non zero for either of the two possible ground states $|\bar{\uparrow}\rangle$ and $|\bar{\downarrow}\rangle$ at $J > 0, h = 0$ and zero for $|\bar{+}\rangle$. The order parameter thus indicates if a state at a specific parameter configuration J, h respects the symmetries of the system's Hamiltonian or not. Concerning the case of second oder phase transitions (as the transverse Ising model), the order parameter changes continuously across the phase transition. The point at which the phase transition takes place, from which point onwards the order parameter takes non vanishing values, is called a quantum critical point h_c. In its vicinity, long ranged quantum fluctuations of the order parameter originating from the Heisenberg uncertainty principle dilute the difference between both phases until they are indistinguishable at h_c. This means that fluctuations occur over all length and time scales requiring a divergent correlation length as it occurs at gap closing (see sec. 3.2). In order for the system to change its phase and spontaneously break symmetries, the system needs to undergo a gap closing (at second order phase transitions). Regarding the context of this thesis MPS, the critical points of a system seem at first infeasible due to the occurrence of long range correlation. Nonetheless, in the following we will see that it is possible to investigate characteristic properties of the system at (to some extend) and next to the critical point.

In order to estimate the performance of the implemented iTEBD routine, we looked into two

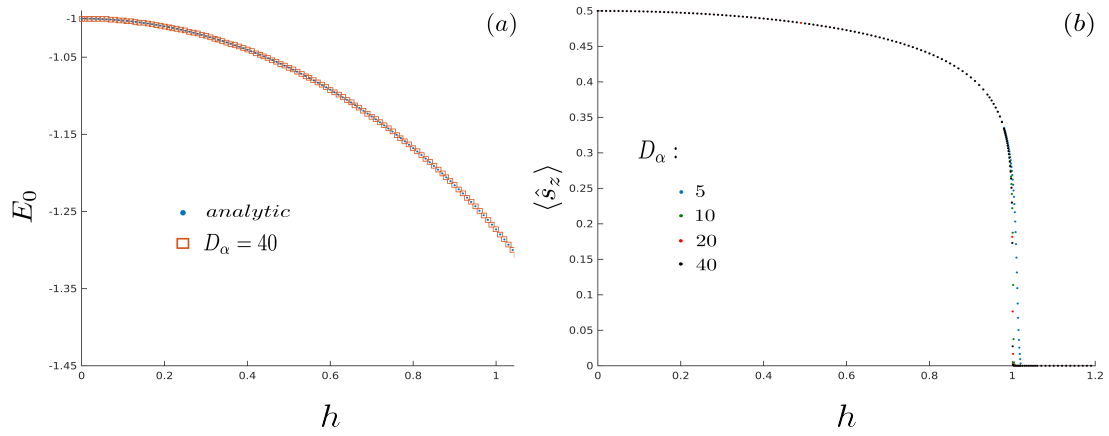

Figure 30: ground state energy & magnetization: a) analytic result of E_0 compared to iTEBD with bond dimension $D_\alpha = 40$, b) magnetization for different bond dimension $D_\alpha = \{5, 10, 20, 40\}$.

quantities, the order parameter $\langle \hat{s}_z \rangle$ and the ground state energy E_0 of the transverse Ising model for different parameters h ($J = 1$). First of all, to evalueate the iTEBD scheme it is essential to state the chosen convergence scheme since results can change significantly. This originates as earlier stated (sec. 4.2) from the susceptiblity of iTEBD/TEBD to get stuck in local minima. We proceeded for the presented results as followed:

- intial state is a random MPS with unit cell 2 of various bond Dimension D_α
- run imaginary-time evolution iTEBD for different external field strengths h. Timesteps start from $\Delta t = 0.1$ and are halved as soon as the relative change in the singular values between the two sites of the unit cell is lower than 10^{-6}. If the the relative error stays above this threshold for a couple of steps, Δt is halved nonetheless since the missmatch in singular values might be caused due to a high trotter error.
- after reaching $\Delta t = 0.0001$ the state is assumed to be the ground state and we compute its magnetization as well as its energy.

For the ground state energy (across the critical point for $h = 0.0$ to $h = 1.2$) we find that the overlap with the analytical result (see Appendix C) for a bond dimension of $D_\alpha = 40$ is up to a relative error of $\sim 10^{-7}$ exact 30. These findings for the ground state energy do not change significantly for smaller bond dimensions. Contrary to that, the plot for the magnetization, see figure 30 b), shows an overall expected slope, which deteriorates notably close to the critical point (see fig. 31 for a close up). For increasing bond dimension we find that the magnetization reaches closer and closer expected vanishsing magnetization at $h = 1$. Nonetheless, the improvement after doubling the bond dimension decreases rapidly, such that it seems to be impossible to reach totally vanishing magnetization. The drawback at cirtical points is not really suprising since the system is gapless and thus cannot be represented faithfully by matrix product states (see sec. 2.3). As a deduction, one may ask if the

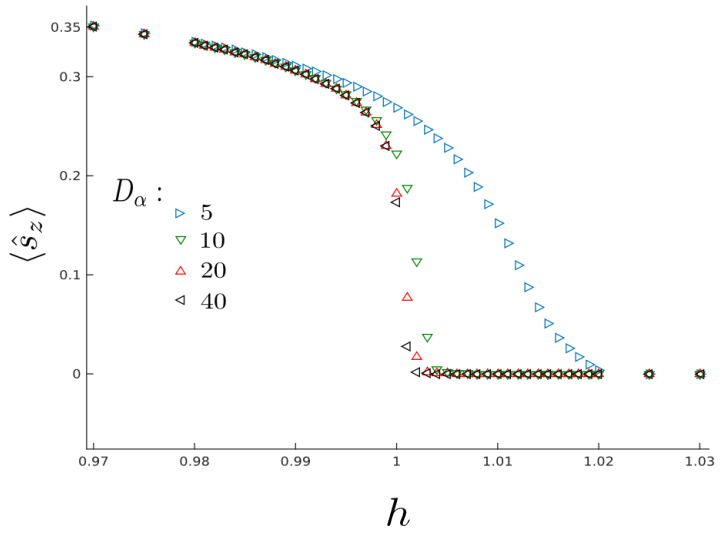

Figure 31: Role of D_α: convergence of $\langle \hat{s}_z \rangle$ at the critical point $h = 1$ with respect to the bond dimension D_α

entanglement at a critical point does not follow the area law, how does it actually scale with the system size?

5.1.1. Entanglement Growth at Criticality

This question of entanglement scaling at the critical point actually arises quite naturally, since the scale invariance of systems contradicts the area law, namely the scaling of entanglement with boundaries. Fortunately, the scale invariance of the system at criticality also allows us to study the system in Conformal Field Theory, in which it can be proven [37] that for generic one dimensional systems at the critical point the entanglement grows logarithmically with the system size L

$$S_{vN} \sim \frac{c}{6} \log(L). \tag{146}$$

Hereby, the constant c, is universal and called the central charge of the Conformal Field Theory. Due to its universality (namely $c = \frac{1}{2}$ for fermionic and $c = 1$ for bosonic systems, in one dimension) the central charge is a perfect candidate to study the performance of our vMPS routine in gapless systems[18].

In order to do so, we calculated the ground state entanglement entropy at half length $S_{vN} = -2 \cdot \sum_{\alpha_{L/2}} \lambda^2_{\alpha_{L/2}} \log(\lambda_{\alpha_{L/2}})$ for the transverse Ising model (142) at the critical point and near critical points $h = \{1.0, 1.02, 1.2\}$ for different chain lengths up to $L = 120$, see figure 32. Each run of the VMPS routine was done by increasing the bond dimension dynamically over 5 sweeps (as explained in sec 4.1). The total bond dimension was restricted to $D_\alpha = 64$ allowing us to represent the full Hilbertspace of (142) up to a system size of $L = 12$ faithfully. As figure 32 a) highlights the bad performance of our iTEBD routine for h close to the critical point can be explained, since besides the expected logaritmic growth at $h = 1$

[18] for more benchmark of the vMPS routine applied on the spin $\frac{1}{2}$ Heisenberg chain see Appendix D

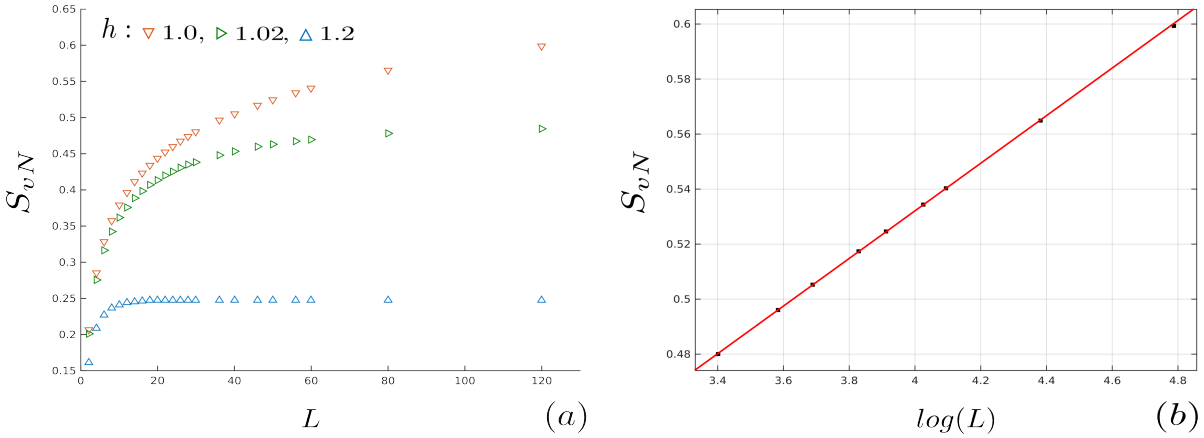

Figure 32: S_{vN} **near critical point:** a) entanglement growth with system size for the transverse Ising model close and on the critical point. b) logaritmic plot of S_{vN} at half length, *fit: slope: 0.08602 (0.08549,0.08654), intercept: 0.1875 (0.1858,0.19), residual: 1*

also systems close to one as $h = 1.02$ possess significant entanglement growth with system size. Even though the entanglement for those near critical points might saturate[19] for very long chains, it seems that it is impossible to incorporate its ground state with a feasible bond dimension.

Regarding the central charge at the critical point (fig. 32 b)), we find with a linear fit on the log plot of S_{vN} at half lenght for our numerical results (for $L = \{30, 36, 40, 46, 50, 56, 60, 80, 120\}$ to exclude finite size effects) that $\frac{6}{c} = 11.6256 \pm 0.0761$. Considering that c can either be $\frac{1}{2}$ or 1 this result even though being off by a bit is strong indication to which class the system belongs. In this manner, even tough MPS routines have significant shortcoming at the critical points, they can still predict the systems critical exponents (which follow from the central charge [38]).

[19] which is not necessarily the case considering subleading corrections of (146)

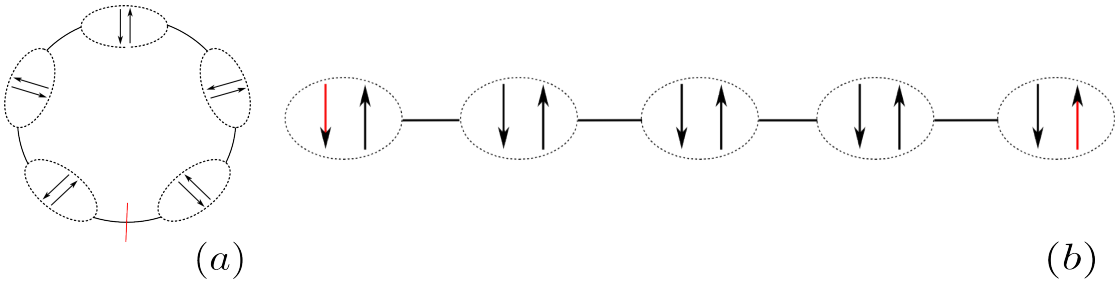

Figure 33: AKLT model: a) the ground state with periodic boundary conditions, becomes the one with obc b) after cutting it at an arbitrary bond (red). The unconnected spin from the former spin singlet are now completely free an can take up to four configurations (four fold degenerate ground state).

5.2. Symmetry Protected Topological Phase in the Spin 1 Heisenberg Chain

What happens if a system undergoes a gap closing but does not show any sign of symmetry breaking and it is impossible to define a meaningful order parameter? Is there simply no phase transition? The answer to this question can be given by looking at an odd integer Heisenberg spin chain

$$\hat{\mathcal{H}} = J \sum_i \mathbf{S}_i \mathbf{S}_{i+1}, \tag{147}$$

which possesses the simplest example of these new type of phases in one dimension. The model initially awakened interest due to Haldane's prediction that the system is gapped [39] rather than the analytic results by Bethe ansatz for fractional spin chains might suggest. Even though the conjecture still lacks a strict mathematical proof, numerical results substantiate a finite energy gap in the thermodynamic limit.

Introducing an exact solvable toy model (the AKLT model) Affleck, Lieb, Kennedy and Tasaki [40] showed that such gapped odd integer spin systems do exist and that they faithfully can be represented by valence bond solids (see Appendix B). The intriguing observation is that the ground state of the AKLT model shares characteristics of topological insulators as edge excitations (see fig. 33) which is an indication of a "topological" phase. To classify these types of phases beyond Landau's theory of phase transitions, Matrix Product States besides being the numerical tool of choice, delivers a powerful analytical language and leads to the full classification of 1D gapped systems by "fractionalization" of symmetry operators [41]. In the following we try to redeem ourselves for introducing new terminology pulled out of thin air, by giving an intuitive picture of these new types of phases in one dimension.[20] Hereby, we will heavily make use of the MPS notation and present numerical results (of our routines) for the Haldane phase, and compare with [42].

As mentioned in the first section of the results of this thesis, symmetries play a crucial role in phase transitions where the spontaneous breaking of a symmetry distinguishes two types of phases. Therefore, it might seem natural to ask what role symmetries, in these new type of "topological" phase transitions, play. To investigate this further let us try to understand

[20] Note, that in one dimension all topological phases are symmetry protected.

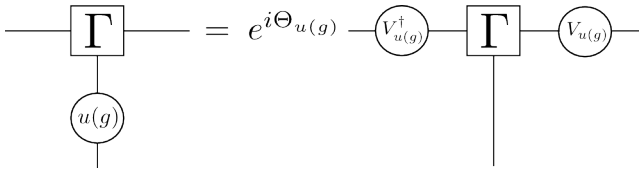

Figure 34: on site symmetries in MPS: application of a linear representation of a on site symmetry group translates into a projective representation of the symmetry on the bond space.

the representation of symmetries in MPS since they faithfully represent all ground states of gapped systems.

Consider a state to be invariant under a global on site symmetry operation $U(g) = \prod_n \bigotimes u_n(g)$, meaning that the state of the system is allowed to change up to a phase under the symmetry operation $|\widetilde{\Psi}\rangle = U(g)\,|\Psi\rangle \Rightarrow \langle\widetilde{\Psi}|\Psi\rangle = e^{i\Phi}$. Let us now express the state in terms of a translation invariant MPS in canonical form. The corresponding transfer matrix $E(X) = \Gamma^{s_i\dagger}\lambda X \lambda \Gamma^{s_i}$ has spectral radius one and the identity as its left and right eigenvector with eigenvalue one, such that it can be proven that the on site linear symmetry operation translates into a projective representation on the virtual index space [16, 43]

$$u(g)_{s_i s_i'}\Gamma^{s_i'} = e^{i\Theta_{u(g)}} V_{u(g)}^\dagger \Gamma^{s_i} V_{u(g)}, \tag{148}$$

where $V_{u(g)}$ are unitary operations commuting with the Schmidt coefficients $[V_{u(g)}, \lambda] = 0$ and the phase $e^{i\Theta_{u(g)}}$ (see fig. 34). In general, a projective representation of a symmetry group G is a linear representation modulo a phase $U(1)$, that means for $g, h \in G$ we have

$$V(gh) = e^{i\Phi(g,h)} V(g)V(h). \tag{149}$$

As a consequence of this phase factor (factor set), the representation splits up into equivalence classes classifying the different phases. Rather than explaining these fundamental and mathematical concepts in a thorough discussion (as in [41, 44]), let us have a look at some physical consequences arising from it and try to give some intuitive understanding.

The periodic AKLT ground state is a prototype of a spin one gapped chain preserving all symmetries of the system is exactly represented by the translation invariant MPS with bond dimension 2, described by the operators:

$$\Gamma^{s_i} = \sigma^s, \qquad \lambda = \begin{pmatrix} \frac{1}{\sqrt{2}} & 0 \\ 0 & \frac{1}{\sqrt{2}} \end{pmatrix}, \tag{150}$$

where the spin one basis is transformed into the new basis

$$|x\rangle = \frac{1}{\sqrt{2}}\left(|1\rangle - |-1\rangle\right), \quad |y\rangle = \frac{i}{\sqrt{2}}\left(|1\rangle + |-1\rangle\right), \quad |z\rangle = |0\rangle\,, \tag{151}$$

and the σ^s with $s \in \{x, y, z\}$ are the Pauli matrices. Since the system is invariant under inversion symmetries $\Gamma^{s_i} \to \Gamma^{s_i T}$, we find for the projective representation (transformation of the bonds) $\sigma^{s_i} \to \sigma^{s_i T} = -\sigma^y \sigma^{s_i} \sigma^y$ ($V_I = \sigma^y$ and $\Theta_I = \pi$)). In general, regarding the

inversion symmetry, it can be shown that Θ has to take values of either 0 or π. Applying the generic expression of inversion symmetry

$$\Gamma^{s_i T} = e^{i\Theta_{u(I)}} V_{u(I)}^{\dagger} \Gamma^{s_i} V_{u(I)}, \tag{152}$$

to itself, yields the equation

$$\Gamma^{s_i} = e^{2i\Theta_{u(I)}} \left(V_{u(I)} V_{u(I)}^{*} \right)^{\dagger} \Gamma^{s_i} V_{u(I)} V_{u(I)}^{*},$$

which can be further transformed into an eigenvalue equation of the transfer matrix by simply multiplying with $\Gamma^{s_i\dagger} \lambda V_{U_I} V_{U_I}^{*} \lambda$

$$\Gamma^{s_i\dagger} \lambda V_{u(I)} V_{u(I)}^{*} \lambda \Gamma^{s_i} = e^{i2\Theta_{u(I)}} V_{u(I)} V_{u(I)}^{*}.$$

By choosing the suitable gauge in the MPS representation (canonical form), the transfer Matrix $E(X) = \Gamma^{s_i\dagger} \lambda X \lambda \Gamma^{s_i}$ is supposed to have a single eigenvalue of value one, such that $e^{i2\Theta_{U_I}} = \{0, \pi\}$ and $V_{u(I)} V_{u(I)}^{*} = e^{i\Phi_{u(I)}} 1$, where $\Phi_{u(I)}$ obeys the same constraint as $\Theta_{u(I)}$,

$$V_{u(I)}^{T} = V_{u(I)} e^{-i\Phi_{u(I)}} \Rightarrow V_{u(I)} = V_{u(I)} e^{-i2\Phi_{u(I)}} \Rightarrow e^{-i2\Phi_{u(I)}} = 1 \Rightarrow \Phi_{u(I)} \in \{0, \pi\}.$$

In the case of the AKLT example $\sigma^y \sigma^{y*} = -1$ and therefore, $\Phi_{u(I)} = \pi$. The choice of this phase Φ has important physical consequences. For $\Phi = \pi$ the symmetry operations on the bonds becomes anti-symmetric $V_{u(I)}^{T} = -V_{u(I)}$, such that $\lambda V_{u(I)}$ is anti-symmetric as well. From linear algebra [] it is known that each anti-symmetric matrix can be brought into real normal form (Jordan Normal form of anti-symmetric matrices). For a generic anti-symmetric matrix M of dimension $dim(M) = d \times d$ with rank $2n$ this reads as

$$M = W^T N W \quad \text{with} \quad diag(N) = \left\{ \begin{pmatrix} 0 & \lambda_{\alpha_1} \\ -\lambda_{\alpha_1} & 0 \end{pmatrix}, ..., \begin{pmatrix} 0 & \lambda_{\alpha_n} \\ -\lambda_{\alpha_n} & 0 \end{pmatrix}, \mathbb{O}_{d-2n} \right\}.$$

Consequently, all Schmidt coefficients (entanglement spectrum) are at least double degenerate (and further can just be even degenerate), since $V_{u(I)}^{\dagger} \lambda^* \lambda V_{u(I)} = \lambda^2 = W^T N^T N W$ and $N^T N = D_1 \oplus D_2 \oplus ... D_n \oplus 0 \oplus 0.. \oplus 0$ with

$$D_i = \begin{pmatrix} \lambda_{\alpha_i}^2 & 0 \\ 0 & \lambda_{\alpha_i}^2 \end{pmatrix}.$$

For the AKLT ground state this can be immediately verified since $diag(\lambda) = \{\frac{1}{\sqrt{2}}, \frac{1}{\sqrt{2}}\}$.
As mentioned above, the phase Φ can be used to classify different phases which cannot be adiabatically connected to each other. But how can we understand this? Once again, let us have a look at the AKLT model (see fig. 33). If we cut the system with pbc in half at an arbitrary bond, its edges correspond to free spin $\frac{1}{2}$'s. If we consider the system to obey a global on site symmetry, we can show that it only manifest itself at the edges of the system since $[V_{u(g)}, \lambda] = 0$ (see fig. 35). This is referred to as symmetry "fractionalization". Note that the free spin $\frac{1}{2}$ at the edges of the AKLT-chain can be in principal infinitely far apart. In order to get rid of the projective representation, the edge states would have to be able

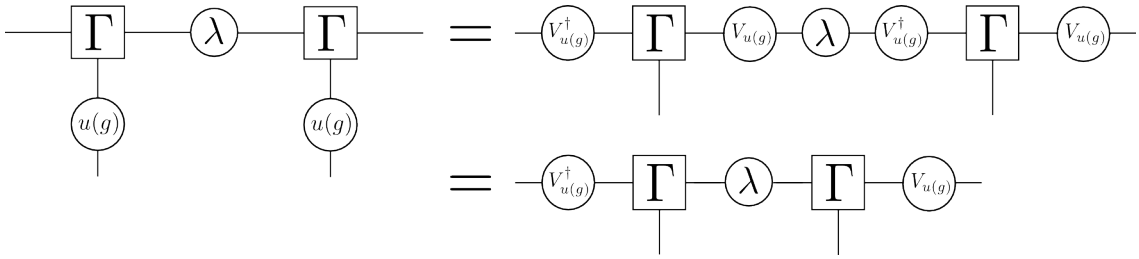

Figure 35: projective rep. at edges: due to the commutation of $[V_{u(g)}, \lambda] = 0$ the action of a global on site symmetry is just reflected at the edges, since everywhere in the bulk we yield $V^{\dagger}_{u(g)} V_{u(g)} = 1$.

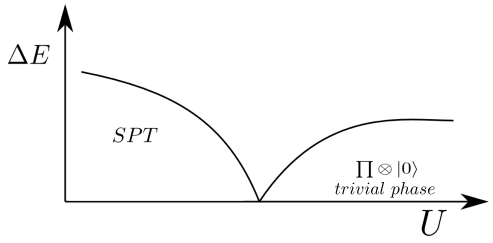

Figure 36: SPT pahse: sketch of the phase transition between a trivial phase at $U \to \infty$ and an SPT phase.

to interact through the whole system. In other words the system should have a divergent correlation and therefore, gap closing. Hence, the projective representation classifies different types of phases which are not possible to connect adiabatically [45]. (To some exctend even though very specifically for this example the free spin $\frac{1}{2}$ at the edges transform under SU(2) while the bulk transforms under SO(3) in order to relief the SU(2) transformation the spin 1/2 have to interact such that they can be represented as a spin 1). Different to the previously discussed phase where breaking of symmetries was essential for classification, in this new case the classification is only possible as long as the system possesses a global on site symmetry, which exhibits a non trivial projective representation. Thus, we refer to these new types of phases as symmetry protected topological phases (SPT).
Let us now come back to the less artificial example of the Heisenberg spin 1 chain and consider an Hamiltonian with an additional anisotropic term

$$\hat{\mathcal{H}} = J \sum_i \mathbf{S}_i \mathbf{S}_{i+1} + U \sum_i \left(S_i^z\right)^2 .$$

For $U \to \infty$ the ground state is in a product state $|\bar{0}\rangle = \prod \otimes |0\rangle$ (referred to as the "trivial" phase). However, different from the phase transition of the transverse Ising model, we do not expect another product state regarding the limit $U = 0$ but rather, due to the similarities with the AKLT model, some state with non vanishing entanglement and furthermore, at least an even number degenerate entanglement spectrum. To compare with previous findings from a different approch, namely Tensor Entanglement Filtering Renormalization (see [46]) and the direct comparison with the results of [42], we will in the following specifically investigate

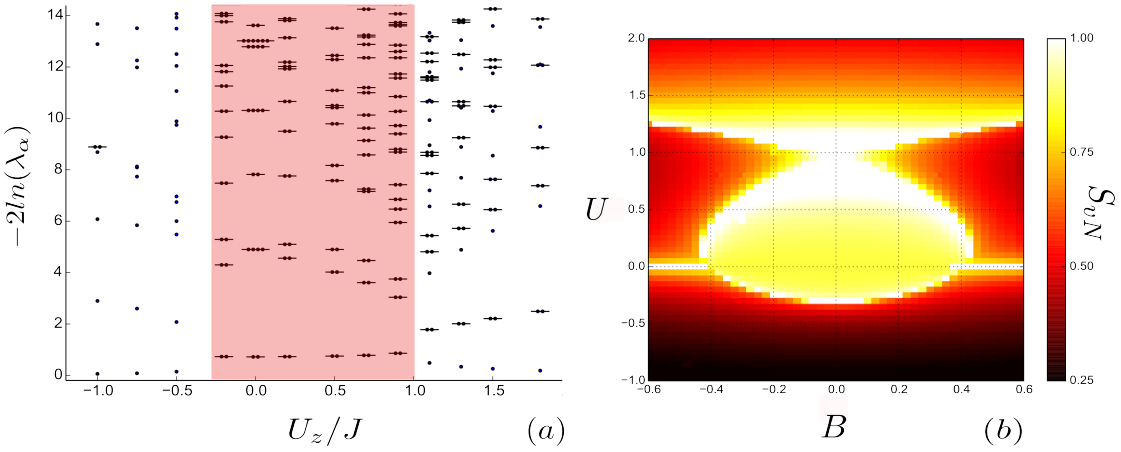

Figure 37: Phasediagram and Ent.-spectrum: a) entanglement spectrum (at $B = 0.0$ for different U, Haldane phase highlighted in red) and entanglement entropy b) of $\hat{\mathcal{H}}$

the slightly adapted Hamiltonian

$$\hat{\mathcal{H}} = J \sum_i \mathbf{S}_i \mathbf{S}_{i+1} + B \sum_i S_i^x + U \sum_i (S_i^z)^2 \,.$$

To be precise, we will investigate for which parameter regimes B, U one can find even degeneracy in the entanglement spectrum and thus the Haldane phase (a symmetry protected topological phase). Further, as it is denoted above, the SPT phase and with it the degeneracy of the entanglement should vanish as soon as the symmetry protecting the phase is broken. Thus, we will break one potentially protecting symmetry after the other by perturbing $\hat{\mathcal{H}}$ with:

- $\hat{\mathcal{H}}_1 = B_z \sum_i S_i^z + U_{xy} \sum_i (S_i^x S_i^y + S_i^y S_i^x)$, which breaks a combination of time reversal and π rotation around the y axis (see fig. 38).
- $\hat{\mathcal{H}}_2 = R \sum_i \left[S_i^z (S_i^x S_{i+1}^x + S_i^y S_{i+1}^y) - S_{i+1}^z (S_i^x S_{i+1}^x + S_i^y S_{i+1}^y) + H.c. \right]$, which breaks inversion symmetry (see fig. 39)

The entanglement spectrum of each ground state corresponding to a set of parameter ($J = 1.0$, B, U) is hereby obtained with iTEBD with a bond dimension of $D_\alpha = 60$ starting from a random matrix product state. The step size of the imaginary time evolution is dynamically minimized (from $\Delta t = 0.8$ to $\Delta t = 0.0001$) by tracking convergence of the eigenenergy. Notice that the symmetry of time reversal and π rotation around the y acts trivially on the AKLT state and thus does not lead to an anti-symmetric projective representation and double degenerate entanglement. Hence, it can be claimed that this symmetry is in fact not sufficient for the Haldane phase. In fact, as figure 38 suggests, we still find a parameter region where the ground state possesses even degenerate entanglement spectrum while this changes instantly when perturbing with $\hat{\mathcal{H}}_2$ (see fig. 39). Therefore, the inversion symmetry seems to be the necessary protecting symmetry of the Haldane phase. Next to the shown

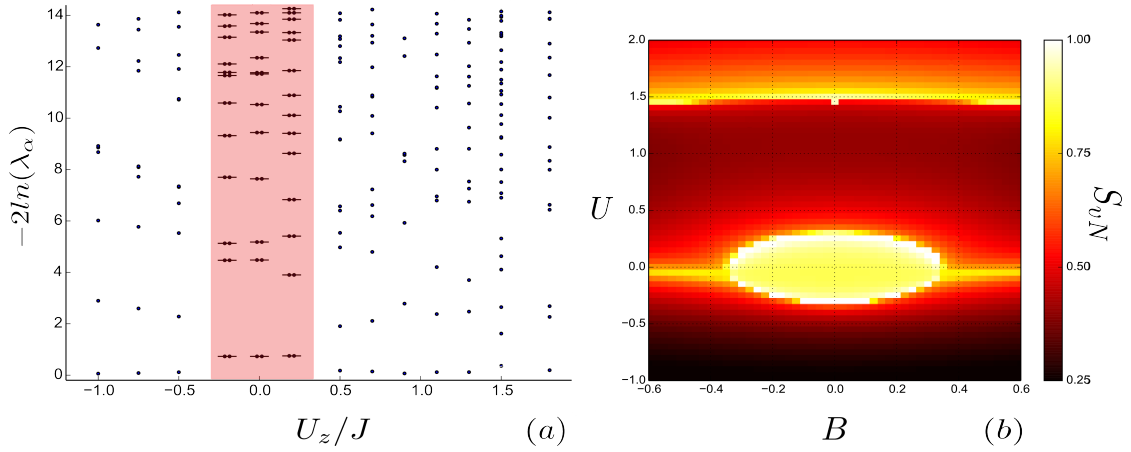

Figure 38: Phasediagram and Ent.-spectrum: a) entanglement spectrum (at $B = 0.0$ for different U, Haldane phase highlighted in red) and entanglement entropy b) of $\hat{\mathcal{H}}+\hat{\mathcal{H}}_1$

entanglement spectra we plotted the von Neumann entanglement entropy for each parameter configuration. Even though the entropy alone is not a sufficient indication for the Haldane phase, it shows phase transition by divergent entanglement (white spots). Looking at figure 39 b) we thus see that the necessary division to the trivial phase ($U \to \infty$) is no longer visible [21].

At last let us demonstrate that indeed as a consequence of the double degeneracy the Haldane phase is not adiabatically connected to the trivial phase. Remember that the trivial phase is characterized by being adiabatically connected to a product state, in the present case to $|\bar{0}\rangle = \prod \otimes |0\rangle$. Thus, we would suspect that for a state belonging to the trivial phase, the entanglement entropy at any cut can be reduced to zero by adiabatically weakening the according bond. This is illustrated in figure 40 where the centre bond of a 80 site unit cell of ground states belonging to different parameter configuration of $\hat{\mathcal{H}}$ are adiabatically weakened. The procedure is as follows, first the ground state is computed with iTEBD and in a second step time evolved with the same Hamiltonian, while the nearest neighbour interaction J of the centre bond is slowly reduced by $J_{weak.} = J - t\frac{J^2}{40}$. For the trivial phase we therefore, obtain a completely disentangled bond after $t = 40$ ($J = 1.0$). In the contrary, for a ground state belonging to the SPT phase, we find that the entanglement entropy cannot be lowered below $ln(2)$, since as explained without gap closing the projective representation of the symmetries at the edges, and as a consequence the double degeneracy in the entanglement spectrum, persists.

[21] this is no proof since the phase transition might just lie beyond the investigated parameters

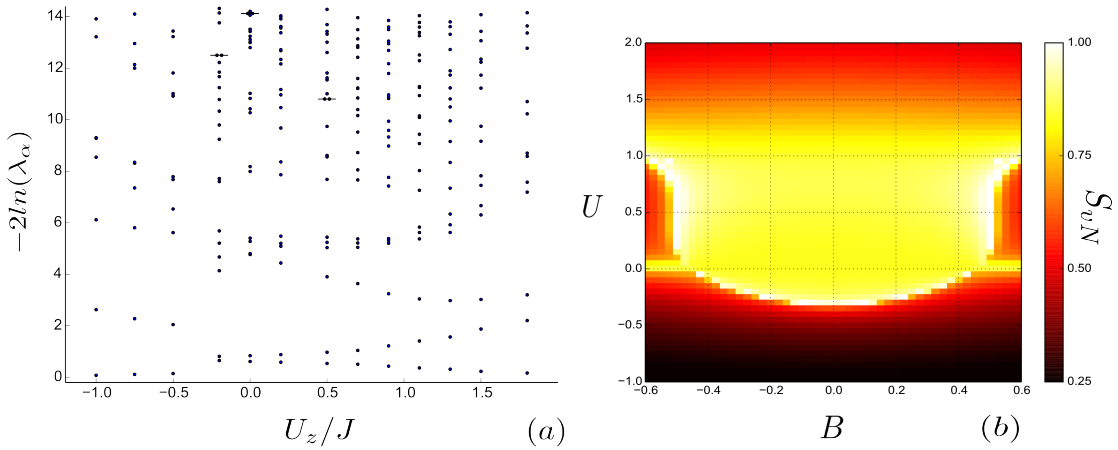

Figure 39: Phasediagram and Ent.-spectrum: a) entanglement spectrum (at $B = 0.0$ for different U, Haldane phase highlighted in red) and entanglement entropy b) of $\hat{\mathcal{H}} + \hat{\mathcal{H}}_2$. No double degeneracy detectable $\rightarrow$ inversion symmetry necessary to protect topological phase

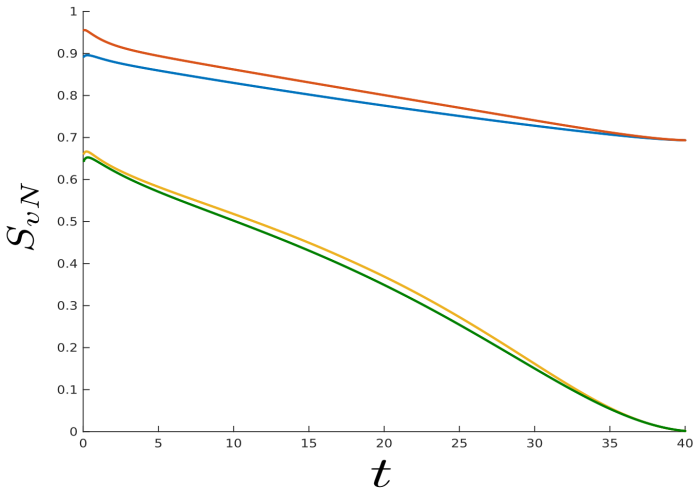

Figure 40: adiabaticall bond weakening: entanglement entropy at the centre bond with time, while weakening the bond $J_{weak.} = J - t\frac{J^2}{40}$ for different ground states of $\hat{\mathcal{H}}$: red = (J=1.0,U=0.2,B=0.3), blue = (J=1.0,U=0.4,B=0.3), yellow = (J=1.0,U=0.8,B=0.3), green = (J=1.0,U=1.0,B=0.3)

5.3. Many Body Localization and Logarithmic Growth of Entanglment

So far we studied static ground state quantum phases, trivial and topolical ones. Beyond these phases, recent thoughts and experimental findings [47, 48] suggest yet another type of phase. Unlike the others (studied in 5.2 and 5.1) this phase is a phase of the dyanmics of highly excited states. Since it makes no sense to speak about a phase without a counter part in which the physical behaviour (as an order parameter or the entanglement spectrum in the previous sections) of the system is sharply distinct from an other, let us try to answer the question of what distinguishs the MBL phase.

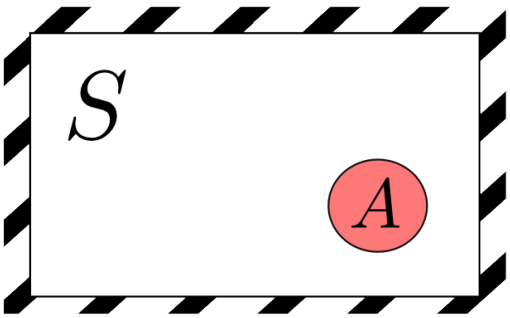

Figure 41: Thermalization: schematics of a completely isolated system S with subsystem A

To answer this question, we have to ask ourselves what is the long time behaviour of a many-body system. For systems in contact with a reservoir, we know that no matter the initial state, after waiting long enough the system will be completely thermalized and described by its canonical ensemble

$$\rho_{th} = \frac{1}{Z} e^{-H/k_B T}. \tag{153}$$

But what happens if we look at a completely isolated system S and question the thermalization behaviour of a subsystem A (see fig. 41)? Is it possible the complement $C = S/A$ serves as an effective reservoir for the subsystem A, such that the subsystem A after a long time becomes thermal $\rho_{th}^{(C)} = tr_C \left(\frac{1}{Z} e^{-H/k_B T}\right)$? As it was disovered over the last 30 years there are two distinct possibilities, either all possible initial states of the system thermalize (behave ergodic) or they do not. The latter is referred to as many-body localization, the prime example of such a system is the multi-particle equivalent to the single particle Anderson model [49]. After a Jordan-Wigner transformation, this model can effectively be rewritten as the XX-model with a random on site potential h_i (disorder)

$$\hat{\mathcal{H}}_0 = J \sum_i \left(\hat{\sigma}_i^x \hat{\sigma}_{i+1}^x + \hat{\sigma}_i^y \hat{\sigma}_{i+1}^y\right) + \sum_i h_i \hat{\sigma}_i^z. \tag{154}$$

Even though, the phase transition, of this model and other related ones, depending on the strenght of the disorder is still the focus of ongoing research, let us look instead to an intriguing feature of the MBL phase. In particular, let us consider how does the termalization of arbitrary initial states behave with an additional weak interaction

$$\hat{\mathcal{H}} = \hat{\mathcal{H}}_0 + J_z \sum_i \hat{\sigma}_i^z \hat{\sigma}_{i+1}^z. \tag{155}$$

In order to do so we created samples of random initial product states with either spin up or spin down for a system of size $N = 10$. Each single one of the initial states is then time evolved under the Hamiltonian (155) with and without interaction ($J_z = \{0.0, 0.1\}$, $J = 1.0$) and a disorder h_i, randomly picked out of a uniform distribution between the interval $[-5, 5]$. During the evolution, conducted with our TEBD routine up to a total time $t = 10^4$ with time steps $\Delta t = 0.05$, we tracked the evolution of the entanglement entropy S_{vN} at a cut of the system at half length (see fig. 42, compare findings[22] with [50]). In the non

[22] note that in the reference the state is initialized in a Néel state rather than in a completely random product state.

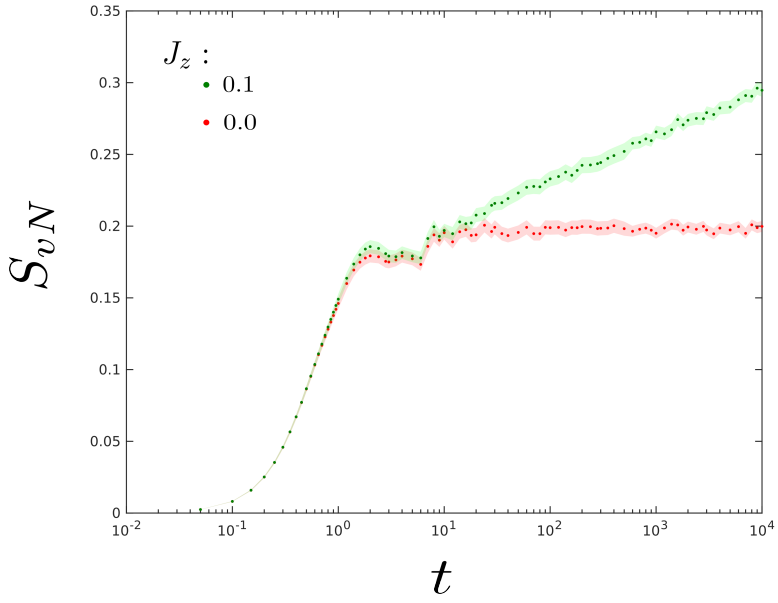

Figure 42: **MBL:** growth of entanglement in a many-body localized system depending on the interaction strenght J_z.

interacting case $J_z = 0.0$ the graph shows the expected behaviour of a many-body localized system. The entanglment starts to spread as in any usual ergodic state until a length scale, referred to as the localization length ξ, is reached. As it is expected for many-body localized states, the growth stops abruptly and the entanglement entropy saturates to a finite value and remains constant for arbitrarily long times. Note that the saturation does not depend on the system size which is a clear evidence that the entropy, as opposed to the case of thermal (ergodic) systems, is not extensive but rather follows the area law. Surprisingly, even for very weak interactions, this behaviour changes qualitatively as soon as particles interact. The entropy after reaching saturation no longer remains constant but instead grows logarithmically in time. However, the findings of [50] prove that this cannot be explained due to the transport of particles. This opposes the generic linear growth of entanglement, as discussed in section 4.2, where the linear growth of entanglement is understood as a balistic transport of entangled quasiparticles. But what else could lead to an increase of entanglement, if not the spread of entangled particles across the two halfs of the system? In an attempt to explain this very briefly, note that even though the particles are localized their wavefunctions have exponentially decaying overlaps with other particles in the system. Considering the system to be cut in halfs, these exponentially supressed interactions $\sim J_z e^{-\frac{x}{\xi}}$ lead to a dephasing (decoherence) of spins (particles) across the cut of the system and thus to an increase in the entanglement (see [51] for a thorough discussion). Note that after complete decoherence, the system saturates to a finite entanglement which scales with system size (see [50]). A weak interaction on a many-body localized system, thus, can be seen as a sub-thermalization of the system since the reached saturation of entanglement entropy is lower than that of ercodic systems but possesses extensive scaling with system size.

6. Conclusion & Outlook

Throughout this thesis, we thoroughly analyzed several Matrix Product State routines, which are useful for the calculation of ground states as well as the dynamics of states of strongly correlated systems. Since a clear physical picture of a problem often starts to emerge after possible findings with numerical techniques, such as Matrix Product State algorithms, it is important to be confident in their accuracy as well as to know under which drawbacks the routines suffer. Therefore, we first presented a detailed introduction of the broad aspects of Matrix Product States as the description of physical states into a product of tensors. Even though this decomposition is a pure mathematical aspect, we demonstrated in section 2.3 that this rewriting of states described by their coefficents into tensor products is essentially a describtion of the state by its entanglement ("entanglement picture"). As for any other mathematical notation (as for instance Dirac's braket notation), we discussed in detail basic algebra of the Matrix Product State tensors (see sec. 3.1) before approaching more complicated equations that occur in the implemented numerical MPS routines. In particular, we looked into the following routines:

- variational Matrix Product States (vMPS), as an algorithm for ground state search,
- Tensor Evolving Block Decimation (TEBD) and its siblings for inifinite systems (iTEBD), for time evolution and ground state annealing by imaginary time evolution,
- Time Dependent Variational Principle (TDVP), for time evolution which preserves energy as other symmetries the system might possess.

Furthermore, besides a meticulous error analysis, we attempted to explain implementation details as well as underlying fundamental concepts of the routines.
Apart from these theoretical conclusions about the MPS routines, it was found necessary to test our implementation on actual problems in many-body physics to estimate their accuracy and see whether they are reliable to be used on further unresolved physical problems. The physical problems we encountered to solve with our routines were:

- quantum phase in the transverse Ising model,
- growth of entanglement at criticality,
- symmetry protected topological phase in the spin 1 Heisenberg chain (compare with [42]),
- logarithmic growth in the many-body localized phase (compare with [50]).

Especially the last two problems are of recent interest in condensed matter physics and we can directly compare our results with findings in literature. The qualitatively behaviour is in direct agreement with the cited publications. [23] This helps us to believe that our implemented routines indeed perfom as expected and therefore, can be used for unsolved issues in many-body physics.

[23] more quantitative benchmark results are given in Appendix D

A. Singular Value Decomposition (SVD)

Brief summary of singular value decomposition and its relation to the Schmidt decomposition.

In general, we can decompose any rectangular matrix M, with $dim(M) = A \times B$, into 3 matrices

$$M = USV^\dagger,$$

with the following properties:

- U is of dimension $A \times min(A, B)$ and build out of orthonormal columns referred to as left singular values.
- $V^\dagger$ is of dimension $min(A, B) \times B$ and has orthonormal rows referred to as right singular values.
- From the orthonormality it follows $U^\dagger U = 1$ respectively $V^\dagger V = 1$. In both cases unitary follows iff U respectively $V^\dagger$ is a square matrix.
- S is a non-negative diagonal matrix of dimension $min(A, B) \times min(A, B)$.

For the connection to the Schmidt coefficients of a composed system $\hat{\mathcal{H}}_{AB}$, consider a pure state $|\Psi\rangle$ in $\hat{\mathcal{H}}_{AB}$. Defining an arbitrary basis, $\{|i\rangle_A\}$ and $\{|j\rangle_B\}$, of the subspaces A respectively B we can compose $|\Psi\rangle$

$$|\Psi\rangle = \sum_{ij} C_{ij} |i\rangle_A \otimes |j\rangle_B ,$$

such that it is represented by some coefficients C_{ij}. These coefficients $M = C_{ij}$ can be identified with the matrix M of the singular value decomposition

$$|\Psi\rangle = \sum_{ij\alpha} U_{i\alpha} S_{\alpha\alpha} (V^\dagger)_{\alpha j} |i\rangle_A \otimes |j\rangle_B ,$$

leading to a decomposition in the 3 matrices $U, S, V^\dagger$. Subjecting $|i\rangle_A$ and $|j\rangle_B$ to a basis transformation defined by U respectively $V^\dagger$

$$|\Phi_\alpha\rangle_A \coloneqq \sum_i U_{i\alpha} |i\rangle_A \qquad |\Phi_\alpha\rangle_B \coloneqq \sum_j (V^\dagger)_{\alpha j} |j\rangle_B ,$$

we obtain new basis states referred to as left $\{|\Phi_\alpha\rangle_A\}$ and right $\{|\Phi_\alpha\rangle_B\}$ Schmidt basis (orthonormality directly follows from the above described properties). The Schmidt decomposition is then directly given by the diagonal elements of $S_{\alpha\alpha}$ referred to as λ_α

$$|\Psi\rangle = \sum_\alpha \lambda_\alpha |\Phi_\alpha\rangle_A \otimes |\Phi_\alpha\rangle_B .$$

Singular values and Schmidt coefficients are hence, the same terminology and the Schmidt *rank* is exactly the same number of non-vanishing singular values.

B. AKTL-model

Valence bond picture of the AKTL-model [5]

The AKLT-model

$$\hat{\mathcal{H}} = \sum_i \bar{\hat{S}}_i \bar{\hat{S}}_{i+1} + \frac{1}{3}\left(\bar{\hat{S}}_i \bar{\hat{S}}_{i+1}\right)^2,$$

introduced by Affleck, Lieb, Kennedy and Tasaki in 1987 is a prototyp of a gapped spin 1 chain. The Hamiltonian is given by an projector in the total spin 2 sector (see [52])

$$\hat{\mathcal{H}} = 2\mathcal{P}_2 - \frac{2}{3},$$

such that its ground state is a valence bond solid state (with total $S = \{0, 1\}$) [40], as depicted in fig. 43. Each spin 1 is represented by two auxiliary spin $\frac{1}{2}$, which are projected into the

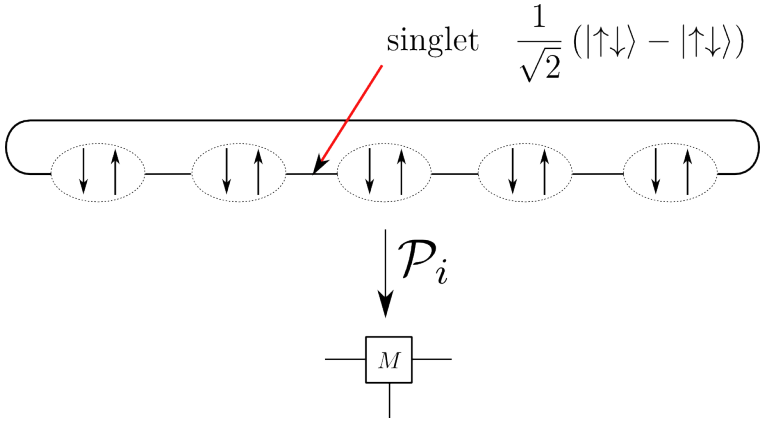

Figure 43: ground state of the AKLT model:

total spin $S = 1$ physical basis at site i by

$$\mathcal{P}_i = |1\rangle_i \langle\uparrow\uparrow|_i + \frac{1}{\sqrt{2}} |0\rangle_i \left(\langle\uparrow\downarrow|_i + \langle\downarrow\uparrow|_i\right) + |-1\rangle_i \langle\downarrow\downarrow|_i .$$

The bonds between each site i are hereby, formed out of singlet states $S = 0$

$$|\Psi\rangle_i = \sum_{\beta\alpha} \Sigma_{\beta\alpha} |\beta_i\rangle |\alpha_{i+1}\rangle \qquad \text{with} \quad \Sigma_{\beta\alpha} = \begin{pmatrix} 0 & \frac{1}{\sqrt{2}} \\ -\frac{1}{\sqrt{2}} & 0 \end{pmatrix},$$

where $|\beta_i\rangle = |\alpha_{i+1}\rangle = \{|\uparrow\rangle, |\downarrow\rangle\}$. Note that this is in fact a simple example of the Valence Bond Picture (VBP) introduced in section 2.4. In analogy to the VBP the valence states (auxiliary state) of a periodic system, form a dimer of the spin $\frac{1}{2}$ singlet states

$$|\Psi_{auxiliary}\rangle = \sum_{\bar{\alpha}\bar{\beta}} \Sigma_{\beta_1\alpha_2} \Sigma_{\beta_2\alpha_3} ... \Sigma_{\beta_{N-1}\alpha_N} \Sigma_{\beta_N\alpha_1} |\bar{\beta}\rangle |\bar{\alpha}\rangle .$$

Projecting state from the valence spin $\frac{1}{2}$ space to the physical spin 1 yields

$$|\Psi\rangle = \sum_{\bar{s}} \sum_{\bar{\alpha}\bar{\beta}} X^{s_1}_{\alpha_1\beta_1} \Sigma_{\beta_1\alpha_2} X^{s_2}_{\alpha_2\beta_2} \Sigma_{\beta_2\alpha_3} .... \Sigma_{\beta_{N-1}\alpha_N} X^{s_N}_{\alpha_N\beta_N} \Sigma_{\beta_N\alpha_1} |\bar{s}\rangle ,$$

where we expressed the projector $\mathcal{P}_i$ as

$$\mathcal{P}_i = \sum_{\alpha_i \beta_i} X^{s_i}_{\alpha_i \beta_i} |s\rangle_i \langle\alpha|_i \langle\beta|_i ,$$

with the matrices

$$X^1 = \begin{pmatrix} 1 & 0 \\ 0 & 0 \end{pmatrix} \quad X^0 = \begin{pmatrix} 0 & \frac{1}{\sqrt{2}} \\ \frac{1}{\sqrt{2}} & 0 \end{pmatrix} \quad X^{-1} = \begin{pmatrix} 0 & 0 \\ 0 & 1 \end{pmatrix}.$$

In order to obtain an expression of the from (13) simply group $M^{s_i} \coloneqq X^{s_i}\Sigma$ together, which results in

$$|\Psi\rangle = \sum_{\bar{s}} M^{s_1} M^{s_2} ... M^{s_N} |\bar{s}\rangle ,$$

where the M^{s_i} read as

$$M^1 = \begin{pmatrix} 0 & \frac{1}{\sqrt{2}} \\ 0 & 0 \end{pmatrix} \quad M^0 = \begin{pmatrix} -\frac{1}{2} & 0 \\ 0 & \frac{1}{2} \end{pmatrix} \quad M^{-1} = \begin{pmatrix} 0 & 0 \\ -\frac{1}{\sqrt{2}} & 0 \end{pmatrix}.$$

Cutting the system at an arbitrary valence bond, the singular values decomposition of the bond

$$\Sigma_{\beta\alpha} = \begin{pmatrix} 0 & \frac{1}{\sqrt{2}} \\ -\frac{1}{\sqrt{2}} & 0 \end{pmatrix} = \begin{pmatrix} 0 & -i \\ -i & 0 \end{pmatrix} \underbrace{\begin{pmatrix} \frac{1}{\sqrt{2}} & 0 \\ 0 & \frac{1}{\sqrt{2}} \end{pmatrix}}_{=:\lambda_{\alpha\alpha}} \begin{pmatrix} i & 0 \\ 0 & -i \end{pmatrix},$$

leads to the Schmidt decomposition $|\Psi\rangle = \lambda_\alpha |\Phi[L]_\alpha\rangle |\Phi[R]_\alpha\rangle$ with $\lambda_\alpha = \{\frac{1}{\sqrt{2}}, \frac{1}{\sqrt{2}}\}$. Note that the double degeneracy of the entanglement spectrum (Schmidt coefficients) do represent the edge excitation of the open chain (as it was worked out in more detail in section 5.2 or see [53]).

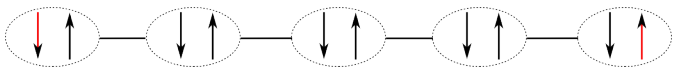

Figure 44: free edge excitations: free spin $\frac{1}{2}$ can be in 4 different configurations leading to a four fold degenerate ground state.

C. transverse Ising Model

Exact analytic solution of the transvers Ising modell as pointed out in [54].

Besides the numerical solutions throughout the thesis, we present here the analytic solutions for the transverse Ising model, to be precise: ground state energy, dispersion, entropy at criticality. Moreover, we will make use of the Jordan-Wigner transformation, a very useful

method in the context of MPS. The Hamiltonian of interest, the transverse Ising model is given by

$$\hat{\mathcal{H}} = -J \sum_i \hat{\sigma}_i^x \hat{\sigma}_{i+1}^x - B \sum_i \hat{\sigma}_i^z,$$

a nearest neighbour spin $\frac{1}{2}$ interaction in x-direction and a transverse external field in z-direction acting on each single spin. For $J > 0$ ($J < 0$) the system describes a ferromagnetic (anti-ferromagnetic) spin chain in an external magnetic field applied perpendicular. To solve this spin $\frac{1}{2}$ model exactly it is first transformed into a model of spinless fermions, using the Jordan-Wigner transformation. Starting with a naive approach, assigning spin lowering and raising to annihilation and creation operators

$$\hat{a}_i^\dagger \coloneqq \frac{1}{2}\left(\hat{\sigma}^x + i\hat{\sigma}^y\right) \qquad \hat{a}_i \coloneqq \frac{1}{2}\left(\hat{\sigma}^x - i\hat{\sigma}^y\right),$$

respectively, the Hamiltonian can be reformulated into

$$\hat{\mathcal{H}} = -\frac{J}{4} \sum_i \left(\hat{a}_i^\dagger + \hat{a}_i\right)\left(\hat{a}_{i+1}^\dagger + \hat{a}_{i+1}\right) - B \sum_i \left(\hat{a}_i^\dagger \hat{a}_i - \frac{1}{2}\right)$$

Even though, from the spin lowering and rising operators $\hat{S}^-$ and $\hat{S}^+$ the new particles have hardcore properties, namely at each lattice site the maximal occupation number is one, they possess inconsistent commutation/anti-commutation relations. On one hand they behave as fermions (hardcore property)

$$\{\hat{a}_i^\dagger, \hat{a}_i\} = 1,$$

and on the other, as the spin operators they commute at different sites

$$\left[\hat{a}_i^\dagger, \hat{a}_j\right] = \left[\hat{a}_i^\dagger, \hat{a}_j^\dagger\right] = [\hat{a}_i, \hat{a}_j] = 0 \quad \forall i \neq j.$$

To transform these effective hardcore bosons further into spin-less fermions, we apply the Jordan-Wigner transformation

$$\hat{c}_i = exp\left[i\pi \sum_{j=1}^{i-1} \hat{a}_j^\dagger \hat{a}_j\right] \hat{a}_j \qquad \hat{c}_i^\dagger = \hat{a}_j^\dagger \; exp\left[-i\pi \sum_{j=1}^{i-1} \hat{a}_j^\dagger \hat{a}_j\right],$$

which accounts for sign change by an additional phase counting modes between i and j. Considering a periodic system ($\hat{\sigma}_{N+1}^x = \hat{\sigma}_1^x$), previous Hamiltonian yields

$$\hat{\mathcal{H}} = -\frac{J}{4} \sum_i \left(\hat{c}_i^\dagger - \hat{c}_i\right)\left(\hat{c}_{i+1}^\dagger + \hat{c}_{i+1}\right) - \frac{B}{2} \sum_i \left(\hat{c}_i^\dagger \hat{c}_i - \hat{c}_i \hat{c}_i^\dagger\right) + \frac{J}{4}\left(exp(i\pi L) + 1\right)\left[(\hat{c}_N^\dagger - \hat{c}_N)(\hat{c}_1^\dagger + \hat{c}_1)\right],$$

where the last term can de dropped for large enough systems, such that $\hat{\mathcal{H}}$ is quadratic in the fermion operators $\hat{c}^\dagger$ and $\hat{c}$. By Fourier transforming the system into momentum space ($a = 1$)

$$\hat{c}_j = \frac{1}{\sqrt{N}} \sum_{k=-\pi}^{\pi} e^{-ikj} \Phi_k \qquad \hat{c}_j^\dagger = \frac{1}{\sqrt{N}} \sum_{k=-\pi}^{\pi} e^{ikj \cdot} \Phi_k^\dagger,$$

and symmetrization of the Hamiltonian, we arrive at an effective two level system

$$\hat{\mathcal{H}} = -B \sum_{k=-\pi}^{\pi} \begin{pmatrix} \Phi_k^\dagger & \Phi_{-k} \end{pmatrix} \begin{pmatrix} \epsilon_k & i\lambda \sin(k) \\ -i\lambda \sin(k) & -\epsilon_k \end{pmatrix} \begin{pmatrix} \Phi_k \\ \Phi_{-k}^\dagger \end{pmatrix}$$
$$\text{with} \quad \epsilon_k = 1 - \lambda cos(k), \quad \lambda = \frac{J}{B}.$$

Diagonalization of the two level system is referred to as the Bogoliubov-transformation, where quasiparticle creation and annihilation operators are introduced

$$\eta_k^\dagger = u_k \Phi_k^\dagger + i v_k \Phi_{-k} \qquad \eta_k = u_k \Phi_k - i v_k \Phi_{-k}^\dagger \quad \text{with} \quad |u_k|^2 + |v_k|^2 = 1,$$

as the normalized eigenvectors. This allows us to write the Hamiltonian in diagonal form

$$\hat{\mathcal{H}} = B \cdot \sum_k \epsilon_k \left(\eta_k^\dagger \eta_k - \frac{1}{2} \right),$$

with

$$\epsilon_k = \sqrt{1 + \lambda^2 - 2\lambda cos(k)}.$$

The ground state energy is thus given as $E_0 = -\frac{B}{2} \sum_k \epsilon_k$, which in thermodynamic limit ($J = 1$) transforms into the integral (see fig. 30)

$$E_0 = -\frac{1}{4\pi} \int_{-\pi}^{\pi} \sqrt{1 + B^2 - 2B cos(k)} \mathrm{d}k.$$

D. Pseudocode:

Pseudocode and further benchmark results of the implemented routines.

D.1. vMPS

Pseudocode of the vMPS routine without usage of U(1) symmetry

In the following we present the pseudocode 1 for the variational matrix product state routine (short vMPS) and some further benchmark results of a spin $\frac{1}{2}$ Heisenberg chain

$$\hat{\mathcal{H}} = J \sum_i \mathbf{S}_i \mathbf{S}_{i+1} \tag{156}$$

in form of a comparison with exact diagonalization.
Note that the here (in pseudocode) presented vMPS routine, does not, other than the actual implemented one, possesses the possibility to restrict the ground state search to a specific U(1) symmetry sector (if present in the system at hand). That this leads to significant improvement can be seen in our benchmark results for the Heisenberg chain (156) with $J = 1.0$. All tables of the benchmark results are build up in the same fashion, the top row present given parameters as the maximal bond dimension D_α and n number of sweeps used in the routine. Table 1 and table 4 thus have the same parameters except that the results of table 4 use the U(1) symmetry sector. The columns are labled as follows:

- N: system size (number of sites the model possesses)
- E_0: the ground state energy our routine found
- $var(E)$: variance of the expectation value of $\hat{\mathcal{H}}$ as measure of the quality of the ground state
- δE: relative error with respect to results obtained by direct diagonalization.

As one can see for longer chain lengths the vMPS routine with U(1) symmetry delivers more accurate results. Further, we give obtained results for different routine parameters (table 2 - table 4). Comparison of the table reveals that an increase of the bond dimension does not necessarily improve the result significantly (table 2 with table 3). It is a combintation of increase in bond dimension and increase in sweeps which leads to better results (table 3 with table 4). This can be understood considering that an increase in the bond dimension leads also to an increase in the complexity of the optimization problem, since more parameters are involved.

Data: n: number of sweeps, D_{max}: max bond dimension, $\hat{\mathcal{H}}$ as MPO
Result: ground state for strongly correlated systems

Function *vMPS(n,D_{max},$\hat{\mathcal{H}}_{MPO}$)*:
    initialize:
    random MPS trial state $|\Psi_{trial}\rangle_{MPS}$ with bond dimension D_{max} (or any other state, which has a non zero overlap with the true ground state $|\Psi\rangle_0$).;
    for $\#_{sweep}$ *in n* **do**
        sweep($\hat{\mathcal{H}}_{MPO}$,$|\Psi_{trial}\rangle_{MPS}$);
        while sweeping check for convergence of $\langle\hat{\mathcal{H}}\rangle$ and quality $|\Psi_{trial}\rangle_{MPS}$ to be an eigenstate by *var* $\left(\hat{\mathcal{H}}\right)$;
    end
return $|\Psi_{trial}\rangle_{MPS}$

Function *sweep($\hat{\mathcal{H}}_{MPO}$,$|\Psi_{trial}\rangle_{MPS}$)*:
    initialize:
    right canonical form $|\Psi_{trial}\rangle_{MPS}$ up to site 1;
    construct *right block* **R** as list containing $F[i]$ (see fig. 16) from last to second site;
    construct *left block* **L** as empty list;
    % forward sweep upper fig in 20
    for $i = \#_{site}$ *from 1 to N (system size)* **do**
        W= MPO tensor of $\hat{\mathcal{H}}_{MPO}$ at site i;
        M_i= reshape tensor of $|\Psi_{trial}\rangle_{MPS}$ at site i into a vector;
        eig_vec=optSite(**L**,**R**,W,M_i);
        update(i,**L**,W,eig_vec,direction=right);
    end
    % backward sweep lower fig in 20
    for $i = \#_{site}$ *from N to 1* **do**
        W= MPO tensor of $\hat{\mathcal{H}}_{MPO}$ at site i;
        M_i= reshape tensor of $|\Psi_{trial}\rangle_{MPS}$ at site i into a vector;
        eig_vec=optSite(**L**,**R**,W,M_i, site i);
        update(i,**R**,W,eig_vec,direction=left);
    end
end

Table 1: vMPS without U(1) sym., $D_\alpha = 10$, $n = 8$

N	E_{vMPS}	$var(E)$	δE
4	-1.616025403784437	$8.881784197001252323 \cdot 10^{-16}$	$2.347116568290005 \cdot 10^{-14}$
6	-2.493577133887924	$2.664535259100375697 \cdot 10^{-15}$	$9.624727334012640 \cdot 10^{-15}$
8	-3.374929869269498	$1.030097845600153050 \cdot 10^{-5}$	$8.087333686109398 \cdot 10^{-7}$
10	-4.258020596661840	$4.796290196296126851 \cdot 10^{-5}$	$3.431317610688470 \cdot 10^{-6}$

Table 2: vMPS with U(1) sym. $S_z = 0.0$, $D_\alpha = 5$, $n = 5$

N	E_{vMPS}	$var(E)$	δE
4	-1.616025403784438	$8.881784197 \cdot 10^{-16}$	$2.349568722945963 \cdot 10^{-14}$
6	-2.493577133887928	$2.6645352591 \cdot 10^{-15}$	$1.121987358655791 \cdot 10^{-14}$
8	-3.374932453484985	$7.00176117974 \cdot 10^{-7}$	$0.0430 \cdot 10^{-6}$
10	-4.258034499844214	$3.17199074118 \cdot 10^{-6}$	$0.1661 \cdot 10^{-6}$

Table 3: vMPS with U(1) sym. $S_z = 0.0$, $D_\alpha = 10$, $n = 5$

N	E_{vMPS}	$var(E)$	δE
4	-1.616025403784438	$8.881784197 \cdot 10^{-16}$	$3.796962744218035 \cdot 10^{-14}$
6	-2.49357713388793	0	$2.620126338115369 \cdot 10^{-14}$
8	-3.374932453485286	$7.00175091239 \cdot 10^{-7}$	$1.45202613932582 \cdot 10^{-7}$
10	-4.258034499850337	$3.17196803223 \cdot 10^{-10}$	$7.074325623079858 \cdot 10^{-7}$

Table 4: vMPS with U(1) sym. $S_z = 0.0$, $D_\alpha = 10$, $n = 8$

N	E_{vMPS}	$var(E)$	δE
4	-1.616025403784439	$4.4408920985 \cdot 10^{-16}$	$3.885780586188048 \cdot 10^{-14}$
6	-2.493577133887926	0	$2.575717417130363 \cdot 10^{-14}$
8	-3.374932598687888	$5.3290705182 \cdot 10^{-15}$	$1.243449787580175 \cdot 10^{-14}$
10	-4.258035207229238	$2.96203950256 \cdot 10^{-10}$	$5.366196376144217 \cdot 10^{-11}$

Table 5: vMPS with U(1) sym. $S_z = 1.0$, $D_\alpha = 5$, $n = 5$

N	E_{vMPS}	$var(E)$	δE
4	-0.9571067811865475	$1.11022302463 \cdot 10^{-16}$	$2.612038749637414 \cdot 10^{-15}$
6	-2.001995356898534	$2.6645352591 \cdot 10^{-15}$	$1.698305637065630 \cdot 10^{-14}$
8	-2.9822404877628848	$5.3290705182 \cdot 10^{-15}$	$5.096839125607276 \cdot 10^{-15}$
10	-3.930673558816132	$1.53327135877 \cdot 10^{-7}$	$7.806669147371796 \cdot 10^{-9}$

Function *optSite(**L**,**R**,W,M_i,site i)*:

construct H_{eff} with **L**, **R** and W (see fig. 18);

eig_vec=Laczos(H_{eff}) with initial vector M_i % search only for the lowest eigenvector

return eig_vec

Function *update(i,(**L**,**R**),W,eig_vec,direction)*:

if *direction is right* **then**

reshape eig_vec into a matrix M of the form $d_i \cdot D_{\alpha_i} \times D_{\alpha_{i+1}}$;

U,S,$V^\dagger$=svd(M); % svd: singular value decomposition

reshape U back into a tensor $A_i = U^{s_i}_{\alpha_i \alpha_{i+1}}$; % Note that A_i is in left canonical form

update $|\Psi_{trial}\rangle_{MPS}$ by exchanging M_i with A_i and contract $M'^{s_{i+1}}_{\alpha_{i+1}\alpha_{i+2}} = (SV)_{\alpha_i \alpha_{i+1}} B^{s_{i+1}}_{\alpha_{i+1}\alpha_{i+2}}$;

construct and store new element $F[i]$ of **L**[i] with updated $|\Psi_{trial}\rangle_{MPS}$;

else if *direction is left* **then**

reshape eig_vec into a matrix M of the form $D_{\alpha_i} \times d_i \cdot D_{\alpha_{i+1}}$;

U,S,$V^\dagger$=svd(M); % svd: singular value decomposition

reshape $V^\dagger$ back into a tensor $B_i = V^{s_i}_{\alpha_i \alpha_{i+1}}$; % Note that B_i is in right canonical form

update $|\Psi_{trial}\rangle_{MPS}$ by exchanging M_i with B_i and contract $M'^{s_{i-1}}_{\alpha_{i-1}\alpha_i} = A^{s_{i-1}}_{\alpha_{i-1}\alpha_i} (US)_{\alpha_i \alpha_{i+1}}$;

construct and store new element $F[i]$ of **R**[i] with updated $|\Psi_{trial}\rangle_{MPS}$;

end

end

Algorithm 1: vMPS scheme without U(1) symmetry

D.2. TEBD

Pseudocode of the TEBD routine with benchmark.

Besides the results for iTEBD/TEBD given throughout the thesis, we will present here the total magnetization $\langle \hat{s}_z \rangle$ dynamics of a quenched transverse Ising model as a benchmark of our TEBD routine. We hereby, initialize the system in a ferromagnetic spin up state $|\uparrow\rangle = \prod_i^N \otimes |\uparrow\rangle$ of size $N = 10$ and let the state evolve under

$$\hat{\mathcal{H}} = J \sum_i \hat{\sigma}_i^x \hat{\sigma}_{i+1}^x + B \sum_i \hat{\sigma}_i^z, \tag{157}$$

for specific parameters J, B but different maximal bond dimension D_α (see fig. 45). The evolution is hereby compared with results obtained from exact diagonalization. As expected we see that by increasing the bond dimension, it is possible to trace the excat solution for longer time. At the maximum bond dimension $D_\alpha = 32$ (Hilbert space is completely incorporated in the MPS representation) the evolution becomes completely identical to the one obtained by exact diagonalization up to an error of the order $\mathcal{O}(10^{-3})$

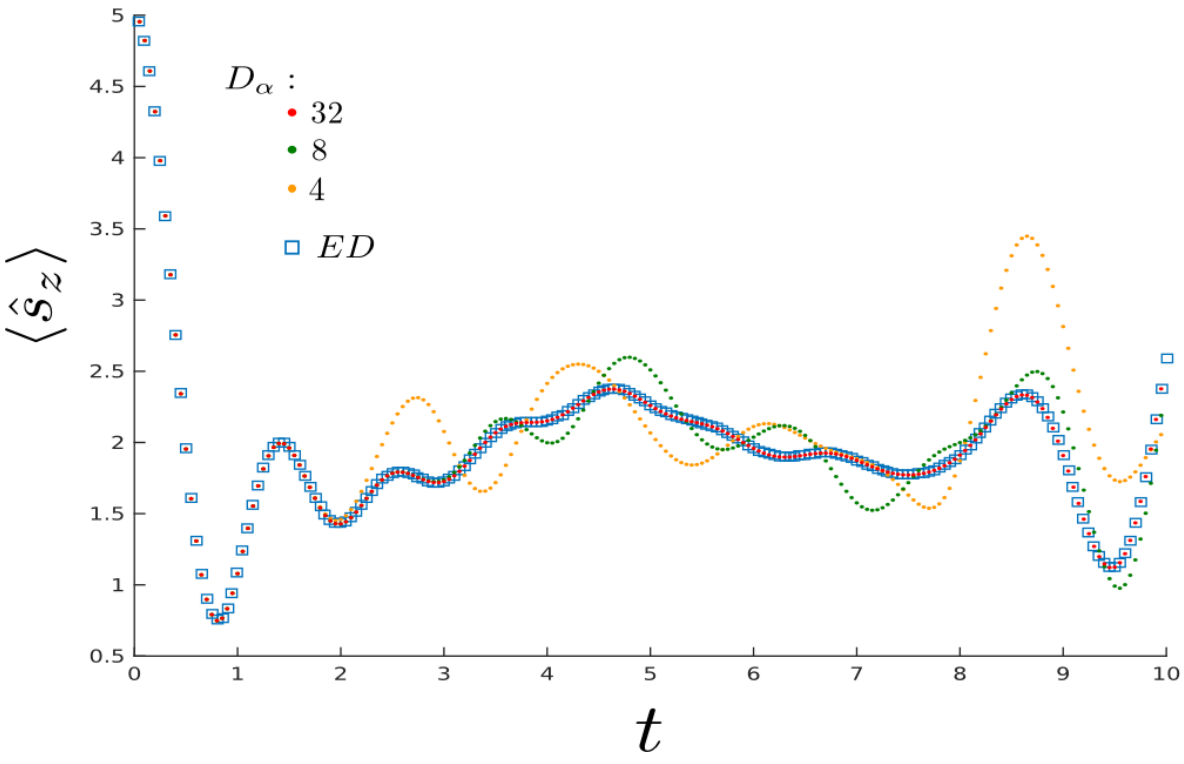

Figure 45: TEBD vs. ED of quenched transverse Ising model (157): for $J = 1.0$, $B = 0.5$, $\Delta t = 0.05$ and system size $N = 10$ initial state is $|\uparrow\rangle = \prod_i^N \otimes |\uparrow\rangle$

Data: $|\Psi(t=0)\rangle_{MPS}$: state at time $t=0$,$[\widetilde{H}]$: list of bond Hamiltonian after Trotter decomposition, D_{max}: maximum of bond dimension possible during evolution,T_{max}: time until state should be evolved, Δt: time step

Result: $|\Psi(t=T_{max})\rangle_{MPS}$: final state at $t=T_{max}$, expectation values and other quantities of operators with time

Function *TEBD(*$|\Psi(t=0)\rangle_{MPS}$,$[\widetilde{H}]$,D_{max},T_{max},Δt*)*:

initialize:

$[\widetilde{U}]$=$exp\left(-i\cdot[\widetilde{H}]\Delta t\right)$ creat list of bond unitary operator;

measurement_list: list for storying exp. values and other quantities during the evolution;

t=0;

for *timestep from 0 to* $T_{max}/\Delta t$ **do**

evolveChain($|\Psi(t)\rangle_{MPS}$,$[\widetilde{U}]$,D_{max});

t=t+Δt;

add measurements or other quantities to measurement_list;

end

return $|\Psi(t=T_{max})\rangle_{MPS}$**,**

Function *evolveChain(*$|\Psi(t)\rangle_{MPS}$,$[\widetilde{U}]$,D_{max}*)*:

% first sequentially evolve all even than all odd bonds

for *even,odd* **do**

for *i in even/odd sites* **do**

evolveBond(i,$\widetilde{U}_{ii+1}$,$|\Psi(t)\rangle_{MPS}$)

end

end

end

Function *evolveBond(i,*$\widetilde{U}_{ii+1}$,$|\Psi(t)\rangle_{MPS}$*)*:

% follows entirely the routine described in fig. 23

contract $\lambda[i-1]\,\Gamma[i]\lambda[i]\,\Gamma[i+1]\lambda[i+1]$ into $M^{s_i s_{i+1}}_{\alpha_{i-1}\alpha_{i+1}}$;

evolve $\widetilde{U}^{s'_i s'_{i+1} s_i s_{i+1}} M^{s_i s_{i+1}}_{\alpha_{i-1}\alpha_{i+1}}$ into $M^{s'_i s'_{i+1}}_{\alpha_{i-1}\alpha_{i+1}}$;

U,λ[i],$V^\dagger$=svd($M_{(s'_i\alpha_{i-1}),(s'_{i+1}\alpha_{i+1})}$); % svd: singular value decomposition

form $\Gamma[i]^{s'_i}=\lambda[i-1]^{-1}U^{s'_i}$ and $\Gamma[i+1]^{s'_{i+1}}=V^{s'_{i+1}}\lambda[i+1]^{-1}$;

end

Algorithm 2: TEBD scheme

D.3. TDVP

Pseudocode of the TDVP routine with benchmark.

As in the previous section we will compare our results obtained with the implemented TDVP routine against result from exact diagonalization for quenched initial state in the transverse Ising model (157). The choosen parameters (system size $N = 10$, $J = 1.0$, $B = 0.5$ as well as the intial state) are hereby, exactly the same as the ones above. The overlap between the ED results and the TDVP results for $D_\alpha = 32$ come with an error of $\mathcal{O}(10^{-7})$. The conservation of energies as other symmetries is still pending.

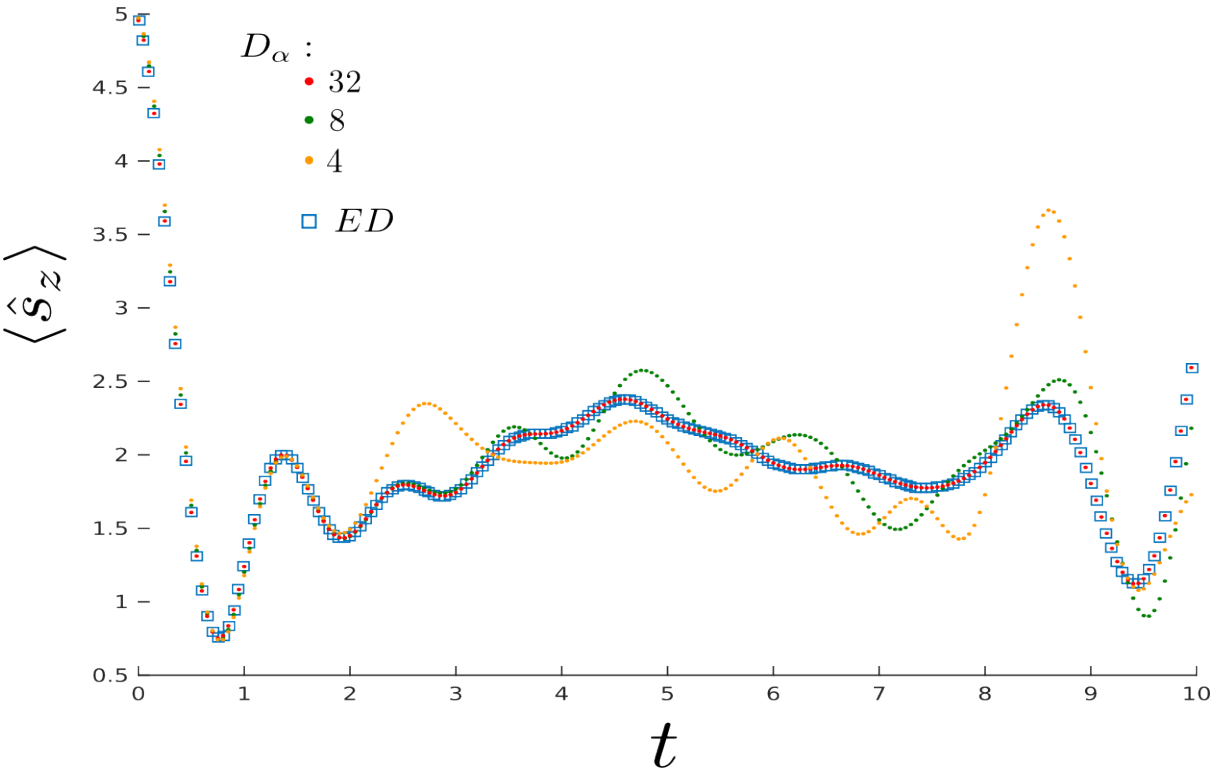

Figure 46: TDVP vs. ED of quenched transverse Ising model (157): for $J = 1.0$, $B = 0.5$, $\Delta t = 0.05$ and system size $N = 10$ initial state is $|\uparrow\rangle = \prod_i^N \otimes |\uparrow\rangle$

Data: $|\Psi(t=0)\rangle_{MPS}$: state at time $t=0$ with specific bond dimension D_α, $\hat{\mathcal{H}}$ as MPO,T_{max}: time until state should be evolved, Δt: time step

Result: $|\Psi(t=T_{max})\rangle_{MPS}$: final state at $t=T_{max}$ with bond dimension D_α, expectation values of operators and other quantities with time

Function *TDVP(*$|\Psi(t=0)\rangle_{MPS}$,$\hat{\mathcal{H}}_{MPO}$,T_{max},Δt*)*:

initialize:
bring $|\Psi(t=0)\rangle_{MPS}$ in right canonical form;
construct *right block* $\mathbf{R}$ as list containing $F[i]$ (see fig. 16) from last to second site;
construct *left block* $\mathbf{L}$ as empty list;
measurement_list: list for storying exp. values and other quantities during the evolution;
t=0;
for *timestep from 0 to* $T_{max}/\Delta t$ **do**
  evolveChain($|\Psi(t)\rangle_{MPS}$,$\mathbf{L}$,$\mathbf{R}$, $\hat{\mathcal{H}}_{MPO}$); % by sweeping back and forth
  t=t+Δt;
  add measurements or other quantities to measurement_list;
end

return $|\Psi(t=T_{max})\rangle_{MPS}$**,**

Function *evolveChain(*$|\Psi(t)\rangle_{MPS}$,$\boldsymbol{L}$,$\boldsymbol{R}$, $\hat{\mathcal{H}}_{MPO}$*)*:

for *n from 1 to system size-1* **do**
  direction=right;
  evolveSite(n,direction,$|\Psi(t)\rangle_{MPS}$,$\mathbf{L}$,$\mathbf{R}$, $\hat{\mathcal{H}}_{MPO}$);
end
% evolve last site seperately
construct effective matrix of last site N: $(H_N)_{(s'_N\alpha'_N),(s_N\alpha_N)}$;
get tensor of MPS at last site N and rearange it into vector $M_{s_N\alpha_N}$;
evolve vector $M_{s_N\alpha_N}$ forward in time:
$M'_{s'_N\alpha'_N} = exp\left[-i(H_N)_{(s'_N\alpha'_N),(s_N\alpha_N)}\Delta t\right]M_{s_N\alpha_N}$;
for *n from system size-1 to 1* **do**
  direction=left;
  evolveSite(n,direction,$|\Psi(t)\rangle_{MPS}$,$\mathbf{L}$,$\mathbf{R}$, $\hat{\mathcal{H}}_{MPO}$);
end

end

Function *evolveSite(n,direction,*$|\Psi(t)\rangle_{MPS}$*,**L**,**R**,* $\hat{\mathcal{H}}_{MPO}$*)*:

if *direction is right* **then**

construct with **L**,**R** and $W[n]$ tensor of $\hat{\mathcal{H}}_{MPO}$ at site n: effective matrix $(H_n)_{(s'_n\alpha'_n\alpha'_{n+1}),(s_n\alpha_n\alpha_{n+1})}$ see fig. 29;

get tensor of MPS at site n and rearange it into vector $M_{s_n\alpha_n\alpha_{n+1}}$;

evolve vector $M_{s_n\alpha_n\alpha_{n+1}}$ forward in time:

$M'_{s'_n\alpha'_n\alpha'_{n+1}} = exp\left[-i(H_n)_{(s'_n\alpha'_n\alpha'_{n+1}),(s_n\alpha_n\alpha_{n+1})}\frac{\Delta t}{2}\right]M_{s_n\alpha_n\alpha_{n+1}}$;

U,S,$V^\dagger$=svd($M'_{(s'_n\alpha'_n),\alpha'_{n+1}}$);

form $A^{s_n}_{\alpha_n\alpha_{n+1}} = U^{s_n}_{\alpha_n\widetilde{\alpha}_{n+1}}$ and $\lambda_{\widetilde{\alpha}_{n+1}\alpha_{n+1}} = SV^\dagger$;

construct with new fromed $A^{s_n}_{\alpha_n\widetilde{\alpha}_{n+1}}$ the new element of **L**, $F[n]$;

construct $(K_n)_{(\widetilde{\alpha}'_{n+1}\alpha'_{n+1}),(\widetilde{\alpha}_{n+1}\alpha_{n+1})}$ see fig. 29;

evolve $\lambda_{\widetilde{\alpha}_{n+1}\alpha_{n+1}}$ backwards in time:

$\lambda_{\widetilde{\alpha}'_{n+1}\alpha'_{n+1}} = exp\left[i(K_n)_{(\widetilde{\alpha}'_{n+1}\alpha'_{n+1}),(\widetilde{\alpha}_{n+1}\alpha_{n+1})}\frac{\Delta t}{2}\right]\lambda_{\widetilde{\alpha}_{n+1}\alpha_{n+1}}$;

contract $\lambda_{\widetilde{\alpha'}_{n+1}\alpha'_{n+1}}$ with MPS tensor to the right;

end

else if *direction is left* **then**

get tensor of MPS at site $n+1$ and rearange it into matrix $M_{\alpha_{n+1},(s_{n+1}\alpha_{n+2})}$;

U,S,$V^\dagger$=svd($M_{\alpha_{n+1},(s_{n+1}\alpha_{n+2})}$);

form $B^{s_{n+1}}_{\widetilde{\alpha}_{n+1}\alpha_{n+2}} = V^{s_{n+1}}_{\widetilde{\alpha}_{n+1}\alpha_{n+2}}$ and $\lambda_{\alpha_{n+1}\widetilde{\alpha}_{n+1}} = US$;

construct with new fromed $B^{s_{n+1}}_{\widetilde{\alpha}_{n+1}\alpha_{n+2}}$ the new element of **R**, $F[n]$;

construct $(K_n)_{(\alpha'_{n+1}\widetilde{\alpha'}_{n+1}),(\alpha_{n+1}\widetilde{\alpha}_{n+1})}$ see fig. 29;

evolve $\lambda_{\alpha_{n+1}\widetilde{\alpha}_{n+1}}$ backwards in time:

$\lambda_{\alpha'_{n+1}\widetilde{\alpha'}_{n+1}} = exp\left[i(K_n)_{(\alpha'_{n+1}\widetilde{\alpha'}_{n+1}),(\alpha_{n+1}\widetilde{\alpha}_{n+1})}\frac{\Delta t}{2}\right]\lambda_{\alpha_{n+1}\widetilde{\alpha}_{n+1}}$;

contract $\lambda_{\alpha_{n+1}\widetilde{\alpha}_{n+1}}$ with MPS tensor to the left iff present;

construct with **L**,**R** and $W[n]$ tensor of $\hat{\mathcal{H}}_{MPO}$ at site n: effective matrix $(H_n)_{(s'_n\alpha'_n\alpha'_{n+1}),(s_n\alpha_n\alpha_{n+1})}$ see fig. 29;

get tensor of MPS at site n and rearange it into vector $M_{s_n\alpha_n\alpha_{n+1}}$;

evolve vector $M_{s_n\alpha_n\alpha_{n+1}}$ forward in time:

$M'_{s'_n\alpha'_n\alpha'_{n+1}} = exp\left[-i(H_n)_{(s'_n\alpha'_n\alpha'_{n+1}),(s_n\alpha_n\alpha_{n+1})}\frac{\Delta t}{2}\right]M_{s_n\alpha_n\alpha_{n+1}}$;

store $M'_{s'_n\alpha'_n\alpha'_{n+1}}$ back as tensor of the MPS;

end

end

Algorithm 3: TDVP scheme

References

[1] Vlatko Vedral, Martin B Plenio, Michael A Rippin, and Peter L Knight. Quantifying entanglement. *Physical Review Letters*, 78(12):2275, 1997.

[2] Martin B Plenio and Shashank Virmani. An introduction to entanglement measures. *arXiv preprint quant-ph/0504163*, 2005.

[3] Guifré Vidal. Efficient classical simulation of slightly entangled quantum computations. *Phys. Rev. Lett.*, 91:147902, Oct 2003.

[4] Román Orús. A practical introduction to tensor networks: Matrix product states and projected entangled pair states. *Annals of Physics*, 349:117 – 158, 2014.

[5] Ulrich Schollwöck. The density-matrix renormalization group in the age of matrix product states. *Annals of Physics*, 326(1):96–192, 2011.

[6] Tom Simonite. Ibm builds biggest data drive ever. *MIT Technology Review*.

[7] M B Hastings. An area law for one-dimensional quantum systems. *Journal of Statistical Mechanics: Theory and Experiment*, 2007(08):P08024, 2007.

[8] Matthew B. Hastings and Tohru Koma. Spectral gap and exponential decay of correlations. *Communications in Mathematical Physics*, 265(3):781–804, 2006.

[9] Mark Srednicki. Entropy and area. *Phys. Rev. Lett.*, 71:666–669, Aug 1993.

[10] J. Eisert, M. Cramer, and M. B. Plenio. Colloquium. *Rev. Mod. Phys.*, 82:277–306, Feb 2010.

[11] F. Verstraete, V. Murg, and J.I. Cirac. Matrix product states, projected entangled pair states, and variational renormalization group methods for quantum spin systems. *Advances in Physics*, 57(2):143–224, 2008.

[12] Steven R. White. Density matrix formulation for quantum renormalization groups. *Phys. Rev. Lett.*, 69:2863–2866, Nov 1992.

[13] I. Peschel, M. Kaulke, and Ö. Legeza. Density-matrix spectra for integrable models. *Annalen der Physik*, 511:153–164, 1999.

[14] Gregory M. Crosswhite and Dave Bacon. Finite automata for caching in matrix product algorithms. *Phys. Rev. A*, 78:012356, 2008.

[15] B Pirvu, V Murg, J I Cirac, and F Verstraete. Matrix product operator representations. *New Journal of Physics*, 12(2):025012, 2010.

[16] D. Perez-Garcia, F. Verstraete, M. M. Wolf, and J. I. Cirac. Matrix product state representations. *eprint arXiv:quant-ph/0608197*, 2006.

[17] Michael M. Wolf, Frank Verstraete, Matthew B. Hastings, and J. Ignacio Cirac. Area laws in quantum systems: Mutual information and correlations. *Phys. Rev. Lett.*, 100:070502, 2008.

[18] Davide Rossini, Vittorio Giovannetti, and Rosario Fazio. Stiffness in 1d matrix product states with periodic boundary conditions. *Journal of Statistical Mechanics: Theory and Experiment*, 2011(05):P05021, 2011.

[19] Kenneth G. Wilson. The renormalization group: Critical phenomena and the kondo problem. *Rev. Mod. Phys.*, 47:773–840, Oct 1975.

[20] Ralf Bulla, Theo A. Costi, and Thomas Pruschke. Numerical renormalization group method for quantum impurity systems. *Rev. Mod. Phys.*, 80:395–450, Apr 2008.

[21] S. R. White and R. M. Noack. Real-space quantum renormalization groups. *Phys. Rev. Lett.*, 68:3487–3490, Jun 1992.

[22] Iztok Pižorn and Frank Verstraete. Variational numerical renormalization group: Bridging the gap between nrg and density matrix renormalization group. *Phys. Rev. Lett.*, 108:067202, Feb 2012.

[23] Naomichi Hatano and Masuo Suzuki. *Finding Exponential Product Formulas of Higher Orders*, pages 37–68. Springer Berlin Heidelberg, Berlin, Heidelberg, 2005.

[24] Pasquale Calabrese and John Cardy. Evolution of entanglement entropy in one-dimensional systems. *Journal of Statistical Mechanics: Theory and Experiment*, 2005(04):P04010, 2005.

[25] Elliott H. Lieb and Derek W. Robinson. The finite group velocity of quantum spin systems. *Comm. Math. Phys.*, 28(3):251–257, 1972.

[26] J. Schachenmayer, B. P. Lanyon, C. F. Roos, and A. J. Daley. Entanglement growth in quench dynamics with variable range interactions. *Phys. Rev. X*, 3:031015, 2013.

[27] G. Vidal. Classical simulation of infinite-size quantum lattice systems in one spatial dimension. *Phys. Rev. Lett.*, 98:070201, 2007.

[28] M. Saraceno P. Kramer. Geometry of the time-dependent variational principle in quantum mechanics. 1981.

[29] P Kramer. A review of the time-dependent variational principle. *Journal of Physics: Conference Series*, 99(1):012009, 2008.

[30] Jutho Haegeman, J. Ignacio Cirac, Tobias J. Osborne, Iztok Pižorn, Henri Verschelde, and Frank Verstraete. Time-dependent variational principle for quantum lattices. *Phys. Rev. Lett.*, 107:070601, Aug 2011.

[31] Sebastian Holtz, Thorsten Rohwedder, and Reinhold Schneider. On manifolds of tensors of fixed tt-rank. *Numerische Mathematik*, 2012.

[32] Laurens Vanderstraeten. Tangent space methods for matrix product states. 2016.

[33] Jutho Haegeman, Tobias J. Osborne, and Frank Verstraete. Post-matrix product state methods: To tangent space and beyond. *Phys. Rev. B*, 88:075133, 2013.

[34] Jutho Haegeman, Christian Lubich, Ivan Oseledets, Bart Vandereycken, and Frank Verstraete. Unifying time evolution and optimization with matrix product states. *Phys. Rev. B*, 94:165116, Oct 2016.

[35] Christian Lubich, Ivan V. Oseledets, and Bart Vandereycken. Time integration of tensor trains. *SIAM Journal on Numerical Analysis*, 53(2):917–941, 2015.

[36] C. Lubich and I. Oseledets. A projector-splitting integrator for dynamical low-rank approximation. *ArXiv e-prints*, 2013.

[37] Pasquale Calabrese and John Cardy. Entanglement entropy and conformal field theory. *Journal of Physics A: Mathematical and Theoretical*, 42(50):504005, 2009.

[38] J. Cardy. Conformal Field Theory and Statistical Mechanics. *ArXiv e-prints*, July 2008.

[39] F.D.M. Haldane. Continuum dynamics of the 1-d heisenberg antiferromagnet: Identification with the o(3) nonlinear sigma model. *Physics Letters A*, 93(9):464 – 468, 1983.

[40] Ian Affleck, Tom Kennedy, Elliott H. Lieb, and Hal Tasaki. Rigorous results on valence-bond ground states in antiferromagnets. *Phys. Rev. Lett.*, 59:799–802, Aug 1987.

[41] Xie Chen, Zheng-Cheng Gu, and Xiao-Gang Wen. Classification of gapped symmetric phases in one-dimensional spin systems. *Phys. Rev. B*, 83:035107, Jan 2011.

[42] Frank Pollmann, Ari M. Turner, Erez Berg, and Masaki Oshikawa. Entanglement spectrum of a topological phase in one dimension. *Phys. Rev. B*, 81:064439, 2010.

[43] R. Orús and G. Vidal. Infinite time-evolving block decimation algorithm beyond unitary evolution. *Phys. Rev. B*, 78:155117, 2008.

[44] Xie Chen, Zheng-Cheng Gu, and Xiao-Gang Wen. Complete classification of one-dimensional gapped quantum phases in interacting spin systems. *Phys. Rev. B*, 84:235128, Dec 2011.

[45] Frank Pollmann and Ari M. Turner. Detection of symmetry-protected topological phases in one dimension. *Phys. Rev. B*, 86:125441, Sep 2012.

[46] Zheng-Cheng Gu and Xiao-Gang Wen. Tensor-entanglement-filtering renormalization approach and symmetry-protected topological order. *Phys. Rev. B*, 80:155131, 2009.

[47] Rahul Nandkishore and David A. Huse. Many-body localization and thermalization in quantum statistical mechanics. *Annual Review of Condensed Matter Physics*, 6(1):15–38, 2015.

[48] Michael Schreiber, Sean S. Hodgman, Pranjal Bordia, Henrik P. Lüschen, Mark H. Fischer, Ronen Vosk, Ehud Altman, Ulrich Schneider, and Immanuel Bloch. Observation of many-body localization of interacting fermions in a quasirandom optical lattice. *Science*, 349(6250):842–845, 2015.

[49] P. W. Anderson. Absence of diffusion in certain random lattices. *Phys. Rev.*, 109:1492–1505, Mar 1958.

[50] Jens H. Bardarson, Frank Pollmann, and Joel E. Moore. Unbounded growth of entanglement in models of many-body localization. *Phys. Rev. Lett.*, 109:017202, Jul 2012.

[51] Maksym Serbyn, Z. Papić, and Dmitry A. Abanin. Universal slow growth of entanglement in interacting strongly disordered systems. *Phys. Rev. Lett.*, 110:260601, Jun 2013.

[52] VLADIMIR E. KOREPIN and YING XU. Entanglement in valence-bond-solid states. *International Journal of Modern Physics B*, 24(11):1361–1440, 2010.

[53] N. Regnault. Entanglement Spectroscopy and its Application to the Quantum Hall Effects. *ArXiv e-prints*, 2015.

[54] Elliott Lieb, Theodore Schultz, and Daniel Mattis. Two soluble models of an antiferromagnetic chain. *Annals of Physics*, 16(3), 1961.